Cytotoxic activity of biosourced astins against malignant pleural mesothelioma cells

Auteur : Redouté, Gaëlle
Promoteur(s) : Willems, Luc
Faculté : Gembloux Agro-Bio Tech (GxABT)
Diplôme : Master en bioingénieur : chimie et bioindustries, à finalité spécialisée
Année académique : 2017-2018
URI/URL : http://hdl.handle.net/2268.2/5156

LIÈGE université
Gembloux
Agro-Bio Tech

CYTOTOXIC ACTIVITY OF BIOSOURCED ASTINS AGAINST MALIGNANT PLEURAL MESOTHELIOMA CELLS

GAËLLE REDOUTÉ

MASTER THESIS PRESENTED IN ORDER TO OBTAIN THE BIOENGINEER MASTER

DIPLOMA ORIENTATION CHEMISTRY AND BIO-INDUSTRIES

ACADEMIC YEAR 2017-2018

SUPERVISOR: LUC WILLEMS

[1] L'autorité académique est représentée par le promoteur membre du personnel enseignant de GxABT (Luc Willems)

LIÈGE université
Gembloux
Agro-Bio Tech

CYTOTOXIC ACTIVITY OF BIOSOURCED ASTINS AGAINST MALIGNANT PLEURAL MESOTHELIOMA CELLS

GAËLLE REDOUTÉ

MASTER THESIS PRESENTED IN ORDER TO OBTAIN THE BIOENGINEER MASTER

DIPLOMA ORIENTATION CHEMISTRY AND BIO-INDUSTRIES

ACADEMIC YEAR 2017-2018

SUPERVISOR: LUC WILLEMS

HOST LABORATORY

This master thesis has been conducted in the lab of molecular and cellular biology at Gembloux Agro Bio-Tech (university of Liege) in cooperation with «Diagenode» company (supplier for sample preparation products for next generation sequencing).

ACKNOWLEDGMENTS

Tout d'abord, j'aimerais remercier mon promoteur Luc Willems pour m'avoir donné l'opportunité de travailler sur un sujet qui me passionne énormément ainsi que pour son aide et ses conseils.

Merci à Rugi Safari pour son encadrement et son soutien tout au long de ce TFE. Je la remercie également pour avoir trouvé des solutions et des idées lors des nombreuses réunions de « crise ».

Je remercie également la dream team, à savoir Micheline Vandenbol, Nuts, Isaline Black et Arsène Burny pour leur constante bonne humeur et leur gentillesse incomparable, Jean-Rock Jacques le MacGyver du laboratoire pour son talent de réparateur et pour ses blagues continuelles et enfin Clothilde Hoyos, la maitre du microscope confocal pour son soutien, le partage de son savoir-faire, ses relectures et ses conseils très précieux.

Merci à Gilles Brocart de « Diagenode » pour m'avoir accueillie et aidée à réaliser le séquençage ARN d'un nombre interminable d'échantillons. De même, je remercie Benoit Charloteaux pour avoir pris le temps de m'expliquer les bases de la bio-informatique ainsi que pour les réponses fournies à mes mails contenant une infinité de questions.

Un tout grand merci à ma famille pour avoir cru en moi depuis le début et sans qui je ne serais pas arrivée jusque-là. Plus particulièrement, merci à l'incroyable Mouchette pour les plats préparés, les lessives, sa capacité à supporter mon caractère horripilant se manifestant de manière indéterminée et surtout pour m'avoir donné le courage durant toutes mes études.

Je tiens aussi à remercier Yohann pour sa complicité et pour avoir su me faire rire même dans les moments difficiles.

J'aimerais également remercier mes amis, avec qui j'ai passé 5 magnifiques et trop courtes années à Gembloux, pour leur sens de l'humour complètement dépassé, leur folie perpétuelle, leur compassion lors des moments de doute (BDR) et pour tous ces souvenirs qu'ils m'ont permis de créer à jamais.

Enfin, je remercie mon kot, le KDR, pour leur talent de cuisinier et tous les bons moments passés à leur cotés.

ABSTRACT

Malignant pleural mesothelioma is an aggressive cancer which develops from mesothelial cells lining the surface of lungs. This deadly disease, whose major etiological agent is asbestos, affects an increasing number of people every year. Currently, the main therapeutic strategies comprising radiotherapy, surgery and chemotherapy extend life expectancy of patients of only a few months, demonstrating their low effectiveness. Therefore, the objectives of this work are to study the cytotoxic potential of astin C against mesothelioma cells with the aim of improving standard chemotherapy treatment, to demonstrate the link between the structure of this molecule and its activity as well as to understand the mechanisms involved. Astins are natural compounds produced by an endophyte fungus, which can exhibit an antitumoral activity depending on their chemical structure (cyclic backbone and adjacent chlorides on the proline residue). The results revealed the cytotoxic activity of astin C, highlighted the link between this activity and the chlorides present in the structure of this compound and demonstrated the ability of this molecule to improve the chemotherapeutic treatment based on the association of cisplatin and pemetrexed. This work also led to a better understanding of mechanisms of action of astin C cytotoxicity. Hence, the contribution of this molecule to new therapeutic strategies could be considered in order to develop more efficacious treatments against mesothelioma.

RÉSUMÉ

Le mésothéliome malin pleural est un cancer agressif qui se développe à partir des cellules mésothéliales recouvrant les poumons. Cette maladie mortelle, dont le principal agent étiologique est l'amiante, atteint un nombre croissant de personnes chaque année. Actuellement, les principales stratégies thérapeutiques comprenant la radiothérapie, la chirurgie et la chimiothérapie permettent d'allonger l'espérance de vie des patients de quelques mois seulement, démontrant leur faible efficacité. Dès lors, les objectifs de ce travail consistent à étudier le potentiel cytotoxique de l'astine C contre les cellules du mésothéliome afin d'améliorer le traitement chimiothérapeutique standard, de démontrer l'importance de la structure de cette molécule dans son activité ainsi que de comprendre les mécanismes impliqués. Les astines sont des composés naturels produits par un champignon endophyte, qui selon leur structure (squelette cyclique et deux chlores adjacent sur le résidu proline) peuvent présenter une activité antitumorale. Les résultats ont permis de mettre en évidence l'activité cytotoxique de l'astine C, de la mettre en lien avec les chlorures présents dans la structure de ce composé et de démontrer la capacité de cette molécule à améliorer le traitement chimiothérapeutique reposant sur l'association de cisplatine et de pemetrexed. Ce travail a également mené au développement de mécanismes d'actions pouvant être à l'origine de la cytotoxicité de l'astine C. De ce fait, l'introduction de cette molécule dans de nouvelles stratégies thérapeutiques pourrait être envisagée en vue de développer des traitements plus efficaces contre le mésothéliome.

LIST OF ABBREVIATIONS AND ACRONYMS

Abbreviations	Meaning
%	Percentage
°C	Celsius degree
µ	Micro
ABP	Actin binding proteins
ACTA2	Actin alpha 2
ACTG2	Actin gamma 2
AICARFT	Aminoimidazole carboxamide ribonucleotide formyltransferase
ATP	Adenosine triphosphate
Bcl-2	B-cell lymphoma 2
Bcl2-L11	Bcl-2-like 11
bp	Base pair
BrdU	Bromodeoxyuridine
CARMN	Cardiac mesoderm enhancer-associated non-coding RNA
CCNA1	Cyclin A1
CCNA2	Cyclin A2
CCNB1	Cyclin B1
CCNB2	Cyclin B2
CCND1	Cyclin D1
CCND2	Cyclin D2
CCND3	Cyclin D3
CCNE1	Cyclin E1
CCNE2	Cyclin E2
Cdc25C	Cell division cycle 25C
CDDP	Cis-dichlorodiammineplatinum (II)
CDK1	Cyclin dependent kinase 1
CDK2	Cyclin dependent kinase 2
CDK4	Cyclin dependent kinase 4
CDK6	Cyclin dependent kinase 6
CDKN1A	Cyclin dependent kinase inhibitor 1A
CDKN1B	Cyclin dependent kinase inhibitor 1B
CDKN1C	Cyclin dependent kinase inhibitor 1C
Chem	Chemotherapy
Cl-	Chloride ion
CO2	Carbon dioxide
CT	Computed tomography
CTGF	Connective tissue growth factor
CTLA-4	Cytotoxic T-lymphocyte-associated protein 4
CTR1	Copper transporter 1
DAPI	4′,6-diamidino-2-phenylindole
DAPP1	Dual adaptor of phosphotyrosine and 3-phosphoinositides 1

DGE	Differential gene expression
DHFR	Dihydrofolate reductase
DISC	Death inducing signaling complex
DMEM	Dubelcco's Modified Eagle Medium
DMSO	Dimethyl sulfoxide
DNA	Deoxyribonucleic acid
DNase	Deoxyribonuclease
DOPEY2	DOP1 leucine zipper like protein B
E2F1	E2F transcription factor 1
E2F2	E2F transcription factor 2
E2F3	E2F transcription factor 3
ECM	Extracellular matrix
EDTA	Ethylenediaminetetraacetic acid
ELF3	E74 like ETS transcription factor 3
EPPK1	Epiplakin 1
ES	Enrichment score
FAs	Focal adhesions
FADH2	Flavin-adenine dinucleotide fully reduced form
FAT3	FAT atypical cadherin 3
FBS	Fetal bovine serum
FDH	Flavin dependent halogenase
FDR	False discovery rate
FGF18	Fibroblast growth factor 18
FL2-A	Filter 2-Area
FL2-W	Filter 2-Width
FLNA	Filamin A
FPGS	Folylpolyglutamate synthase
FSC	Forward scatter channel
g	Gravitational acceleration
GADD45	Growth arrest and DNA damage
GARFT	Glycinamide ribonucleotide formyltransferase
GO	Gene Ontology
GSEA	Gene set enrichment analysis
Gy	Gray
H	Hour
HPLC	High pressure liquid chromatography
IFN-α	Interferon aplha
IL-2	Interleukin-2
ITGA5	Integrin subunit alpha 5
LATS1/2	Large tumor suppressor kinase 1/2
m	Milli
M	Molarity
MBNL1-AS1	MBNL1 antisense RNA 1
MDM2	Murine double minute 2
MDM4	Murine double minute 4

miR-143	MicroRNA 143
miR-145	MicroRNA 145
MM	Malignant mesothelioma
MPM	Malignant pleural mesothelioma
MSRB3	Methionine sulfoxide reductase B3
MYL9	Myosin light chain 9
NaCl	Sodium chloride
NCBI	National center for biotechnology information
NER	Nucleotide excision repair
NES	Normalized enrichment score
NKX2-2	NK2 homeobox 2
NRPS	Non-ribosomal peptide synthetase
O2	Dioxygen
P21	Cyclin dependent kinase inhibitor 1A
P53	Tumor suppressor p53
P/D	Pleurectomy/Decortication
PBS	Phosphate buffered saline
PCP	Peptidyl carrier protein
PCR	Polymerase chain reaction
PD-1	Programmed death 1
PD-L1	Programmed death ligand 1
Pen-Strep	Penicillin and streptomycin
Pgp	P-glycoprotein
PI	Propidium iodide
PPP1R3B	Protein phosphatase 1 regulatory subunit 3B
PRUNE2	Prune homolog 2
PTCHD4	Patched domain containing 4
RB1	RB transcriptional corepressor 1
RFC	Reduced folate carrier
RNA	Ribonucleic acid
RNase	Ribonuclease
ROS	Reactive oxygen species
SARM1	Sterile alpha and TIR motif containing 1
SH3BGRL2	SH3 domain binding glutamate rich protein like 2
siRNA	Small interfering RNA
SLAMF7	SLAM family member 7
SMs	Secondary metabolites
SSC	Side Scatter Channel
STC1	Stanniocalcin 1
SULT1E1	Sulfotransferase family 1E member 1
SV40	Simian virus 40
SYNPO2	Synaptopodin 2
TAGLN	Transgelin
TEM	Transmission electron microscopy
TNFR	Tumor necrosis factor receptor
TPM	Tropomyosin

TRPC4	Transient receptor potential cation channel subfamily C member 4
TrPM	Transcript per kilobase million
TS	Thymidylate synthase
UV	Ultraviolet
WHO	World health organization
YAP	Yes associated protein

LIST OF FIGURES

LIST OF TABLES

TABLE OF CONTENTS

INTRODUCTION

1. Malignant pleural mesothelioma

1.1. GENERALITIES

Malignant mesothelioma (MM) is an aggressive cancer originating from mesothelial cells lining several body cavities (Peake, 2009). It can affect the surface tissues of the pleura, the pericardium and the peritoneum (Ho and al, 2001). The pleura consists in the serosae lining the chest wall (parietal pleura) and surrounding the lung (visceral pleura). The serous membranes covering the heart and the abdomen correspond to the pericardium and the peritoneum respectively (Marieb and Hoehn, 2007). However, the most frequently observed mesothelioma in the worldwide population is the malignant pleural mesothelioma (MPM) (Figure 1). This deadly disease is resistant to various treatment options such as radiotherapy, surgery that have been proven ineffective up to now (Tsao and al, 2009). This indicates that this cancer can only be controlled in order to increase lifetime of patients at this time but not cured (Raja and al, 2011). The malignant pleural mesothelioma is mainly associated with asbestos exposure and the development of the disease appears from 20 to 60 years later, corresponding to the latency period (Jänne and al, 2006; Tsao and al, 2009). In addition, it appears that the MPM occurs preferentially in men than women. Once the patient is diagnosed for this illness, the median overall survival is estimated from 9 to 17 months depending on the stage (Tsao and al, 2009). The incidence of this tumor is increasing in frequency around the world and is expected to reach a peak between 2010 and 2020 in Europe (Boutin and al, 1998). For all those reasons, the implementation of new therapeutic strategies is a priority to enhance the results obtained from current treatments.

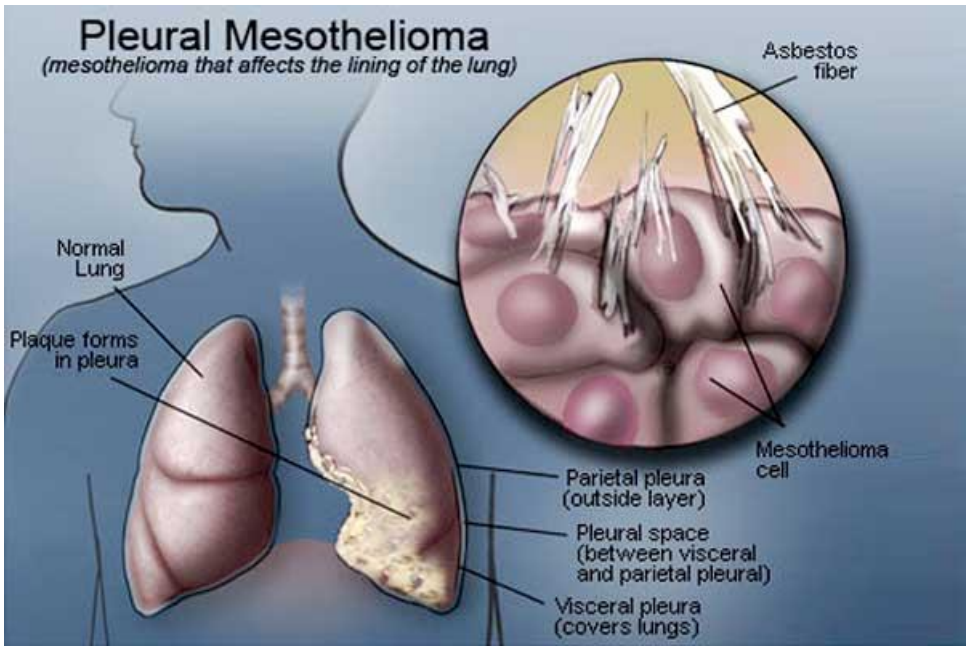

Figure 1. Schematic representation of a healthy lung and a lung affected by MPM
The MPM is an aggressive cancer which develops from mesothelial cells affecting the pleura. This deadly disease is mainly associated with the inhalation of asbestos fibers (CENTRAMIC Pleural Mesothelioma. Symptoms, Causes, Treatment Options. Accessed 30 Jun. 2018).

1.2. INCIDENCE

The occurrence of malignant mesothelioma is taking an ever-greater importance over time in many countries. In fact, it is considered that there are around 43,000 people worldwide dying from this disease each year (Delgermaa and al, 2011; Robinson, 2012). This gradual increase of the disease incidence can be related to the broad use of asbestos from World War II until the half of the last century. Indeed, asbestos was a material commonly exploited in various construction applications such as shipbuilding or insulator for houses (Raja and al, 2011; Boutin and al, 1998). Therefore, the world health organization (WHO, 2007) recognized all asbestos types as carcinogen and drew the attention to asbestos-related diseases (Delgermaa and al, 2011; Robinson, 2012). Following those statements, asbestos was banned from several countries in Europe in the last 1970s and from European Union in 2005 (Røe and Stella, 2015).

The most robust data on the occurrence of malignant mesothelioma have been recorded in UK and in Australia with an annual incidence rate of approximately 30 cases per million (Bianchi and Bianchi, 2007; Robinson, 2012). Belgium is also considered as a country with a high incidence rate since 273 cases were registered in 2011 (Bianchi and Bianchi, 2014). On a global scale, it appears that countries with a high incidence rate are mainly represented by Australia, New Zealand and some countries in Europe (UK, Belgium…). The other countries from Europe as well as the US have intermediate incidence rates and lower ones are attributed to several countries of Asia (Bianchi and Bianchi, 2014) (Figure 2).

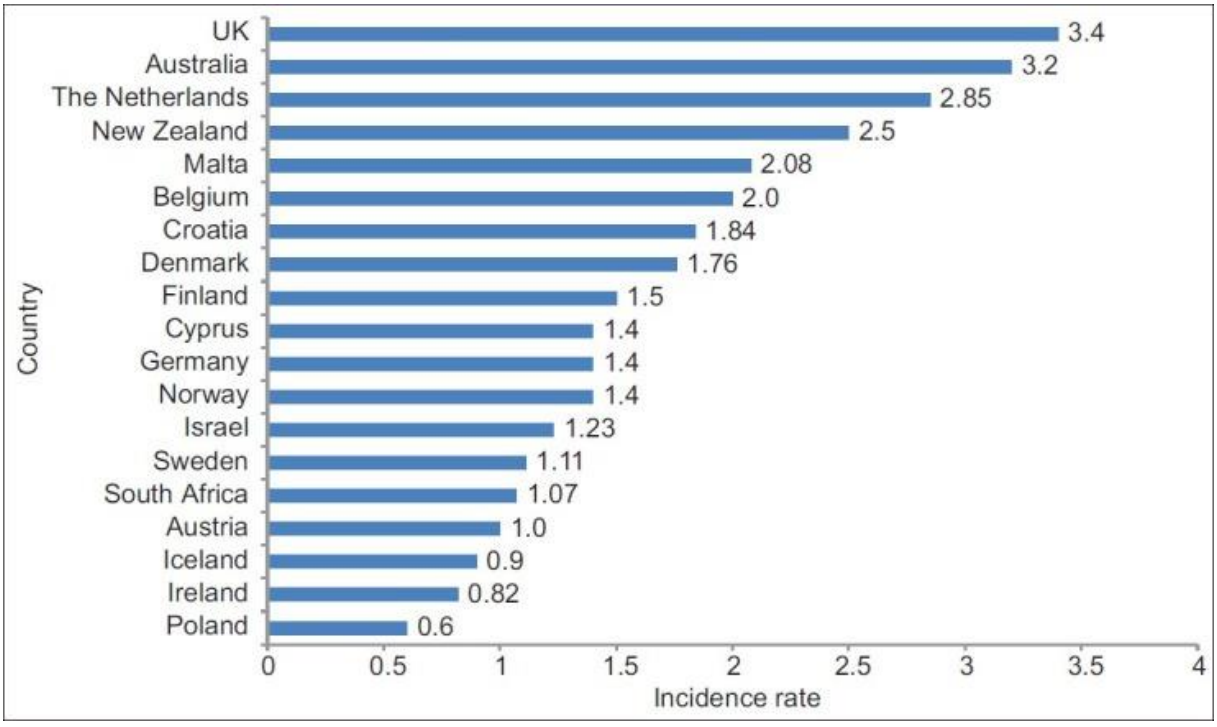

Figure 2. Incidence rate of mesothelioma in 19 countries
Countries with a high incidence rate are represented by Australia and Northern Europe in this figure. This is related to early industrialization involving the use of asbestos in various sectors. However, a significant reduction of incidence rate is expected in a few decades thanks to the banishment of asbestos utilization in different countries (Bianchi and Bianchi, 2014).

Following those data that allow the representation of the global geographical distribution of mesothelioma, a significant difference between developed and developing countries can be highlighted (Røe and Stella, 2015; Bianchi and Bianchi, 2007). Indeed, the low occurrence of mesothelioma in developing countries can be described by two alternative explanations. The first one concerns the diagnostic strategies and the data collection that are still in process (Delgermaa and al, 2011). The other one is related to the fact that the industrialization and then the use of asbestos took place much later in developing countries (Bianchi and Bianchi, 2007).

Concerning the predictions for the future, it appears that countries with high and intermediate incidence rates will reach a peak around 2020 (2015-2020 in Europe, 2014-2021 in Australia) (Yang and al, 2009; Robinson, 2012). Nevertheless, there are some exceptions such as the US and Sweden that have already reached their peaks thanks to restrictive measures applied to asbestos use that have been set up earlier (Robinson, 2012; Bianchi and Bianchi, 2007). The case of Asian countries is totally different given that some of them are still using asbestos and the others have stopped its exploitation but only since around 2000 (Kazan-Allen, 2015; Røe and Stella, 2015; Bianchi and Bianchi, 2007; Stayner and al, 2013). It makes sense to predict that the mesothelioma incidence peak of those countries will occur in the coming decades, such has Japan with a predicted peak between 2030 and 2039 (Delgermaa and al, 2011; Stayner and al, 2013).

1.3. EPIDEMIOLOGY

Since the breakout of MPM in the population, extensive studies have been conducted in order to determine the possible causes of this disease. As a result of those investigations, a strong link has been established between the occurrence of MPM and the exposure to mineral fibers such as asbestos and erionite. However, other factors have also been identified as relevant causative agents (Zandwijk and al, 2013).

1.3.1. Asbestos

The association between the increasing risk of MPM and the exposure to asbestos was introduced for the first time in asbestos miners toward the half of the last century (Raja and al, 2011). Currently, asbestos is classified as an occupational carcinogen by the WHO and its use as a product was banned in a wide range of countries (WHO, 2007).

By definition asbestos is a natural fibrous silicate mineral that is resistant to heat and chemically inert. Depending on the chemical composition and structure, those minerals can be assigned to the serpentine (chrysotile) or amphibole (amosite, actinolite, anthophyllite, crocidolite and tremolite) groups. In fact, serpentine asbestos is characterized by tubular fibers while amphibole asbestos is composed by linear and needle like fibers (Wylie, 2017) (Figure 3).

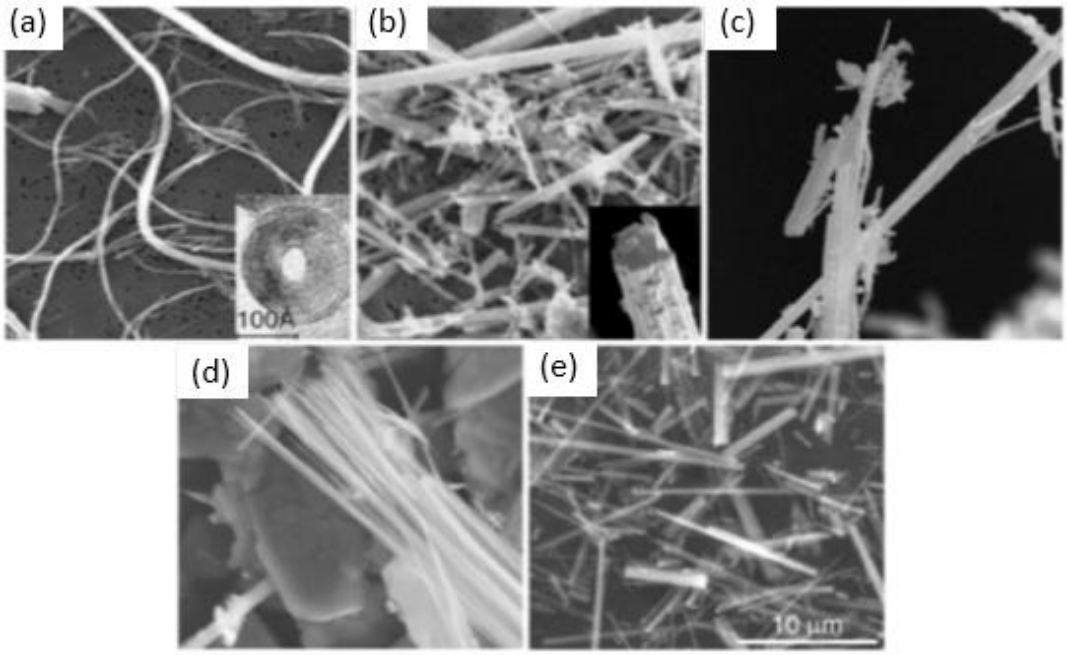

Figure 3. Physical structure of asbestos fibers obtained by transmission electron microscopy (TEM)
The picture (a) represents serpentine asbestos characterized by tubular fibers and pictures from (b) to (e) correspond to amphibole asbestos characterized by linear and needle like fibers. (a) Chrysotile is the only member of serpentine asbestos and (b) Crocidolite, (c) Anthophyllite, (d) Tremolite, (f) Amosite fibers belong to the amphibole group. Those differences between the structures can be explained by their specific chemical composition. In addition, their particular geometry is partly responsible for the distinct effects on health, amosite and crocidolite having the most carcinogenic impact. Scale bar = 10 µm (Sanchez and al, 2010).

Two different forms of exposure to asbestos have been highlighted and depend on the context in which the exposition to those minerals has occurred. The first one is the occupational exposure which takes place in the work environment by the handling of raw asbestos for construction, shipbuilding or pipefitting (Zandwijk and al, 2013; Raja and al, 2011). This work associated with exposure is considered as the principal cause of MPM, explaining the prevalence in males since females are less likely to work in those professional fields. The other one is the non-occupational exposure that can be due to domestic and environmental exposure (Magnani and al, 2000). The transfer of asbestos fibers from workers to cohabitants that occurs usually via contaminated clothes is referred as domestic exposure. However, the environmental exposure is linked to the proximity between the living area and asbestos mines or factories and to the natural presence of asbestos in the soil (Magnani and al, 2000; Zandwijk and al, 2013).

Another important fibrous mineral that has the potential to induce the mesothelioma is the erionite that belongs to the silicate mineral group called zeolite. This mineral is found in geological environment, more precisely in volcanic rocks, and can contaminate the air as fine dust following diverse activities such as digging for road construction and mining (Selçuk and al, 1992; Wylie, 2017). It is also important to notice that some synthetic fibers such as fibrous nanomaterials are sharing some physical and chemical properties with asbestos that are responsible for their carcinogenicity. In fact, considering their

low weight, the exposure to those nanomaterials by inhalation could raise the potential pathogenicity of asbestos (Sanchez and al, 2010).

1.3.2. Health effects of asbestos fibers

Inhaled asbestos fibers passing through the respiratory tract can be responsible for the development of diseases of the lung and the pleura. These include the formation of benign pleural plaques, appearing as lesions on parietal, visceral and diaphragmatic pleura that likely originate from collagen deposition by submesothelial fibroblasts. It is also important to mention two other pathologies associated with asbestos: (i) asbestosis that consists in foci of fibrosis localized in the lower zones of the lungs and (ii) benign pleural effusion characterized by the accumulation of exudate in pleural cavity. However, diseases of concern linked to asbestos exposure are the lung cancer and the malignant pleural mesothelioma as they can lead to human death (Boutin and al, 1998; O'Reilly and al, 2007; Manning and al, 2002; Sanchez and al, 2010).

Various parameters have an impact on the toxicity, pathogenicity and carcinogenicity of asbestos. Among these, the most important are the geometry, the bio-persistence, the chemical composition and the surface reactivity of fibers considering that they have an influence on the production of reactive oxygen species (ROS) (Sanchez and al, 2010). In fact, even if the precise mechanism of injury to the cells is still unknown, the generation of ROS by asbestos fibers should play a significant role through lipid peroxidation and oxidative DNA damage. In addition, interferences with the mitotic spindle and persistent inflammatory response promoting the transformation of mesothelial cells play also an important role in the carcinogenicity of asbestos fibers (Sanchez and al, 2010; Manning and al, 2002; Mossman and Marsh, 1989).

All asbestos fibers do not have the same effect on cells because, as mentioned earlier, it depends on their characteristics. Some studies have demonstrated that the long fibers are not completely engulfed by alveolar macrophages through a mechanism called “frustrated phagocytosis” and then tend to generate more ROS (Figure 4). Besides, the production of ROS is linked to the presence of transition metal at the fiber surface. For this reason, crocidolite and amosite asbestos fibers belonging to the amphibole mineral group are the most carcinogenic. In fact, those fibers generate a higher content of ROS comparatively to others due to their low biodegradability in the lung and their high iron content ranging from 20 to 30% by weight (Sanchez and al, 2010; Mossman and Marsh, 1989; Boyles and al, 2014).

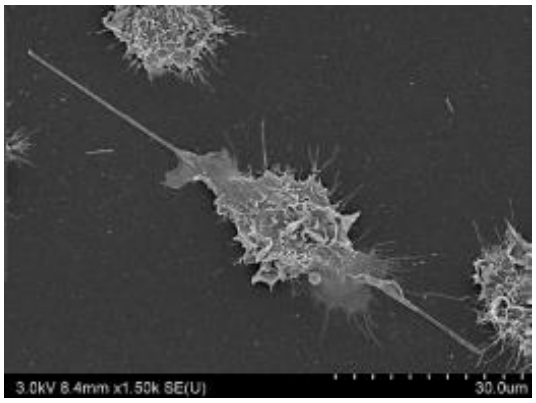

Figure 4. Scanning electron micrograph of monocyte macrophage unable to phagocyte an asbestos fiber measuring over 20µm
As the length of those cells ranges from 10 to 20µm, the complete phagocytosis of a longer or same size fiber is unlikely to occur. This unsuccessful or "frustrated" phagocytosis leads to the overproduction of ROS causing the lipid peroxidation and oxidative DNA damage (Boyles and al, 2014).

1.3.3. Other factors

Some studies suggested that other factors are related to the development of MPM even though they represent a small percentage of cases. These include the simian virus 40, radiation exposure and genetic predisposition (Tsao and al, 2009).

The simian virus 40 (SV40) originates from Africa and has been transmitted to humans through the administration of contaminated polio vaccines produced in monkey kidney cells between 1955 and 1978 (Jasani and al, 2012; Yang and al, 2009). The oncogenic activity of the SV40 is supposed to be mediated principally by the production of two proteins: large T and small t antigens. Those oncogenic proteins act principally by binding and inactivating some proteins involved in tumor suppression. Although several studies have failed to show a correlation between contaminated polio vaccines and occurrence of MPMs, analyses conducted on human MMs have demonstrated the presence of SV40 in tumor cells and its absence in healthy cells (Yang and al, 2009).

The other risk factor is the exposition to radiations that can happen in different contexts: radiotherapy treatment, thorium dioxide administration and atomic energy exposure. There are some reports supporting the relationship between radiation exposure and incidence of MMs but further studies have to be conducted to confirm this putative link (Jasani and al, 2012).

The last suspected etiologic factor is the genetic predisposition. Indeed, it appears that MPM can be inherited following an autosomal dominant pattern. Evidences were provided by Pedigree studies (conducted in the Cappadocian villages of Tuzkoy) showing that MM occurs predominantly in certain families and not in others even if they were exposed to similar amount of erionite. Besides, the progeny resulting from the union between a genetically predisposed family and a family with no history of the

disease is susceptible to develop MM. However, members of high risk MM families who were born and have grown up in regions free of MM have not shown clinical signs of the disease. All these evidences seem to indicate an interaction between the incidence of MM and the genetic predisposition (Dogan and al, 2006; Yang and al, 2009).

1.4. HISTOLOGY

From a histological point of view, the MPM can be classified in three different subtypes, namely the epithelioid, sarcomatoid and biphasic (Kanbay and al, 2014) (Figure 5). Epithelioid MPM predominates, representing approximately 60% of all cases and is characterized by polygonal, oval, cuboidal cells or a mix of them forming the tumor. The sarcomatoid MPM is formed by spindle-shaped cells that can be organized in bundles or randomly oriented and accounts for about 10-20% of mesotheliomas. In addition, the sarcomatoid subtype is the most aggressive and virulent. The last histologic form is the biphasic MPM which is composed of both epithelioid and sarcomatoid cells within the same tumor and represents around 20-30% of all cases (Husain and al, 2013; Zandwijk, 2013; Institut national de la santé et de la recherche medicale, 2008).

The recognition of the MPM subtypes is important to establish the differential diagnosis of patients. However, the variability between mesothelioma cells makes it histopathological diagnosis challenging (Kanbay and al, 2014; Institut national de la santé et de la recherche medicale, 2008). Nevertheless, some technologies such as electron microscopy and immunohistochemistry have been used to distinguish the different patterns of MPM even if they have limited sensitivity and specificity (Kindler, 2000; Philippeaux and al, 2004). Techniques distinguishing MPM subtypes should be improved in order to facilitate the diagnosis of the disease.

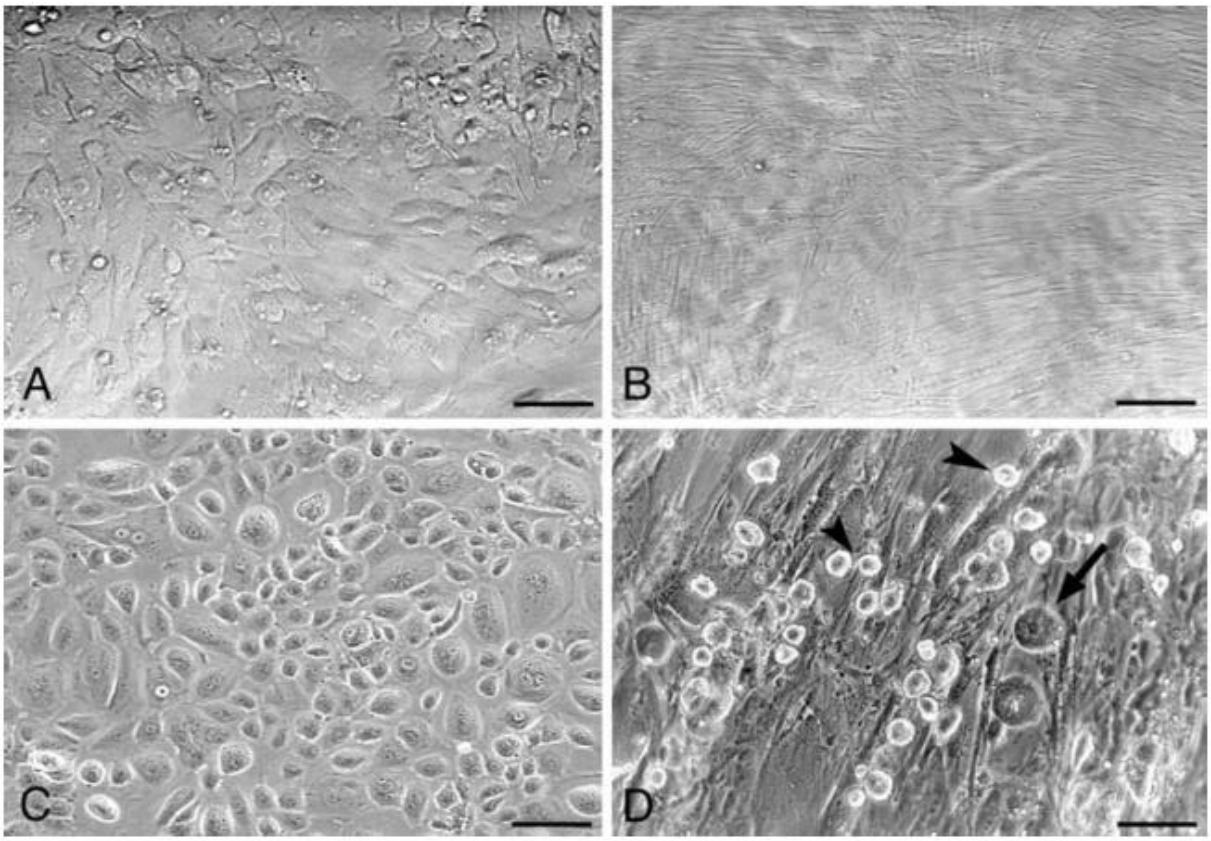

Figure 5. Different subtypes of MM cells obtained by phase-contrast micrographs
(A) Epithelioid subtype characterized by polygonal, oval, cuboidal cells or a mix of them forming the tumor, (B) Sarcomatoid subtype characterized by spindle-shaped cells, (C) Normal mesothelial cells and (D) Biphasic subtype composed of both epithelioid (long arrow) and sarcomatoid cells. (A), (B) and (D) were obtained from untreated MM patients and (C) was derived from patients with benign inflammation. Scale bar = 20 µm (Philippeaux and al, 2004).

1.5. CLINICAL SIGNS

Clinical manifestations of MPM depend on the stage of the illness and are nonspecific explaining the difficulty in establishing a link between the symptoms and the disease. This can be responsible for the late diagnosis in most cases (O'Reilly and al, 2007; Boutin and al, 1998). However, the dyspnea and the chest pain are considered to be the two most frequent presenting symptoms (OncoLogiK Mésothéliome Pleural. Accessed 27 Feb. 2018). The dyspnea corresponds to a dysfunction of the respiratory system mainly due to a pleural effusion while chest pain is caused by an invasion into the chest wall (Ho and al, 2001; Raja and al, 2011). In addition, other symptoms can be developed by the patient such as cough, weight loss and fatigue (O'Reilly and al, 2007). It is also important to highlight that in more advanced stages of the disease some complications can occur leading to superior vena cava syndrome and dysphagia, demonstrating the progressive worsening of the symptoms (Ho and al, 2001; O'Reilly and al, 2007).

1.6. DIAGNOSIS

Due to the similarity between MPM and other diseases, the establishment of a precise diagnosis is complicated and is performed in most cases in the fifth to seventh decades of patient's life (Ho and al, 2001; Zandwijk and al, 2013). Nowadays, various medical technologies have been developed and used in order to diagnose MPM as soon as possible (Ho and al, 2001).

The first steps in diagnosis consist in clinical and radiological analyses that can show a pleural effusion or a diffuse pleural thickening (Zandwijk and al, 2013; Raja and al, 2011; Boutin and al, 1998). Indeed, the thoracoscopy-guided biopsy and the computed tomography (CT) scanning (Kim and al, 2016) are the most widely used modalities for the assessment of MPM and have a diagnostic sensitivity of approximately 90% (Figure 6) (Zandwijk and al, 2013).

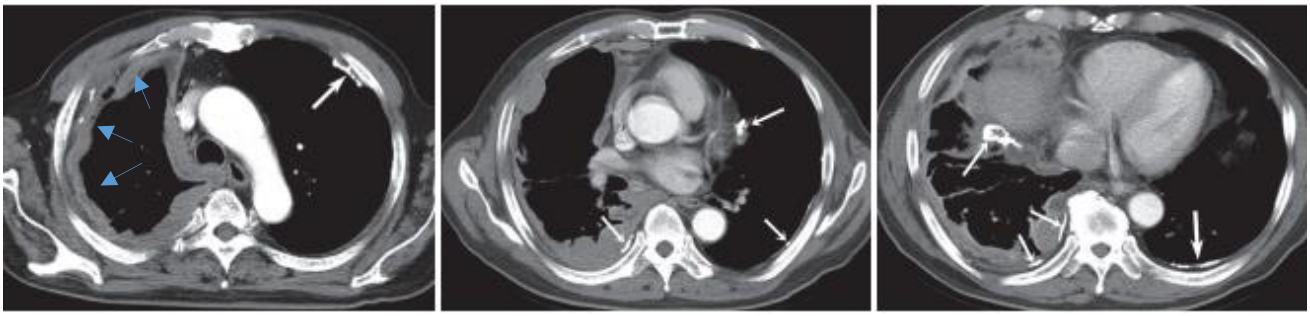

Figure 6. Transverse chest CT images of a 71-year-old man suffering from MPM
The computed tomography (CT) scanning is considered as the first line imaging modality for the diagnosis of MPM. This analysis can detect pleural thickening, calcified pleural plaques, fissural pleural thickening and pleural effusion. The diagnostic yield of this technic reaches around 90% and presents low complication rates, explaining the importance of CT in the assessment of MPM (Kim and al, 2016). The CT shows a circumferential pleural thickening in the hemithorax scan (blue arrows) and calcified pleural plaques (white arrows).

In addition, other examinations can be conducted to confirm and provide a more accurate diagnosis (Zandwijk and al, 2013). Among those, the cytological analysis performed in pleural effusion is the most important and can reveal the presence of carcinoma cells (Husain and al, 2013). Immunohistochemical analyses performed on a thoracoscopic biopsy and combined with electron microscopy provide a definitive diagnosis (Hazarika and al, 2005). Regarding the immunohistochemical tests, some biomarkers such as cytokeratins or calretinins are used to recognize particular molecules expressed by mesothelioma cells (Philippeaux and al, 2004; Husain and al, 2013). As this technique takes an ever-greater importance in the establishment of the diagnosis, some new markers have been developed. Indeed, the mesothelin and osteopontin are two new serum markers that could ameliorate diagnosis of MPM (Tsao and al, 2009).

The identification of the disease stage is also very important to provide the optimal treatment to patients. In fact, MPM is divided into a four-stage system (I, II, III and IV) (Zandwijk and al, 2013), each

characterized by different types of symptoms (Boutin and al, 1998) and by the tumor spread and location (Ho and al, 2001).

1.7. TREATMENTS

Generally, the recommended treatments for patients suffering from MPM consists in surgery, radiotherapy or chemotherapy. The latter can be prescribed in combination (Ceresoli and al, 2007) or separately (Zandwijk and al, 2013). The choice of the treatment advised to each patient will vary according to patient's age, performance status and disease stage (Raja and al, 2011). Nevertheless, it is important to highlight that those treatments are used for palliative purposes since they only moderately increase patient's lifetime (Zandwijk and al, 2013; Ho and al, 2001).

Other treatments are also emerging in the medical field but are still in progress: targeted therapies (Zandwijk and al, 2013), gene therapy (Boutin and al, 1998) and immunotherapy (Tano and al, 2017).

Surgery is considered as the most effective treatment and its purpose is to decrease the size and spread of the tumor by using different techniques such as thoracoscopy, pleurectomy/decortication (P/D) and extrapleural pneumonectomy (Ismail-Khan and al, 2006). The first one consists in the achievement of a pleurodesis that allows the adherence of the visceral pleura to parietal pleura through the injection of a sclerosant in the pleural space (Zandwijk and al, 2013; Ho and al, 2001). The P/D is a surgery performed by an open thoracotomy that aims the ablation of the parietal pleura, comprising the portion over the mediastinum, pericardium, and diaphragm (Tsao and al, 2009; Ismail-Khan and al, 2006). The third one is the most aggressive and intensive surgical procedure that is proceeded by resecting the pleura, as well as the involved lung, pericardium, diaphragm and regional lymph nodes in order to take out macroscopic tumor from the chest (Zandwijk and al, 2013; Ismail-Khan and al, 2006). However, the microscopic residues of the tumor cannot be removed making the total resection of the tumor impossible (Tsao and al, 2009; Ruth and al, 2003). That is why those remaining residues are treated with adjuvant therapies which consist in most cases in radiotherapy and/or chemotherapy (Sugarbaker and Wolf, 2010; Kaufman and Flores, 2011).

Radiotherapy is principally used for patients having already undergone surgical interventions or chemotherapies (Rosenzweiga and Giraud, 2017; Waite and Gilligan, 2007). Indeed, considering that MPM is a diffuse disease that can reach various adjacent organs, it makes difficult to apply radiations on the entire tumor (Ramalingam and Belani, 2008; Ismail-Khan and al, 2006). Moreover, the radiation dose delivered depends on the vital structures because each organ has its specific sensitivity to radiations leading to different limiting doses (e.g. 20 Gy in lung and 30 Gy in liver) (Ismail-Khan and al, 2006). Then, it greatly complicates the treatment of the whole neoplasm at tumoricidal dose without damaging underlying organs (Perrot and al, 2017; Zandwijk and al, 2013). For all those reasons, radiotherapy is

not applied as primary therapy but is widely used in multimodal treatments and in palliative intents (Ramalingam and Belani, 2008; Raja and al, 2011).

Concerning chemotherapy, it is mainly used for patient with an advanced stage of the disease in order to temper symptoms and to modestly improve survival of patients. Indeed, it is assumed that 80% of the patients are not suitable for surgery because of the extent of the tumor making it unresectable or due to their old age or the presence of comorbidities (Cinausero and al, 2018). Initially, chemotherapy consisted in the administration of a single agent presenting anticancer activity (Ramalingam and Belani, 2008). The first family of drugs investigated in the treatment of MPM was the anthracycline. However, they did not show a response rate higher than 15% with a maximal median survival of 8 months (Tomek and al, 2003). Therefore, the focus was placed on new chemotherapeutic agents such as platinum compounds (cisplatin and carboplatin), alkylating agents, antimetabolites (pemetrexed and raltitrexed) … (Cinausero and al, 2018; Tomek and al, 2003) But again, the response was not satisfactory following the administration of those drugs separately (Tsao and al, 2009). In addition, Ellis and al have demonstrated on the basis of 111 relevant phase II trials that combination chemotherapy provides higher response rates than single agents (Ellis and al, 2006). Among those combinations, the administration of cisplatin along with pemetrexed in a phase II trial yielded the best results with a prolongation of the median survival of 3 months compared to cisplatin alone (12.1 vs. 9.3 months) and a response rate of 41%. It is also important to highlight that a supplementation of folic acid plus vitamin B12 during CT treatment decreases the toxicity and increases the number of administrated cycles (Cinausero and al, 2018). Therefore, the combination of cisplatin plus pemetrexed is considered as the standard first line treatment for patients with unresectable MPM (Nowak, 2012). In the event of a relapse or progression of the disease after the first line treatment, a second line chemotherapy could be considered (Nowak, 2012). However, improvements and further investigations have to be performed to select agents with the best results for the second line therapy (Cinausero and al, 2018).

The immunotherapy relies on the modulation of the patient's immune system in order to direct it against its own cancerous cells (Dozier and al, 2017). This approach takes an ever-greater importance because of the limited efficiency of other treatments and the proof of tumor response to immune system stimulation (Grégoire, 2010). The use of cytokines including interferons and interleukins as well as antibodies has already been investigated to this end. Among the cytokines, the IL-2 (interleukin) and IFN-α (interferon) have already shown cytotoxic activity against mesothelioma cells following their administration to patients through the activation of natural killer cells and cytotoxic T-lymphocytes. However, the use of those compounds is limited by the appearance of symptoms (fever, vascular leak and shock) due to the immune activation (Alley and al, 2017). Concerning the antibodies, they can be used for different purposes. Currently, the main application of those antibodies is to block the checkpoints (PD-1, PD-L1 and CTLA-4) involved in the inhibition of immune cells preventing autoimmunity. The use of checkpoint inhibitors hinders the anergy of T-cells in presence of MPM cells (Tano and al, 2017; Alsaab and al, 2017). It is also important to notice that other immunotherapy methods are also evaluated in clinical studies such as anticancer vaccines, adoptive cell therapy and

dendritic cells-based therapy (Dozier and al, 2017; Grégoire, 2010). As recent studies have shown the efficacy of immunotherapy, this approach can be considered as promising for the treatment of MPM but studies still need to be conducted to improve this new treatment (Alley and al, 2017; Tano and al, 2017).

The multimodal therapy was elaborated following the failure of single treatment to increase lifetime of patients suffering from MPM (Ceresoli and al, 2007). The use of treatment combinations aims to limit the occurrence of local, and distant metastasis later or to reduce the tumor as much as possible (Ramalingam and Belani, 2008). This multidisciplinary approach has already shown promising results in clinical trials, particularly for the combination surgery plus chemotherapy plus radiotherapy (Ceresoli and al, 2007; Sterman and Albelda, 2005). Another new combination that should be considered in the future is the immunotherapy plus radiotherapy since they have synergistic effects by inducing an upregulation of lymphocyte-T activity (Alley and al, 2017). Nevertheless, multimodality treatment may be aggressive explaining that an optimal program has to be established for each patient (Su, 2009).

2. Chemotherapy treatment

2.1. GENERALITIES

The term “chemotherapy” was invented in the beginning of the 1900s and was defined as the use of drugs to treat a disease by a German scientist Paul Ehrlich (DeVita and Chu, 2008). The first clinical studies performed on humans to show the efficiency of chemotherapy against cancers started in the mid of the 20th century with folic acid antagonists and nitrogen mustards as chemotherapeutic agents (Galmarini and al, 2012). From this period until now, chemotherapy has evolved considerably with the development of new drugs and a deeper comprehension of their mechanisms of action (DeVita and Chu, 2008; Espinosa and al, 2003).

Chemotherapeutic agents act mainly through the interaction with intracellular molecules (DNA, growth-signaling molecule) leading to some injuries and/or dysfunctions (Luqmani, 2005; Hannun, 1997; Xu and Mao, 2016). Following those perturbations, a signal will be sent to assess the importance of the damages in the tumor cell. Depending on the severity and the extent of the lesion, the tumor cell response will be different. It can result in apoptosis or cell cycle arrest (Hannun, 1997; Johnstone and al, 2002; Xu and Mao, 2016). The purpose of the chemotherapy is to stop tumor cell proliferation and finally to induce their apoptosis (Figure 7) (Johnstone and al, 2002; Xu and Mao, 2016).

One of the major problems linked to this therapy is the cytotoxicity of the drugs on normal cells due to their wide spectrum of activity. Even if some chemotherapeutic agents succeed to target selectively cells with abnormal proliferation, side effects can occur because their activity is not exclusive to tumor cells. In addition to that, tumor cells can show intrinsic resistance (linked to genetic characteristics) or resistance acquired following the exposition to the drugs (Johnstone and al, 2002; Luqmani, 2005).

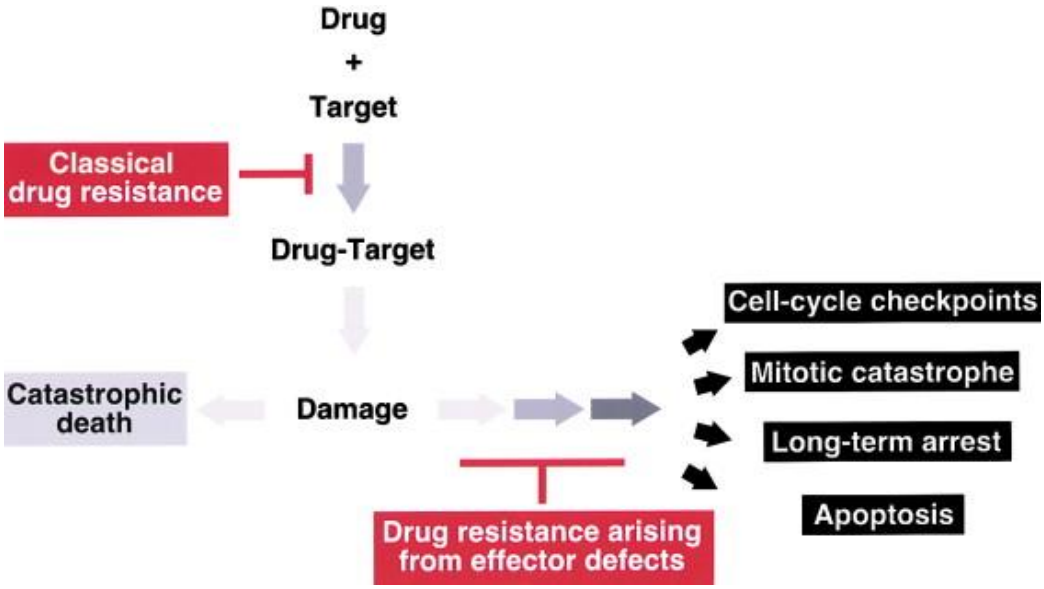

Figure 7. General mechanism of action of chemotherapeutic agents
The administration of drugs to patient suffering from cancers results in interaction between the drugs and their specific intracellular targets. Following those reactions, some damages are generated into tumor cells. Depending on the severity of the lesion, different cell-signaling pathways can be activated leading principally to cell apoptosis or cell cycle arrest. However, tumor cells can show some resistance to those drugs and then can continue their proliferation (Johnstone and al, 2002).

2.2. CHEMOTHERAPEUTIC AGENTS

The drugs used in chemotherapy treatment can be synthetized from building block molecules or extracted from plants. Those natural and synthetic agents are classified on the basis of their mechanism of action on tumor cells. The most important classes are the alkylating agents (nitrogen mustards, aziridines), heavy metals (carboplatin, cisplatin and oxaliplatin), antimetabolites (folic acid antagonist, pyrimidine and purine antagonists), cytotoxic antibiotics (anthracyclines), spindle poisons (vinca alkaloids and toxoids) and topoisomerase inhibitors (I and II) (Luqmani, 2005; Payne and Miles, 2008).

However, as new anticancer drugs with various modes of action appear in chemotherapy, they are not assigned to a particular class but are regrouped together without a specific denomination. For this reason, a new system of classification has been developed based on the kind of target. It can concern DNA, RNA or proteins in the tumor cells or in other structures interacting with the latter (Espinosa and al, 2003).

Because of the high number of chemotherapeutic agents, only the cisplatin and pemetrexed will be described, as there are considered as the standard first line treatment for patients with MPM (Nowak, 2012).

2.2.1. Cisplatin

Cisplatin is a chemotherapeutic agent widely used around the world in the treatment of various cancers (ovary, testicular, neck, lung, bone, muscle), also known as cisplatinum or cis-dichlorodiammineplatinum (II) (CDDP). Its chemical structure consists in a platinum atom in the II oxidation state bound to two inert ammoniac atoms and two labile chloride atoms forming a square planar geometry. The molecular formula established for cisplatin is the following: cis-[Pt(II)(NH(3))(2)Cl(2)] (Florea and Büsselberg, 2011; Dasari and Tchounwou, 2015).

Concerning the mechanism of action of cisplatin, several studies were performed in order to understand its operating principle. It was shown that after the drug administration, cisplatin remains stable and in its neutral state until it circulates in the blood stream. Indeed, the hydrolysis of the drug is hindered thanks to the high concentration of chloride ions present in the blood. Then, the cisplatin can enter into the cell by passive diffusion or by active transport using transmembrane proteins. Once inside the cytoplasm, the low concentration of chloride ions induces the hydrolysis of cisplatin. This process consists in the substitution of chlorides by water molecules resulting in the formation of a highly reactive complex. Owing to its positive charges, the complex will react with cellular nucleophiles such as DNA. This interaction between hydrolyzed cisplatin and DNA occurs through the linkage to the nitrogen located at the seventh position on purine residues. The establishment of those bonds, also called crosslinks, can give rise to different DNA adducts: monoadducts, intra-strand crosslinks and inter-strand crosslinks. Following those crosslinks, the conformation of the double helix is modified and can prevent the DNA replication and transcription inducing apoptotic cell death if DNA adducts are not repaired (Figure 8) (Florea and Büsselberg, 2011; Dasari and Tchounwou, 2015; Browning and al, 2017; Rabik and Dolan, 2007).

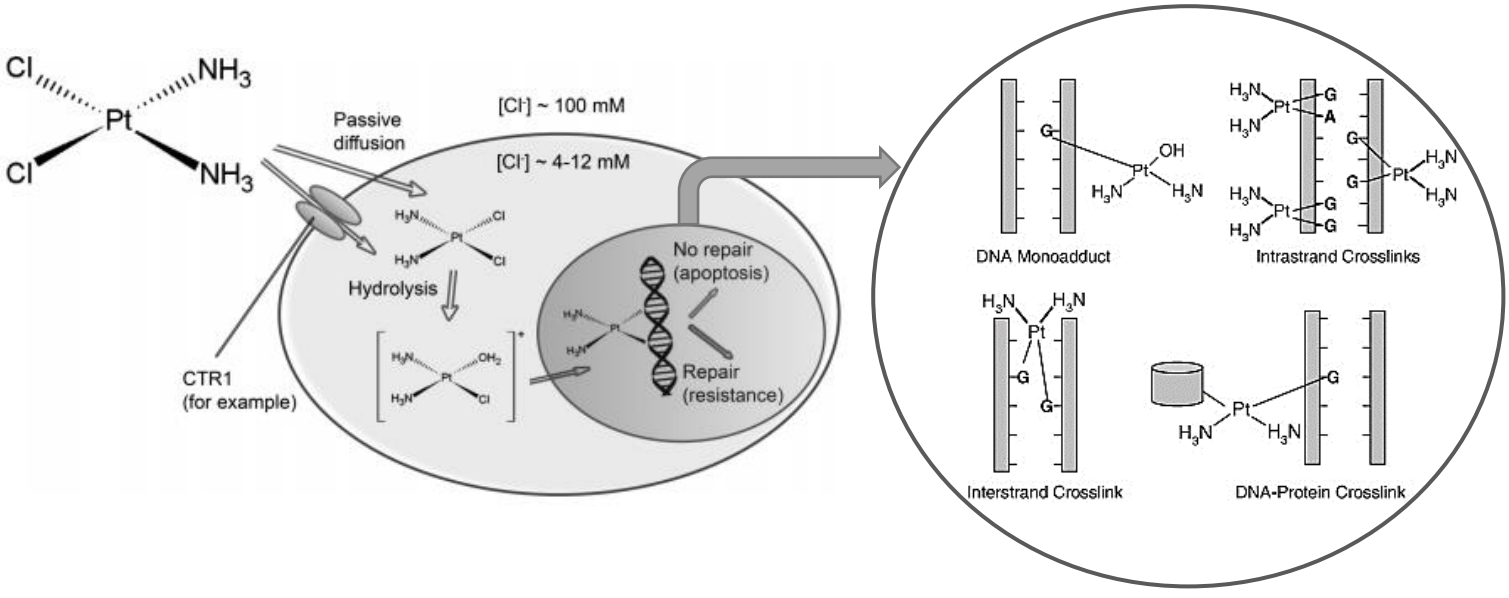

Figure 8. Structure and operating principle of cisplatin
Cisplatin is a platinum compound composed of two chloride atoms and two ammoniac groups that is administrated by intravenous injection to cancerous patient. In the bloodstream, cisplatin remains stable thanks to the high chloride concentration (100mM). However, this drug can leave the blood circulation to enter into tumor cells by active or passive diffusion. Once inside, cisplatin will undergo a hydrolysis due to the low concentration of chloride ions (4-12mM). This process results in the formation of a very reactive positively charged compound that can interact with purine bases of DNA. As the hydrolysis can displace one or both chlorides, each cisplatin can bind DNA in one (monoadduct) or two (crosslink) positions. The crosslinks can be established on the same strand or on opposite strands of the DNA and to a lesser extent between a protein and DNA strand (Browning and al, 2017; Rabik and Dolan, 2007).

However, the DNA damage is not the only mode of action used by cisplatin in order to induce cell apoptosis. In fact, new evidences demonstrated that cisplatin triggers cell apoptosis principally through intrinsic mitochondrial pathway and extrinsic death receptor pathway. In the intrinsic pathway, the hydrolyzed cisplatin can react with mitochondrial glutathione and other antioxidants including a thiol group in their structure. As a result, those compounds with sulfhydryl groups are inactivated leading to the disruption of the cellular redox status and subsequently to cellular oxidative stress. This oxidative stress generated by the accumulation of ROS is responsible for lipid peroxidation, calcium uptake inhibition and DNA damages that can result in apoptotic pathway activation (Dasari and Tchounwou, 2015; Pabla and Dong, 2008). Concerning the extrinsic pathway, its initiation is induced by the binding of ligands to tumor necrosis factor receptor (TNFR). The administration of cisplatin can promote this pathway by the upregulation of ligands (Pabla and Dong, 2008), by increasing expression of surface receptors and by the relocalization of the receptors in the plasma membrane (Blanáthoma and al, 2011). Once the connection between the ligand and the receptor is established, it stimulates the activity of caspases leading to apoptosis (Florea and Büsselberg, 2011; Blanáthoma and al, 2011).

At this time, cisplatin is considered as one of the most effective chemotherapeutic agents (Rabik and Dolan, 2007). Although, the administration of this drug to cancer patients is limited by the severe side effects. Indeed, cisplatin shows also a systemic toxicity to normal cells leading mainly to nephrotoxicity, neurotoxicity, ototoxicity and cardiotoxicity (Mendus, 2010; Dasari and Tchounwou, 2015). To address this problem, platinum analogues (carboplatin, oxaliplatin, nedaplatin) are synthetized because of the lesser toxicity and the potential oral delivery of those drugs (Pabla and Dong, 2008; Florea and Büsselberg, 2011). More recently, a focus of interest was placed on the development of particular systems of drug delivery that would trap the drugs and transport them until tumor cells where they will be released (Browning and al, 2017).

2.2.2. Pemetrexed

Pemetrexed is a drug that belongs to the antimetabolite group and more precisely to the antifolates. This compound works by blocking folate-dependent metabolic processes that are essential for cell replication (Hanauske and al, 2001; Cinausero and al, 2018). Indeed, the pemetrexed enters into the cell mainly thanks to folate transporters. Once inside, the folylpolyglutamate synthase converts it into its more active form, namely the polyglutamated pemetrexed. Those specific forms of pemetrexed will inhibit folate-dependent enzymes involved in the biosynthesis of purine and thymidylate nucleotides: the thymidylate synthase, the glycinamide ribonucleotide formyltransferase, the dihydrofolate reductase and the aminoimidazole carboxamide ribonucleotide formyltransferase (Figure 9) (Powell and Dudek, 2009; Hazarika and al, 2005).

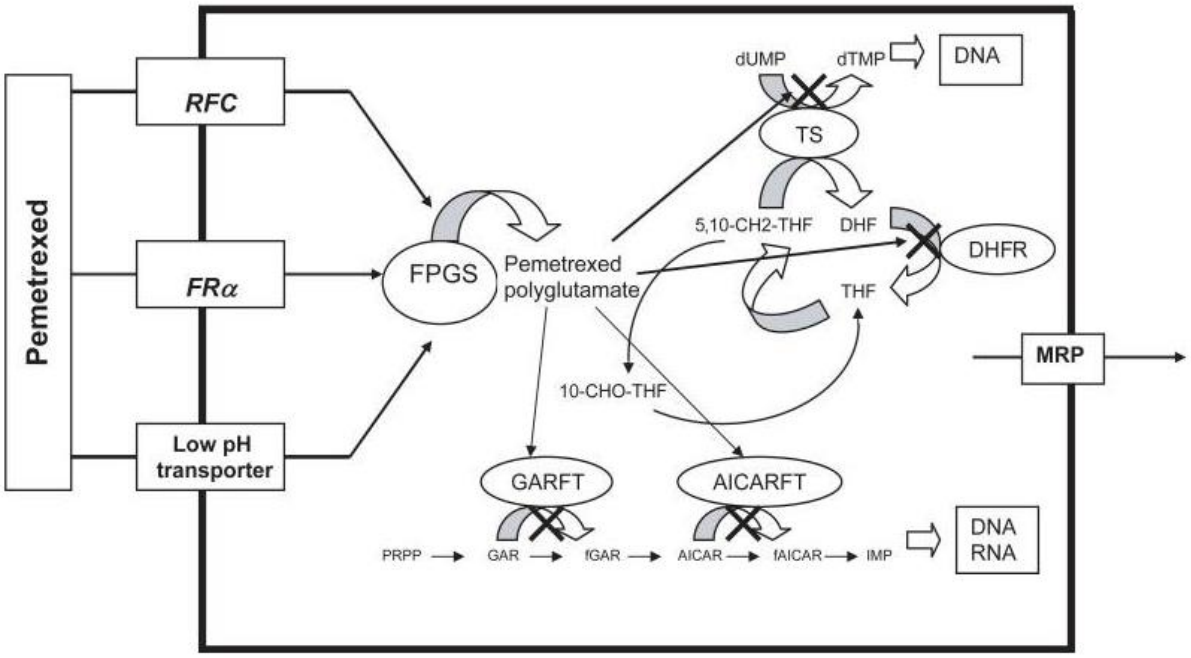

Figure 9. Effect of pemetrexed on folate metabolic processes
Pemetrexed can enter into the cell by different ways but it occurs mainly through folate transporters (RFC). Within the cell, the pemetrexed is polyglutamated by the folylpolyglutamate synthase (FPGS) which results in a much more reactive compound. In this polyglutamated form, the pemetrexed has a higher affinity for folate-dependent enzymes and the interaction between those compounds will lead to the inhibition of the latter. Inhibited enzymes include the thymidylate synthase (TS), the glycinamide ribonucleotide formyltransferase (GARFT), the dihydrofolate reductase (DHFR) and the aminoimidazole caroxamide ribonucleotide formyltransferase (AICARFT) playing a role in the biosynthesis of purine and thymidylate nucleotides (Powell and Dudek, 2009).

Concerning the side effects generated by the intake of this drug, myelosuppression, rash, fatigue, and gastrointestinal toxicity are the most common. Other adverse reactions can be observed such as thrombocytopenia, anemia and fever. However, pemetrexed is considered as a compound with reduced toxicity against normal cells compared to other drugs used as chemotherapeutic agents (Powell and Dudek, 2009).

2.3. MECHANISMS OF DRUG RESISTANCE

Drug resistance refers to the non-responsiveness of tumor cells following the administration of anticancer agents. The resistance can be considered as “acquired”, where the drugs loss gradually their efficiency over time and “intrinsic”, where the drugs never showed any efficiency since the beginning of the treatment (Florea and Büsselberg, 2011; Housman and al, 2014). Currently, this phenomenon represents a serious complication in chemotherapy treatment of mesothelioma tumors and is taking an ever-greater importance (Mujoomdar and al, 2010).

Various mechanisms are involved in drug resistance and act independently of one another or in combination. Among those, the drug inactivation, drug target alteration, drug efflux and influx, DNA damage repair and epigenetic can be mentioned as there are implicated in cisplatin resistance (Florea and Büsselberg, 2011; Housman and al, 2014).

The main mechanism of cisplatin resistance concerns the regulation of drug influx and efflux. This process depends on the expression of cellular membrane transporters. Indeed, the copper transporter 1 (CTR1) is responsible for the uptake of platinum compounds in the cell. Hence, the underexpression of CTR1 decreases the intracellular accumulation of cisplatin. On the contrary, the upregulation of ATP-binding cassette transporter, which acts by pumping out various anticancer drugs, leads directly to the ejection of cisplatin out of the cell (Shen and al, 2012; Housman and al, 2014). Another important mechanism that can be highlighted is the DNA damage repair. In fact, some cancer cells have the ability to remove the cisplatin adducts thanks to the nucleotide excision repair (NER) process (Kartalou and Essigmann, 2001). Briefly, the NER operating principle is based on the recognition of the distortion in the double helix caused by cisplatin crosslinks. Then, the NER opens up the damaged zone and removes it from the DNA. Once performed, the DNA polymerase and ligase can initiate and complete the repair synthesis (Schärer, 2013). Finally, epigenetic mechanisms that are responsible for histone modifications and DNA methylations also play a considerable role in drug resistance. For example, the hypermethylation of a particular promoter gene can result in the loss of DNA mismatch repair processes. In fact, once the hypermethylation is conducted, the gene is not expressed anymore resulting in cell tolerance to cisplatin adducts (Kartalou and Essigmann, 2001).

2.4. STRATEGIES TO COUNTERACT DRUG RESISTANCE

Since the emergence of drug resistances, different strategies have been developed in order to overcome them. The main strategies consist in: the administration of cytotoxic drugs in parallel with pharmaceutical inhibitors subverting mechanisms of drug resistance, the identification and inhibition of genes involved in resistance, the improvement in drug delivery systems (Browning and al, 2017) and the administration of novel drug combinations (Luqmani, 2005).

Specific pharmaceutical agents are used to block cellular mechanisms involved in drug resistance. Indeed, some new inhibitory compounds such as NSC23925, PSC833 and VX710 have already proven their efficiency in the treatment of multiple cancer types. Those molecules act by inhibiting the expression of the P-glycoprotein (Pgp) which is a drug efflux pump, taking out of the cell various chemotherapeutic drugs (Wang and al, 2017).

The comparison of genetic material between drug sensitive and drug resistant cells allows the identification of genes potentially responsible for drug inefficacy (Luqmani, 2005). The inhibition of genes overexpressed in drug resistant cells after chemotherapeutic treatment can overcome this problem. In fact, it has been demonstrated than Bcl-2 expression is up regulated in the presence of some cytotoxic drugs. As Bcl-2 is a protein that represses the apoptosis, the drugs that involve cell death by this pathway are ineffective (Sartorius and Krammer, 2002). Thus, thanks to siRNA transfection, Bcl-2 gene is inhibited allowing the chemotherapeutic agents to recover their potency (Zhao and al, 2009).

Recently, a new approach aimed to deliver the drugs directly in the tumor area is making progress. For this purpose, different systems such as liposomes, micelles, polymers, and inorganic nanoparticles have been developed. The principle is based on the trapping of cytotoxic drugs in one of those specific systems and to transport them until their reach the target zone where they will be released. This emerging technique should decrease concomitantly the drug resistance and the cytotoxicity on normal cells. However, this strategy is not yet operational and requires further studies (Browning and al, 2017).

Finally, the combination of different cytotoxic agents can prevent or avoid mechanisms of drug resistance. In general, the association of drugs is based on their overlapping toxicity, mode and site of action, patterns of cross resistance and effect on tumor cells when used individually (Luqmani, 2005; Yardley, 2013).

3. Astins

3.1. GENERALITIES

Astins are natural compounds that show promising antitumor activities. They were isolated for the first time in 1993 by Morita and al from the biologically active extract of roots of the plant named *Aster tataricus* (Schumacher and al, 1998; Morita and al, 1993). In fact, those plants were used in traditional Chinese medicine in the form of herbal tea for their diverse beneficial effects on health. Nevertheless, the root extract process has resulted in low concentration of astins, namely a few milligrams from 10kg of dried roots (Jahn, 2015). Following the determination of the biomolecule structures, there were assigned to the cyclopentapeptide family and currently, there are 15 different forms of astins that have been discovered, ranging from A to I and K to P (Xu and al, 2013). Only three of them have shown an anticancer activity (A, B and C), this property being attributed to their particular chemical structure (Morita and al, 1996). Recently, it was demonstrated that astins were not produced by the plant itself but by an endophyte fungus denominated *Cyanodermella asteris*. This fungus has a mutual relationship and lives in the tissues of *Aster tataricus* (Jahn and al, 2017; Jahn and al, 2017). Therefore, further studies have to be conducted to precisely determine the impact, side effects and mechanisms of action of the antitumor astins against cancer cells.

3.2. CHEMICAL STRUCTURE

The chemical structure of astins were resolved principally through chemical conversion and nuclear magnetic resonance analysis conducted on isolated and purified molecules (Morita and al, 1995). Those natural compounds present a 16-membered ring system containing two proteinogenic (proline and serine) and three non-proteinogenic (ß-amino phenylalanine, α-aminobutyric acid and allothreonine) amino acids. Besides, all the peptides are present in trans position with the exception of the α-aminobutyric acid or *allo*threonine which is bound in cis conformation to the proline (Jahn, 2015).

The various form of astins have a highly similar structure as all of them present both proteinogenic amino acids and the non-proteinogenic ß -phenylalanine. They differ from each other according to the hydroxylation at the β-carbon atom and the chlorination on the proline residue. Indeed, allothreonine or α-aminobutyric acid can be observed in astin structure in function of the hydroxylation at the β-carbon atom. Concerning the chlorination, it can take place on β, γ or δ carbon atom resulting in mono or dichlorination. Only the astins A, B, C and K present a dichlorination on β and γ carbons. All the others are monochlorinated except the astin G that does not show any chlorination at the proline residue. In addition to those distinctions, the chemical bond established between the γ and δ carbon of the proline residue can be simple or double (Figure10) (Jahn, 2015; Théatre, 2017).

At this time, sixteen different forms of astin were discovered and described, ranging from A to I and K to P. Among these, there are two exceptions that differentiate themselves from other astins according to a structural point of view. In fact, the astin O is characterized by an acetyl group attached at the β carbon atom of serine residue and the astin P has a α-aminovaleric acid that replaces the allothreonine (Figure10) (Xu and al, 2013).

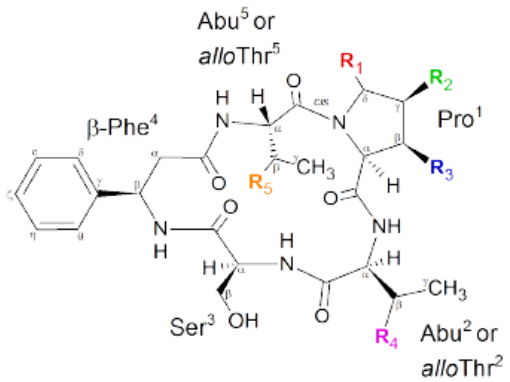

astin	R_1	R_2	R_3	R_4	R_5	γ to δ
A	H	Cl	Cl	H	OH	CH-CH
B	H	Cl	Cl	OH	H	CH-CH
C	H	Cl	Cl	H	H	CH-CH
D	Cl	H	H	H	H	C=C
E	Cl	H	H	OH	H	C=C
F	H	H	Cl	H	H	CH-CH
G	H	H	H	H	H	CH-CH
H	Cl	H	H	H	OH	C=C
I	H	Cl	OH	H	H	CH-CH
K	H	Cl	Cl	OH	OH	CH-CH
L	Cl	H	H	OH	OH	C=C
M	H	Cl	H	H	H	CH-CH
N	H	Cl	H	H	H	C=C

Figure 10. Chemical structure of the different form of astins
The structure of the first nine astins (A-I) was determined by Morita and al and the structure of astin K-P was described by Xu and al. The structural differences between the various astin forms depend on the hydroxylation at the β-carbon atom, the chlorination on the proline residue and the presence or absence of a double bond between the γ and δ carbon of the proline (Jahn, 2015).

3.3. ASTER TATARICUS

Aster tataricus, also called Zi wan, is a perennial plant that belongs to the *Asteraceae* (Compositae) family. This plant is native to Northern Asia (Siberia, China, Mongolia, Korea and Japan) and is widely cultivated in China for its positive impacts on human health. From the morphological point of view, the leaves of *A. tataricus* are disposed in ground rosette and the inflorescence is composed of many flower heads with violet petals supported by branched stems (Jahn, 2015; Théatre, 2017).

The interest devoted to this plant is related to the use of its roots for more than 2000 years in traditional Chinese medicine. In fact, *A. tataricus* roots contain diverse secondary metabolites such as shionone type triterpenes, aster shionones, cyclopeptides and flavonoids that are known for their expectorant, antitussive, antibacterial, antiviral, anti-ulcer activities (Yu and al, 2015; Zhang and al, 2017; Jahn and al, 2017). Among those secondary metabolites, there are astins that are a part of the cyclopeptide group and that have shown a promising antitumor activity (Morita et al, 1996).

3.4. CYANODERMELLA ASTERIS

Cyanodermella asteris is an endophyte fungus that was discovered recently (Jahn and al, 2017; Jahn and al, 2017). The term endophyte refers to an organism that lives inside of the plant without causing adverse effects to the growth and development of the host (Jahn, 2015). In the case of *C. asteris*, the relationship that this fungus shares with *A. tataricus* is considered as mutualistic. It means that the interactions established between the plant and the fungus have beneficial effects for both (Théatre, 2017). At this time, it is supposed that *A. tataricus* is used as a habitat by the fungus and consequently, protects it from the environment. However, further studies have to be conducted in order to determine the benefits conferred on the plant by the fungus (Jahn and al, 2017).

The fungus has been isolated from the inflorescence axis of *A. tataricus* and its genome was sequenced. Following the sequences obtained, phylogenetic analyses were performed. On the basis of the results, it appears that *C. asteris* is a new specie that belongs to the non-lichenized member of the class Lecanoromycetes. This class is particularly well known to produce second metabolites presenting diverse biological activities. Analyses of genes involved in the biosynthesis of secondary metabolites (SMs) have been conducted on *C. asteris*. Findings indicate that the fungus has a huge potential of SMs production. This information confirms the fact that astins are produced by *C. asteris* and not by the plant itself (Jahn and al, 2017).

3.5. ENZYMES INVOLVED IN ASTIN BIOSYNTHESIS

The biosynthesis of astin is assumed to be performed by three different enzymes: the non-ribosomal peptide synthetase (NRPS), the monooxygenase and the flavin dependent halogenase (FDH). Each of them should play an important role in particular processes of formation which, taken together, will result in the achievement of astin structure (Jahn, 2015).

3.5.1. Non-ribosomal peptide synthetase

The non-ribosomal peptide synthetase consists in a large complex composed of diverse modular enzymes. NRPS is responsible for the synthesis of peptides structurally independent from ribosomes. Those peptides can contain 500 different monomers including proteinogenic and non-proteinogenic amino acid residues. In addition, the peptides produced by NRPS have important medicinal applications, such as antibiotics, antitumor and immunosuppression. At this time, the NRPS has only been observed in the secondary metabolism of bacteria and fungi (Strieker and al, 2010; Miller and Gulick, 2016).

Regarding the operation process of the NRPS, four main catalytic domains ensure a substantial role. Firstly, there is the A-domain that activates by adenylation the amino acids and load downstream a

pantetheine thiol group. Secondly, the peptidyl carrier protein (PCP) acts by transferring the amino acids between the different domains. The condensation domain is in charge of the peptide bond formation between the various amino acid residues. Finally, the thioesterase domain catalyzes the hydroxylation or cyclisation, releasing the peptide (Figure 11) (Miller and Gulick, 2016; Mitchell and al, 2012).

In this context, the interest for NRPS as an enzyme involved in the astins synthesis is based on the fact that: (i) astins are molecules composed by proteinogenic and non-proteinogenic amino acids, (ii) the NRPS generates compounds particularly active in medicinal field and (iii) astins have shown antitumor activity (Jahn, 2015). Another relevant indication that should be highlighted concerns the synthesis of cyclochlorotine. Indeed, this compound, that is really close to astin structurally, is synthetized by the NRPS (Schafhauser and al, 2016).

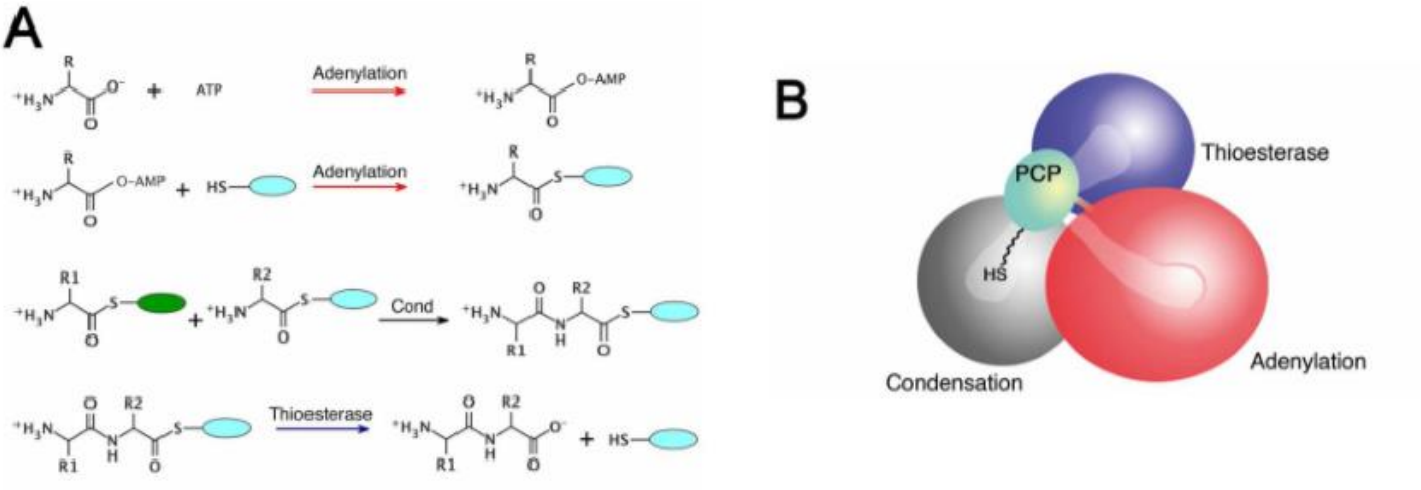

Figure 11. Steps involved in the synthesis of astin backbone structure by the non-ribosomal peptide synthetase and schematic representation of the connections between the four catalytic domains of NRPS
(A) The first step consists in the adenylation of the amino acid at its carboxyl extremity followed by the binding downstream of a pantetheine thiol group (blue oval + SH group). The second step concerns the peptide bond formation between the amino acids. Finally, a hydrolysis or cyclisation is performed in order to release the peptide. (B) Structural conformation of the four catalytic domains highlighting the central position of the PCP that transfers the amino acid between the different domains (Mitchell and al, 2012).

3.5.2. Monooxygenase

The monooxygenase is an enzyme belonging to oxidoreductase subclasses that catalyzes oxygenation reactions. Specifically, this enzyme introduces one atom of oxygen in the compound and the other one is reduced to water (Hrycay and Bandiera, 2015; Huijbers and al, 2013). In the case of astin, monooxygenase inserts the oxygen at the β-carbon atom resulting in the conversion of α-aminobutyric acid into allothreonine. This phenomenon of hydroxylation is responsible for a part of the diversity in astin structure. For example, astins A, B, C and K are dichlorinated at the same position on the proline residue but differ on the basis of the hydroxylation process. In addition to this primary function, monooxygenases play also an important role in biological processes such as detoxification, biosynthesis and pathogen defense (Huijbers and al, 2013; Jahn, 2015).

3.5.3. Flavin dependent halogenase

As mentioned previously, astins can partly be differentiated on the basis of the number of chlorides present in their structure as well as through their position on the proline residue. The only exception concerns the astin G that is non-chlorinated. This process of chlorination indicates the presence of halogenating enzymes. Nevertheless, there is only one that is considered in the astin case thanks to its substrate specificity and regioselectivity. In fact, the flavin dependent halogenase is able to specifically introduce halogen atoms on particular position of secondary metabolites (Van Pée and Patallo, 2006; Jahn, 2015).

Flavin dependant halogenase is an enzyme that needs FADH2 to achieve the halogenation reaction. For this purpose, a flavin reductase reduces the FAD in FADH2. Then, FADH2, O_2 and Cl^- that are present in the enzyme active sites will interact together. Firstly, the reaction between FADH2 and O_2 gives rise to flavin hydroperoxide (FAD(C4a)-OOH) production. This intermediate molecule generated reacts subsequently with Cl^- resulting in the formation of hypochlorous acid. Finally, the hypochlorous acid interacts with lysine residue also present in the active site and then, halogenation of the substrate occurs (Zhu and al, 2009; Jahn, 2015).

3.6. STRUCTURAL ANALOG OF ASTIN: CYCLOCHLOROTINE

Cyclochlorotine is a chlorinated cyclic pentapeptide that was recognized as the causing agent of the yellow-rice syndrome in Japan. In fact, this compound was isolated from a mold occurring on foodstuffs, called *Penicillium islandicum*, known for the production of hepatotoxic mycotoxins (Schafhauser and al, 2016).

The interest in cyclochlorotine can be explained by its structural similarity to astins. In fact, this compound contains also the non-proteinogenic acids L-2-aminobutyrate, L-β-phenylalanine, L-cis-3,4-dichloroproline and two L-serines. The only difference between cyclochlorotine and astin C is the substitution of the serine by a second 2-aminobutyrate. Apart from being structural analogs, the non-ribosomal peptide synthetase is also involved in the biosynthesis of both compounds (Schafhauser and al, 2016; Jahn, 2015).

However, despite these similarities, astin C and cyclochlorotine show completely different activities. Indeed, astin C has demonstrated anticancer activity when tested in vivo on sarcoma 180A in mice (Morita and al, 1996). In contrast, cyclochlorotine has proven toxic and carcinogenic effects to liver cells (Uraguchi and al, 1972).

3.7. ANTICANCER PROPERTIES

The first evidence of astin antitumor activity was highlighted by Morita and al in 1996 through in vivo experiments conducted on sarcoma 180 ascites in mice (Morita and al, 1996). However, only astins with cyclic backbone and cis-dichlorinated proline residue, namely astin A, B and C, have demonstrated the antitumor property (Morita and al., 1996; Itokawa and al., 2000; Rossi and al., 2004; Saviano and al., 2004). In fact, since acyclic and mono or non-chlorinated astins did not inhibit tumor growth of sarcoma 180A, it seems evident that the cyclic conformation as well as the presence of two chlorides in cis position on the proline residue play a critical role (Morita and al, 1996). Other experiments have been conducted in vitro on nasopharynx carcinoma and in vivo on P388 lymphocytic leukemia and sarcoma 180A by Itokawa and al. and have extended former conclusions (Itokawa and al., 2000).

Since the 2000s, scientists have synthetized structural analogues of astins and have tested their effects on human cancer cell lines. Once again, no antitumor activity was observed for synthetized acyclic astins. Nevertheless, a different result has been obtained for synthetic astin G-related cyclopeptides which have shown a similar biological activity than natural astin A and B (Rossi and al., 2004; Saviano and al., 2004).

A first indication concerning the mechanism of action of astin against carcinoma cells has been elaborated by Cozzolino and al in 2005. They have synthetized astin-related cyclopeptides to test their antitumor activity on human papillary thyroid carcinoma cell line. Those synthetic cyclopeptides differ from natural astins by some non-proteinogenic amino acid residues and a peptide bond surrogate. It appears from this investigation that the newly synthesized cyclic astins induce apoptosis through the activation of the caspase pathway. In fact, they have observed that, in presence of caspase family inhibitor, the synthetic cyclic astins did not induce apoptosis anymore. This indicates that the anticancer activity of astins is linked to the subsequent activation of caspase 8, 9 and 3 (Cozzolino and al, 2005).

OBJECTIVES

The malignant pleural mesothelioma is a very aggressive cancer that affects the tissues of the pleura. The development of this disease is most predominantly associated with asbestos fiber exposure and occurs only 20 to 60 years later. Following the onset of the illness, a low survival time is estimated, ranging from 9 to 17 months. Each year, MPM is responsible for around 43,000 deaths in the world and this number is expected to rise due to the late implementation of restrictive measures applied to asbestos use in most countries. At this time, mesothelioma treatments are limited and have not been proven sufficiently effective. Therefore, new studies have to be conducted in order to develop novel therapeutic strategies.

In many cases, the standard chemotherapy treatment, consisting in the administration of cisplatin plus pemetrexed, is recommended to patients suffering from MPM. Nevertheless, the development of resistances limits considerably the use of those chemotherapeutic agents. It is therefore necessary to seek out new compounds that could overcome this issue.

Based on the antitumor activity of astin, the first objective focuses on the characterization of the cytotoxic effect of astin C and astin C plus chemotherapeutic agents (cisplatin plus pemetrexed) against a malignant pleural mesothelioma cell line. The second objective consists in demonstrating the importance of the two chlorides in the astin structure by comparing the effects of astin C (carrying two chlorides on the proline residue) and astin G (carrying no chlorides) against mesothelioma cells. Finally, the last objective consists in understanding the mechanisms of action involved in the cytotoxic effect of astin C.

MATERIALS AND METHODS

1. Cell culture

A malignant pleural mesothelioma cell line, the M14K (RRID:CVCL_8102) that belongs to the epithelioid subtype, was cultivated. The cells were maintained at 37°C in a humidified atmosphere with 5% CO2 and cultivated in DMEM (Dubelcco's Modified Eagle Medium, Lonza) medium with L-glutamine supplemented with 10% of fetal bovine serum (FBS, Gibco) and 1% of penicillin and streptomycin (Pen-Strep, 10 000U/mL, Lonza).

2. Cell treatment

Cells were treated with two chemotherapeutic agents, cisplatin and pemetrexed and with astins in combination or alone.

Cisplatin is an alkylating antineoplastic agent used to prevent the replication of cancer cells, leading to their death (Browning and al, 2017). Aliquots of cisplatin 10mM were prepared by the solubilization of the powder (Calbiochem) in dimethyl sulfoxide (DMSO) and a second dilution was conducted in 0.9% NaCl solution. The product was stored at -20°C for 3 weeks maximum as a result of cisplatin instability in solution. The treatment consisted in the administration of cisplatin 10µM to M14K cells for 48 hours.

Pemetrexed is an antimetabolite used to block folate-dependent metabolic processes that are essential for cell replication (Hanauske and al,2001; Cinausero and al, 2018). Aliquots of pemetrexed 10mM were prepared by the dissolution of the powder (Eli Lilly) in 0.9% NaCl solution and were stored at -20°C. The treatment consisted in the administration of pemetrexed 10µM to M14K cells for 48 hours.

Two different forms of astin were used in the treatment of the cells: astin C and astin G. The difference between those two compounds lies in the presence of two adjacent chlorides on the proline residue for astin C and the absence of those atoms for astin G (Morita and al, 1996). Both astin powders (EKU Tübingen, department of biology) were dissolved in DMSO to obtain a solution with a final concentration of 10mM and were stored at -20°C. The treatment consisted in the administration of astin C or astin G 20µM to M14K cells for 48 hours.

3. Cell cycle analysis

3.1. CULTURE, TREATMENT, HARVEST AND FIXATION OF CELLS

The M14K cells were cultivated in a 6 well plate with 500,000 cells per well. After one night, the chemotherapeutic agents (cisplatin 10µM + pemetrexed 10µM) and/or the astin C or astin G (20µM) were added to the culture medium containing the cells in the wells. Five different combination of drugs were tested: astin G, astin C, astin C + chemotherapeutic agents, chemotherapeutic agents (Chem) and astin G + chemotherapeutic agents. In addition to those combinations, a control was performed corresponding to untreated cells. After a treatment of 48 hours, the culture medium of each well was transferred into a falcon tube to take into account the whole of the cells and those remaining in the wells were washed with PBS, trypsinized (Tryspsin-EDTA, Lonza) and collected in the related falcons. The falcons were centrifuged at 485g (Hettich Rotina 420R) for 5 minutes and the pellet of cells obtained was washed twice with PBS-10%FBS and fixed with absolute chilled ethanol 70%. The samples were stored at -20°C for at least 1hour.

3.2. RNase TREATMENT, PI LABELING AND ANALYSES

After the incubation at -20°C, fixed cells were washed three times with PBS-10%FBS and treated with a PBS solution containing 50µg/mL of RNase A (Invitrogen) supplemented with 0.1% of tween for 30 minutes at 37°C. This treatment was performed to label only the DNA because propidium iodide (PI) is a fluorescent intercalating agent that can bind to DNA but also to RNA (Martin and al, 2005). Then, the cells were incubated at room temperature in the dark in presence of PBS solution with 20µg/mL of PI (Sigma Aldrich).

The analysis of the samples was conducted by using the flow cytometer BD FACSCalibur (BD Biosciences) and the BD FACSDiva Software (BD Biosciences). For each sample, ten thousand events were recorded. Cells were selected on the basis of their FSC (forward-scattered light) and SSC (side-scattered light) parameters and from this population doublets were excluded using (FL2-A/FL2-W) gating methods.

4. Fluorescent microscopy

4.1. CELL CULTURE AND FIXATION

The M14K cells were cultivated on coverslips previously placed in a 24 well plate at a rate of 50,000 cells per well. After two hours, the cells were treated with the different combination of drugs (astin G, astin C, astin C + chemotherapeutic agents, chemotherapeutic agents and astin G + chemotherapeutic agents) for 48 hours and untreated cells were used as control. The cells were washed two times with PBS and fixed with a solution of paraformaldehyde 4% for 20 minutes at room temperature in the dark. After the fixation step, the cells were again washed twice with PBS.

4.2. CELL LABELING AND FLUORESCENT MICROSCOPIC ANALYSES

Cells were labeled with DAPI, which is a highly specific fluorescent marker for DNA, allowing nuclei viewing (Kapuscinski, 1995). Briefly, one drop of Fluoroshield with DAPI (Sigma Aldrich) was placed on each coverslip and after 5 minutes, the latter were mounted on slides. The analysis of the slides was performed with a fluorescent microscope (Zeiss LSM 510) equipped with a video camera, a UV light and a 20X objective through the LSM Image Browser software.

5. Statistical analyses

The statistical analyses were conducted using the software Minitab 18. Firstly, the normality of the distributions was monitored by applying the Shapiro-Wilk test which is the equivalent of Rayan and Joiner test on Minitab. Secondly, the equality of variances was assessed following the Levene's test. Once the application conditions accepted, a paired student t test was performed to determine the statistical significance of the differences between the samples. The results of the statistical analyses can reveal significant (*), highly significant (**), very highly significant (***) or non-significant differences between the samples.

All the statistical tests were conducted on experiments that were repeated independently three times.

6. RNA sequencing

6.1. RNA EXTRACTION

The M14K cells have been cultivated in a 6 well plate and treated with the different combination of drugs (astin G, astin C, astin C + chemotherapeutic agents, chemotherapeutic agents and astin G + chemotherapeutic agents) for 48h. In addition to this, a control was performed corresponding to untreated cells. Once the treatment finished, the M14K cells were obtained following their trypsinisation, centrifugation and washing. Then, the extraction of RNA from M14K cells was conducted using the miRNeasy Mini Kit (Quiagen). The overall process of this kit is based on two major steps: the lysis of cells and the purification of total RNA.

Briefly, a phenol/guanidine solution is added to the cells in order to promote their lysis and to inhibit RNases. An organic extraction is performed through the addition of chloroform to remove most of the cellular DNA and proteins from the lysate. After this step, all RNA molecules acquire optimal binding conditions as a result of ethanol addition and, subsequently, the sample is applied to the RNeasy Mini spin column. As the total RNA binds to the membrane of the column, the contaminants are washed away and finally, the purified RNA is recovered through the elution in RNase-free water. The quality and the concentration of the RNAs extracted are then assessed thanks to the bioanalyzer (Agilent).

6.2. POLY(A) RNA ISOLATION, LIBRARIES PREPARATION AND SEQUENCING

The isolation of RNA bearing a poly(A) tail and the preparation of the libraries were conducted by following the CATS mRNA-seq kit v2 with poly(A) selection (Diagenode) protocol.

The poly(A) RNA isolation was performed by the means of oligo(dT) beads. The principle of this method is based on the complementarity between the poly(A) tail of RNA and the poly-T oligonucleotide localized at the bead surface, which are then removed from the solution by magnetic attraction.

The preparation of DNA libraries for sequencing consisted in four different steps: RNA fragmentation, RNA de-phosphorylation and tailing, reverse transcription and PCR pre-amplification.

The purification of the libraries obtained was conducted using the 0.9X AMPure XP beads (Agencourt). The concentration of DNA in the purified libraries was determined with Qubit 2.0 fluorometer dsDNA and the size distribution of libraries was monitored with the bioanalyser (Agilent).

Finally, the sequencing of the libraries was conducted using the Illumina HiSeq 4000 sequencing device (1 x 50bp). Duplicates of the libraries were performed for the RNA sequencing.

7. Bioinformatics analyses

The bioinformatics analyses were achieved in several steps involving two different platforms.

Firstly, the raw reads obtained directly from the sequencing facility were filtered. The filtering consisted in the trimming of the extremities of the reads (polyA tail and template switch used in the CATS mRNA-seq kit for DNA libraries preparation) and in the removal of reads with a sequence length of less than 18 base pair. Then, a quality control was performed to determine whether the quality of the reads was sufficient to proceed to the analyses. After this step, the reads were mapped on the human genome (GRCh38, Ensembl), using the STAR software (ultrafast universal RNA-seq aligner) and statistics associated with this mapping were also obtained and analyzed. Finally, differential gene expression (DGE) analysis based on the $\log_2$(fold change) and on the false discovery rate (FDR) were conducted through the use of DESeq2 software to highlight genes with an expression level significantly different between two different conditions. The fold change corresponds to the difference in expression level of a gene between two treatments and the FDR corresponds to the significance of the differences established. Only the genes with at least a FDR of 0.05 and a log2(fold change) of ± 2 were selected. All these operations were done thanks to the Genialis platform that includes the software programs.

In addition to this, the gene set enrichment analysis (GSEA) platform was used to determine the biological pathways that were regulated differently between two conditions. For this purpose, all the genes differentially expressed between two different conditions in the Genialis platform (with a log2(fold change) different from 0 and a FDR higher than 0.05) were selected. Then, a list of the genes selected with their $\log_2$(fold change) was established and loaded on the GSEA platform. This platform contains a collection of gene sets annotated by the same gene ontology (GO) terms (C5 collection), each gene set corresponding to a specific biological pathway. The GO terms describe the gene function along three aspects: the molecular function, the cellular component and the biological process. Therefore, the GSEA software computed the overlaps between the genes of the list and the gene sets annotated to determine which biological pathways were differently regulated. Moreover, it calculated four key statistics, namely the enrichment score (ES), the normalized enrichment score (NES), the false discovery rate and the p-value. The first two parameters are used to determine the degree to which the biological pathway is differently regulated and the FDR and p-value assess the statistical significance of the NES and ES respectively.

RESULTS

1. Analysis of the cytotoxic effect of astin C on mesothelioma cells

1.1. CONSEQUENCES OF ASTIN C TREATMENT ON CELL CYCLE

Numerous chemotherapeutic agents act by interacting with factors that are involved in the regulation of the cell cycle. In most cases, those interactions result in the arrest of the cell cycle. For example, cisplatin and pemetrexed which are used as standard chemotherapy treatment are responsible for the blockage of cells in phases S or G2. To determine the effect of astin C on the cell cycle, M14K mesothelioma cells were treated with astin C and other drug combinations (astin G, astin C + chemotherapeutic agents, chemotherapeutic agents (Chem) and astin G + chemotherapeutic agents) or maintained in normal conditions (control) for 48 hours. Subsequently, the cells were collected, fixed with absolute chilled ethanol 70%, subjected to RNase treatment, labeled with PI and analyzed by flow cytometry (Figure 12A).

The analysis of the cell cycle by flow cytometry gives rise to a DNA content histogram. This graph shows the number of cells analyzed (expressed as a percentage) in function of the intensity of propidium iodide fluorescence. As the propidium iodide is a fluorescent DNA intercalating agent, the intensity of fluorescence gives the cell DNA content. In untreated M14K mesothelioma cells, two distinct peaks appear on the histogram, corresponding to a DNA content of 2n and 4n (Figure 12 B). The 2n peak represents the cells in G1 phase and the 4n peak represents the cells in G2 phase. The S phase, corresponding to cells in replication, is localized between the two peaks on the histogram as the DNA content is intermediate between 2n and 4n. Finally, apoptotic cells are positioned before the 2n peak and polyploid cells are positioned after the 4n peak.

The observation of the DNA content histograms shows that the astin G treatment is similar to the control regarding the general pattern of those two graphs as well as the percentage of cells in the different phases. Concerning the graph of M14K cells treated with astin C, a high percentage of apoptosis is observed (21.7%) that is higher than the ones obtained in the control (1%) and in presence of astin G (1.3%), chemotherapeutic agents alone and in combination with astinG (12.2% and 16.6% respectively). However, the M14K cells treated with astin C plus chemotherapeutic agents generates 9.7% of apoptotic cells more than the astin C treatment alone. Another important observation concerns the blockage of the cells in S phase, that is illustrated in the graphs corresponding to M14K cells treated with chemotherapeutic agents alone (48.9%) and in combination with astin C or astin G (22.3% and 45.6%) by comparison to the control (5.9%). Regarding the G2-M phase, the percentage of M14K cells obtained following the astin C treatment (10.4%) is not higher than the one observed in the control (15.2%). Finally, when astin C is administrated to M14K cells (23.4%) alone and in association with

chemotherapeutic agents, (10.6%) the percentage of polyploid cells is importantly increased compared to the control (1.1%) (Figure 12C).

A

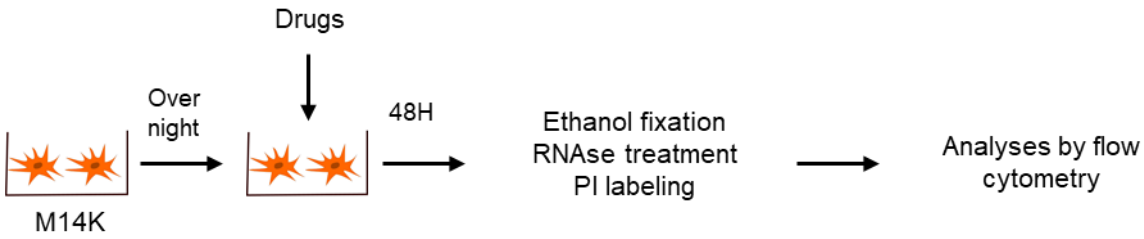

B

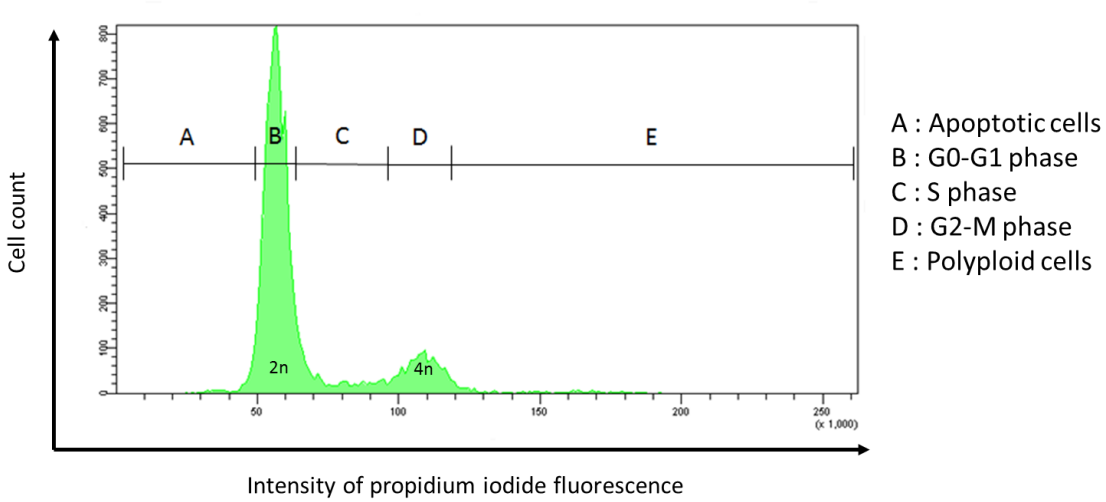

C

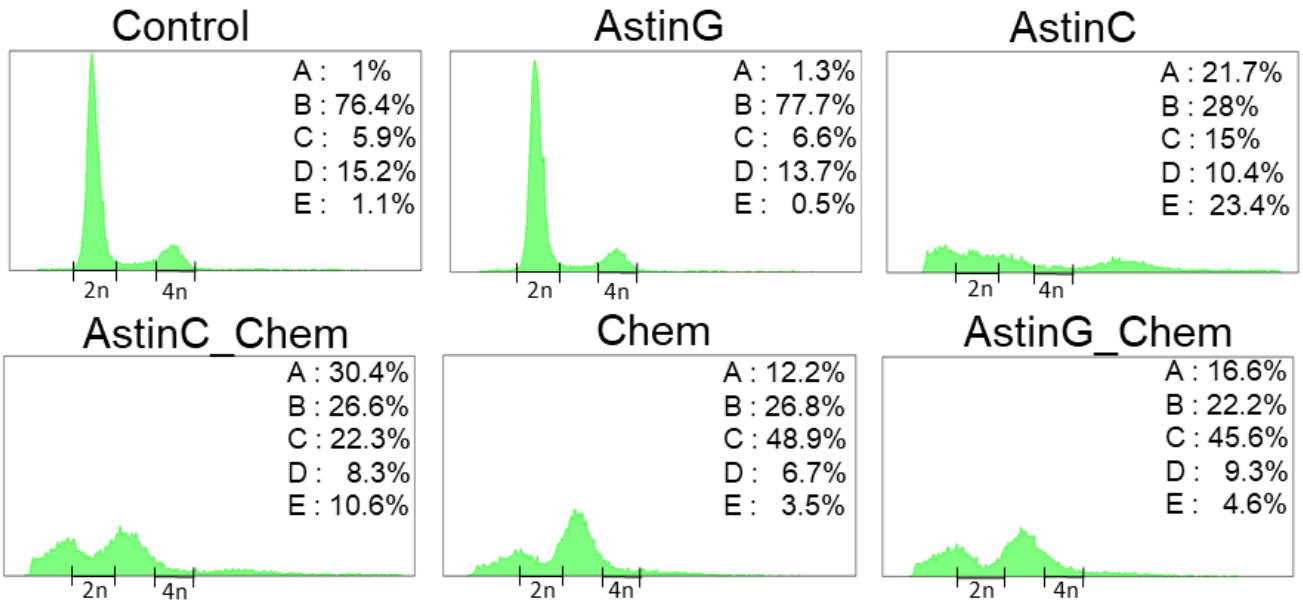

Figure 12. Consequences of astin C treatment and other drug combinations on the different phases of the cell cycle of M14K mesothelioma cells

(A) Experimental design. The M14K cells were cultivated overnight in a 6 well plate and subsequently treated with astin C and other drug combinations (astin G, astin C + chemotherapeutic agents, chemotherapeutic agents (Chem) and astin G + chemotherapeutic agents) or maintained in normal conditions (control) for 48 hours. Then, the cells were collected, fixed with absolute chilled ethanol 70%, subjected to RNase treatment, labeled with PI and analyzed by flow cytometry. **(B) DNA content histogram of untreated M14K mesothelioma cells**. This graph shows the percentage of cells in function of their intensity of propidium iodide fluorescence. The peaks associated with 2n and 4n DNA content correspond to the G0-G1 and G2-M phases respectively. The S phase, characterized by an intermediate DNA content, is localized between the two peaks. The cells before the 2n peak are apoptotic and cells after the 4n peak are polyploid. **(C) DNA content histograms of M14K mesothelioma cells treated with astin C and other drug combinations.** The graphs and percentages shown on this figure illustrate a representative experiment. Those DNA content histograms permit to assess the blockage of the cells in a particular phase of the cell cycle in function of the drugs administrated by comparison to the control as well as the percentage of apoptotic and polyploid cells.

1.2. IMPACT OF ASTIN C ON APOPTOTIC, S PHASE, G2-M PHASE AND POLYPLOID CELLS

Following the study conducted on the effect of astin C on the cell cycle of M14K cells, the S phase, G2-M phase, apoptotic and polyploid cells were submitted to a more detailed analysis. To this end, the same experiment was conducted. Three repetitions were performed to determine the significance level of the differences observed.

Concerning apoptotic cells:

The presence of astin G in the culture medium of M14K cells, being structurally different from astin C by the absence of two chlorides on the proline residue, generates a percentage of apoptosis of 1% that is not significantly different (p-value = 0.329) from the percentage observed in untreated cells (0.7%) (Figure 13A).

Regarding the astin C treatment, it is responsible for a highly significant increase (p-value = 0.005) of the apoptosis percentage (19.5%) compared to astin G treatment (1%) and untreated cells (0.7%) (Figure 13A).

The astin C treatment provokes also a significant increase in the apoptosis percentage of M14K cells (19.5%) in comparison with chemotherapy treatment administrated alone and in combination with astin G to M14K cells (12.7% and 14.3% respectively) (p-value = 0.04 and 0.022 respectively) (Figure 13A).

Finally, the treatment of M14K cells with astin C plus chemotherapeutic agents induces 27.6% of apoptosis and this percentage is significantly higher (p-value = 0.003) than the one generated by the astin C treatment (19.5%) (Figure 13A).

Concerning the S phase:

The M14K cells treated with chemotherapeutic agents and chemotherapeutic agents plus astin G exhibit a percentage of cells in S phase of 53.3% and 51.8% respectively, which are significantly different from the percentage achieved in untreated cells (5.1%) (p-value = 0.004 and 0.004 respectively) (Figure 13B).

The administration of chemotherapeutic agents plus astin C to M14K cells is responsible for a significant increase (p-value = 0.025) of the percentage of M14K cells in S phase (30.6%) compared to untreated cells (5.1%) (Figure 13B).

However, the astin C treatment does not lead to a significant difference (p-value= 0.066) in the percentage of M14K cells in S phase (17.6%) compared to untreated cells (5.1%) (Figure 13B).

Concerning the G2-M phase:

The administration of astin C to M14K cells is not responsible for a significant difference (p-value= 0.406) in the percentage of M14K cells in G2-M phase (18.1%) compared to untreated cells (14.5%) (Figure 13C).

Concerning polyploid cells:

The treatment of M14K cells with astin C and with astin C plus chemotherapeutic agents generates a percentage of polyploid cells of 21.3% and 9.7% respectively, that are significantly different from the percentage obtained in untreated cells (0.6%) (p-value = 0.004 and 0.003 respectively) (Figure 13D).

A

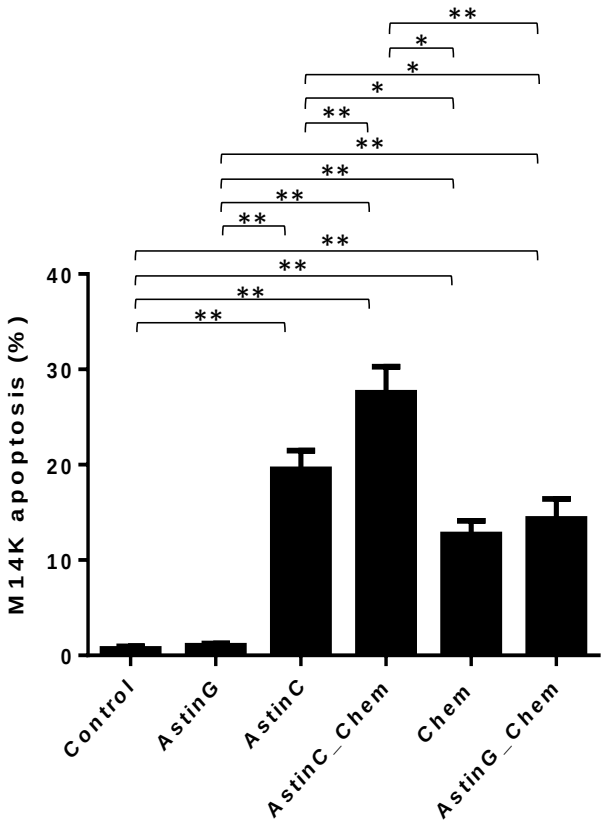

B

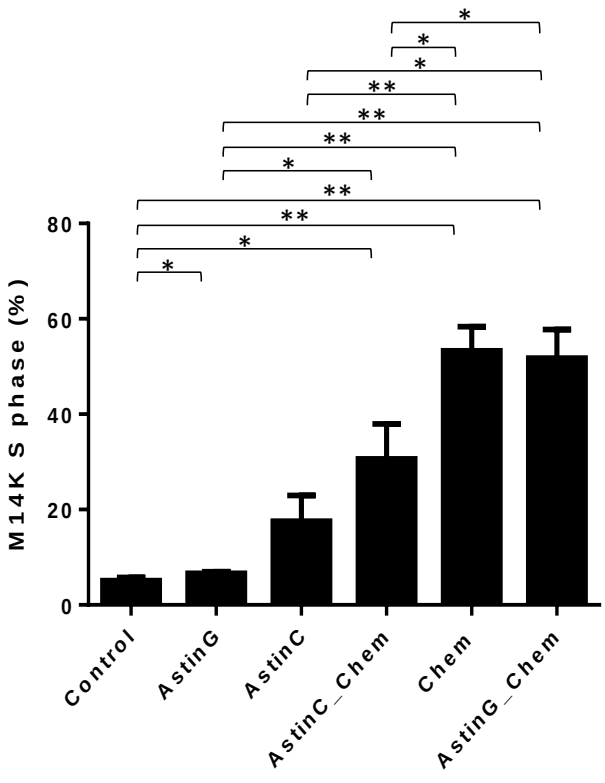

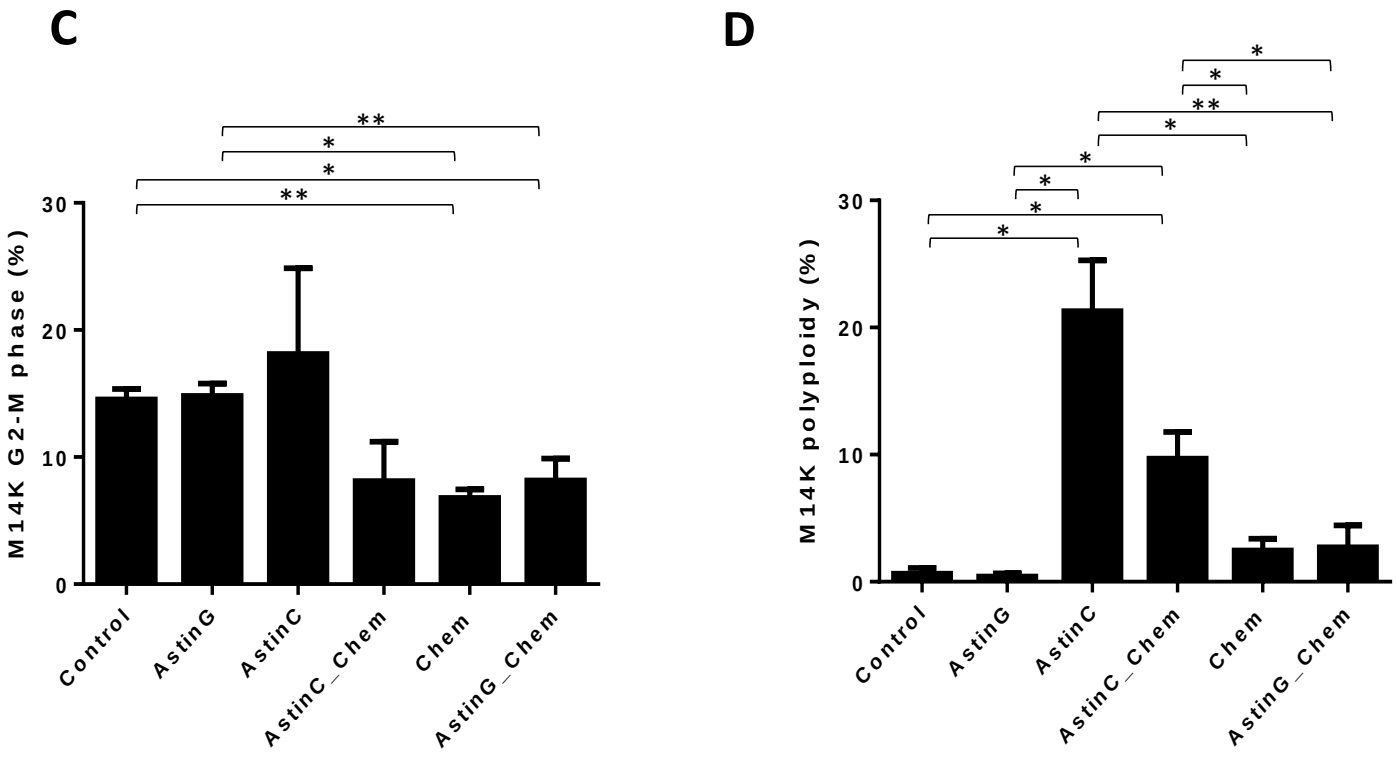

Figure 13. Effect of astin C and other drug combinations on the percentage of apoptotic, S phase, G2-M phase and polyploid M14K cells

The M14K cells were incubated overnight in a six well plate. The cells were cultivated for 48 hours in presence or not (control) of different combination of drugs (astin G, astin C, astin C + chemotherapeutic agents, chemotherapeutic agents (Chem) and astin G + chemotherapeutic agents). Then, the cells were collected, fixed with absolute chilled ethanol 70%, subjected to RNase treatment, labeled with PI and analyzed by flow cytometry. **(A) Bar chart showing the percentage of apoptotic M14K mesothelioma cells. (B) Bar chart showing the percentage of M14K mesothelioma cells in S phase. (C) Bar chart showing the percentage of M14K mesothelioma cells in G2-M phase. (D) Bar chart showing the percentage of polyploid M14K mesothelioma cells.** Those graphs show the means and the standard deviations of apoptotic, S phase, G2-M phase and polyploid M14K cells in normal conditions and in presence of different drugs. The results are presented as the percentage of apoptotic, S phase, G2-M phase and polyploid cells which corresponds to the number of apoptotic, S phase, G2-M phase and polyploid cells counted by comparison to the number of cells analyzed. The statistical analyses were based on a paired t-test and the significance level of the difference observed between two means was established as follows: p-value<0.05 (*), 0.01<p-value<0.05 (**), p-value<0.001 (***). Three repetitions were performed.

1.3. MORPHOLOGICAL CHANGES OF CELLS AFTER EXPOSURE TO ASTIN C

To determine the morphological changes induced by astin C on M14K mesothelioma cells, the overall shape of the cell was examined after exposure to this compound for 48H. In fact, the morphological structure of a cell gives indications concerning its general condition, particularly through the appearance of the nucleus. In the case of a uniform labeling of the nucleus with a clear delimitation of its structure, the cells are considered as normal or necrotic in most cases. However, cells presenting fragmented nucleus with a high fluorescence (due to chromatin condensation) are assumed to be apoptotic. Also, the global aspect of the cell can provide supplementary information on its size modification and membrane discontinuities or disruption for example.

For this purpose, the M14K cells were cultivated on coverslips for 2 hours and were subsequently treated with astin C and other drug combinations (astin G, astin C + chemotherapeutic agents, chemotherapeutic agents (Chem) and astin G + chemotherapeutic agents) or remained in normal conditions (control) for 48 hours. Then, the cells on coverslips were washed, fixed with paraformaldehyde 4% and labeled with DAPI which is a fluorescent DNA intercalating agent. This dye can cross cell membranes and generates a blue fluorescence when irradiated with UV light. Then, the overall shape is obtained under phase-contrast fluorescent microscope (Figure 14 A).

As shown in figure 14 B, untreated cells and cells treated with astin G do not show any typical characteristics of apoptotic cells. Regarding the cells treated with astin C, chemotherapeutic agents alone and in combination with astin C or astin G, nucleus damage and fragmentation (orange arrows) are clearly visible. A modification of the cell configuration by comparison to the control is also observed. Those morphological changes further support onset of apoptosis.

A

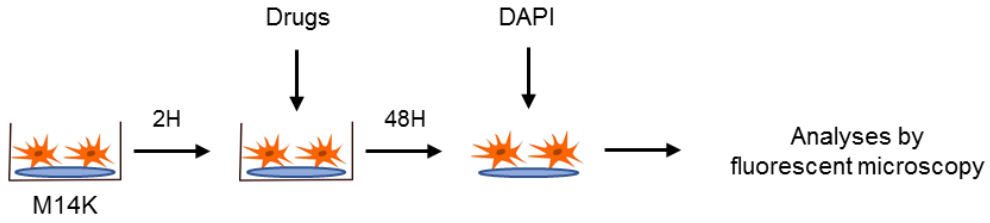

B

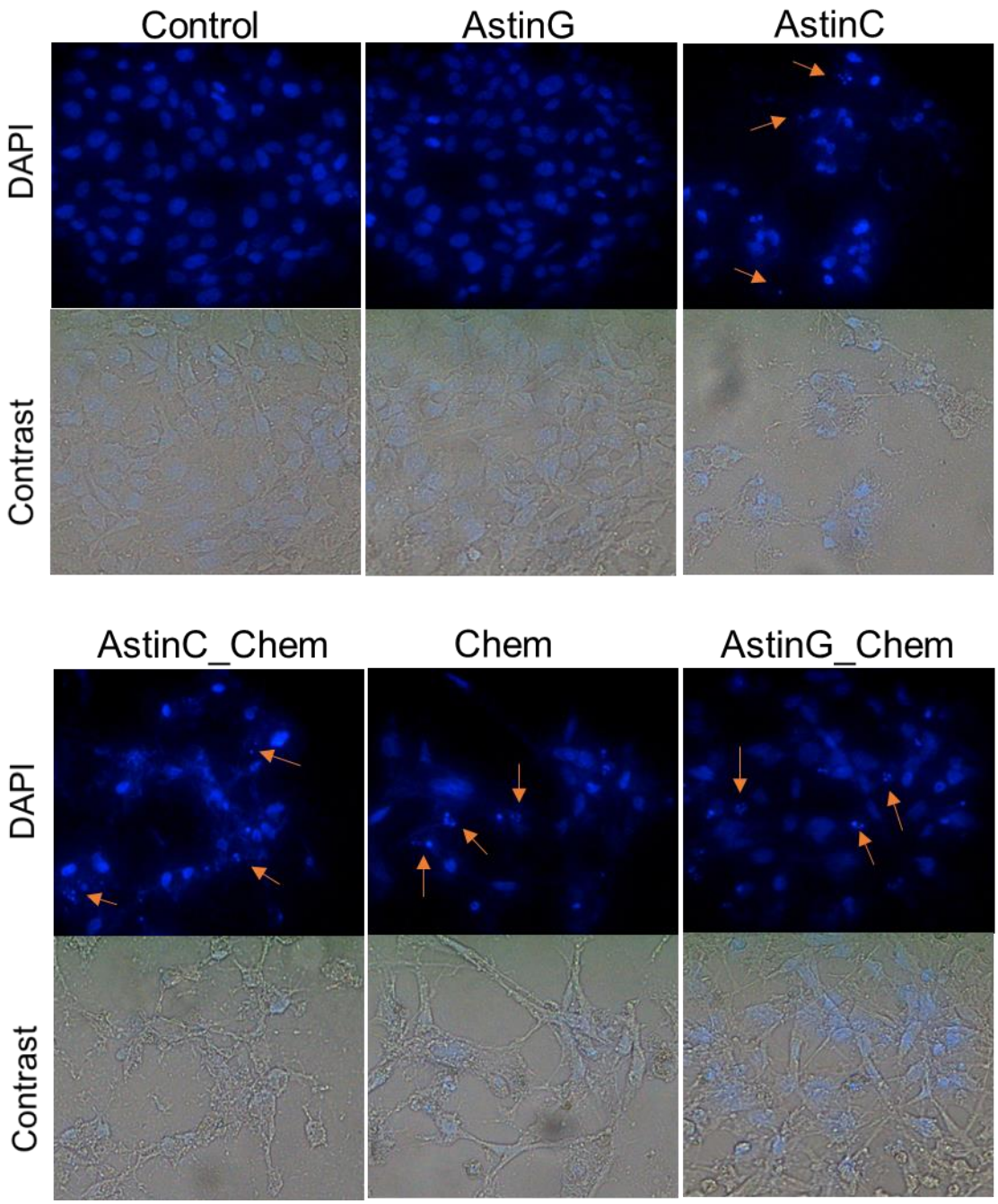

Figure 14. Microscopy of M14K mesothelioma cells treated with astin C and other drug combinations

(A) Experimental design. The M14K cells were cultivated on coverslips in a 24 well plate for 2 hours. The cells were treated or not (control) with the different combination of drugs (astin G, astin C, astin C + chemotherapeutic agents, chemotherapeutic agents (Chem) and astin G + chemotherapeutic agents) for 48 hours. Then, the cells on coverslips were washed, fixed with paraformaldehyde 4% and labeled with DAPI. Finally, the coverslips were mounted on slides and analyzed by fluorescent microscopy. The DAPI is a fluorescent DNA intercalating agent that allows visualization of the nucleus (in blue). **(B) Visualization of the astin C cytotoxic effect on M14K mesothelioma cells by comparison to other drugs.** Fluorescent images after DAPI labeling show fragmented nuclei (orange arrows). Images obtained under phase-contrast show the overall shape of the cells.

2. Determination of potential genes and mechanisms of action involved in the cytotoxic effect of astin C

In order to reveal the genes and mechanisms of action that could be involved in the cytotoxic effect of astin C, a sequencing of the cell transcriptome was performed. This RNA sequencing was conducted on M14K mesothelioma cells untreated and treated with astin C and other drug combinations (astin G, astin C + chemotherapeutic agents, chemotherapeutic agents (Chem) and astin G + chemotherapeutic agents) for 48H.

Before starting the sequencing, the total RNA was extracted from the mesothelioma cells and the concentration and quality of the RNAs were determined using a bioanalyzer. Then, RNAs with a ploy(A) tail were isolated through the use of oligo(dT)-anchored magnetic beads. Subsequently, DNA libraries were prepared in duplicates (for each condition). The DNA concentration as well as the size distribution of the libraries were monitored. Lastly, the libraries were sequenced using the Illumina HiSeq 4000 sequencing device (1 x 50bp) (Figure 15A).

Once the sequencing completed, the raw reads obtained were processed by conducting the filtering, the quality control and the mapping on the human genome. To determine the similarities between the different samples (corresponding to the sequences obtained from M14K cells subjected to the different treatments) and between the duplicates (1 and 2), a hierarchical clustering was performed. The association or dissimilarities between the samples are based on the measurement of the correlation distances (Pearson). As illustrated in the figure 15B, the duplicates are properly associated, except for astin G1 and astin G2 samples that are more distant. Moreover, it appears that the Chem1 and Chem2 samples are dissociated from the others.

The bioinformatic analyses that follow were performed only with the samples corresponding to the sequences obtained from M14K cells untreated and treated with astin C, astin G and chemotherapeutic agents, explaining the absence of the other samples in the hierarchical clustering.

A

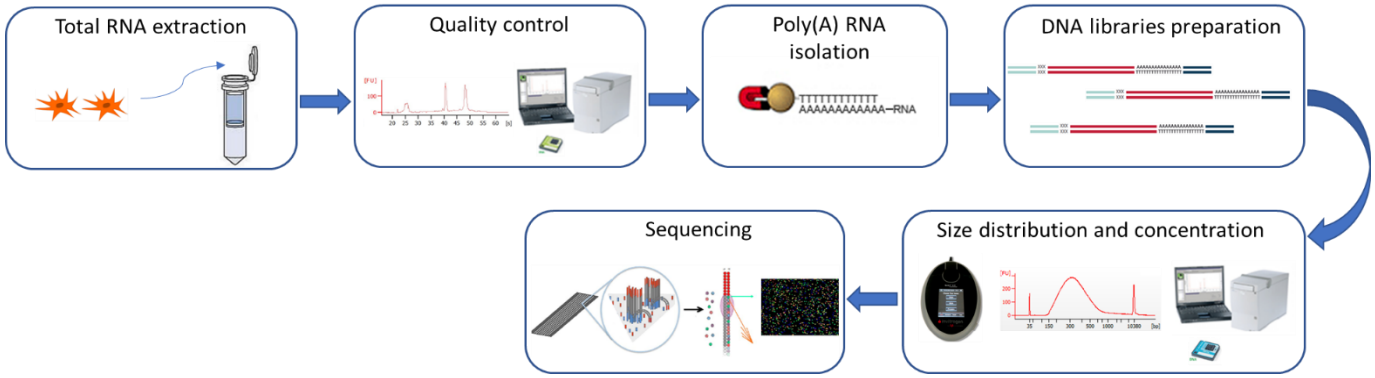

B

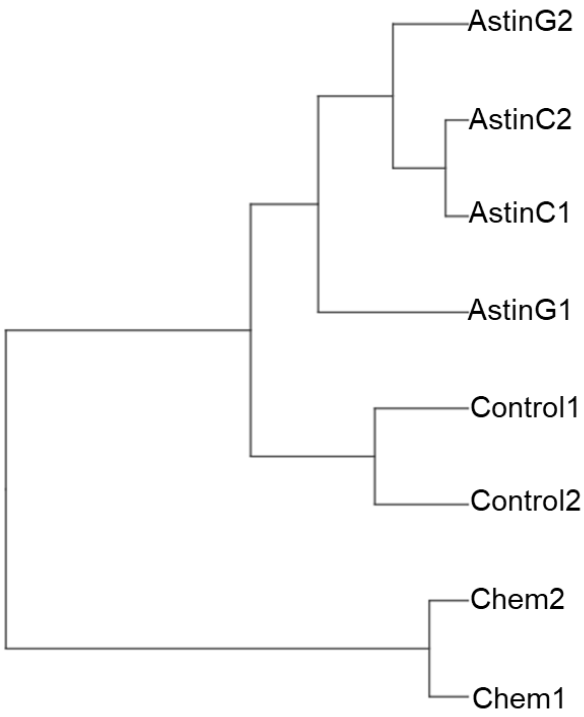

Figure 15. Preliminary stages of bioinformatics analyses
(A) Flow chart of the various steps leading up to the sequencing
Firstly, total RNA is extracted from M14K cells treated or not (control) with the different combination of drugs (astin G, astin C, astin C + chemotherapeutic agents, chemotherapeutic agents (Chem) and astin G + chemotherapeutic agents) for 48 hours. Secondly, the quality and the concentration of the extracted RNA are verified. Then, the poly(A)-tailed RNAs are isolated by using oligo(dT) magnetic beads. After this step, the DNA libraries are prepared in duplicates for each condition. The DNA concentration as well as the size distribution of the libraries are monitored. Finally, the libraries are sequenced using the HiSeq 4000, 1×50bp. **(B) Hierarchical clustering of the samples obtained from the m-RNA sequencing of M14K cells untreated (control) and treated with astin C, astin G and chemotherapeutic agents (Chem).** Following the processing of the raw reads obtained from the sequencing (filtering, quality control and mapping), a cluster analysis is performed to determine the similarities between the different samples and among the duplicates (1 and 2). The similarities are established on the basis of the correlation distances (Pearson) between the different samples.

2.1. GENES DIFFERENTIALLY EXPRESSED IN ASTIN C TREATED CELLS

To determine the genes deregulated in M14K cells treated with astin C by comparison to M14K cells untreated (control), treated with astin G and treated with chemotherapeutic agents (Chem), a DGE analysis was conducted on the Genialis platform. The results of each comparison between two treatments appear in a volcano plot. The x axis of the volcano plot represents the log2(fold change) and the y axis represents the negative log10 of the FDR. Then, each point on the graph represents a gene with a particular log2(fold change) and -log10(FDR). The fold change corresponds to the difference in expression level of a gene between two treatments and the FDR corresponds to the significance of the difference established. For each volcano plot, only the genes with high difference in expression level and high statistical confidence were selected (points indicated in bold) and regrouped in a gene set by setting up a log2(fold change) and a FDR threshold (vertical and horizontal lines) of ±2 and 0.05 respectively. Therefore, three gene sets were obtained, corresponding to the genes differentially expressed in cells treated with astin C by comparison to untreated cells, cells treated with astin G and with chemotherapeutic agents (Figure 16A).

Then, the overlap between the three different gene sets was established by the means of a Venn diagram. This diagram enables to determine the genes that are commonly deregulated in the three gene sets (deep blue) (Figure 16B).

Those genes shared between the three gene sets, whose expression is highly modified by the astin C treatment, are listed in the comparison table (Table 1). This table contains the gene symbols, the main biological processes in which they are involved and the log2(fold change) values corresponding to the number of times that a specific gene is under/overexpressed in M14K cells treated with astin C by comparison to untreated cells and cells treated with astin G and with chemotherapeutic agents.

In addition to the comparison table 1, the genes selected from the Venn diagram were also used to construct a heat map. This map illustrates the expression level of the genes in each individual sample. The rows represent the gene symbols and the columns represent the different samples. A color chart is used to facilitate comparison of gene expression levels across the samples. The values attributed to the various color shades are expressed in transcript per kilobase million (TrPM) transformed by row-wise Z-score. TrPM is a type of expression that takes into account the normalization for gene length and for sequencing depth. The row-wise Z-score transformation gives the value of standard deviation by which the expression level of a gene in one sample differs from the mean of the expression level of the same gene in all the samples (Figure 16C).

The comparison table and the heat map indicate that only five genes are underexpressed (ELF3, FGF18, PTCHD4, SLAMF7 and STC1) in M14K cells treated with astin C. From those five genes, only the ELF3 and FGF18 are also underexpressed, but even more significantly in M14K cells treated with chemotherapeutic agents. The comparison table shows also that the main processes concerned with those genes are the cell migration (ACTA2, ACTG2, EPPK1, STC1), the cell adhesion (CTGF, FAT3, ITGA5, SLAMF7), the regulation of gene expression (ACTA2, ACTG2, CARMN, ELF3), the cell differentiation (ELF3, TAGLN), the signal transduction (CTGF, DAPP1, FGF18, ITGA5, PTCHD4) and the cell death (CTGF, PRUN2, SARM1). Finally, when a « / » is indicated in the process row, it means that the processes in which the gene is implicated have not been discovered yet (Figure 16C and Table 1).

A

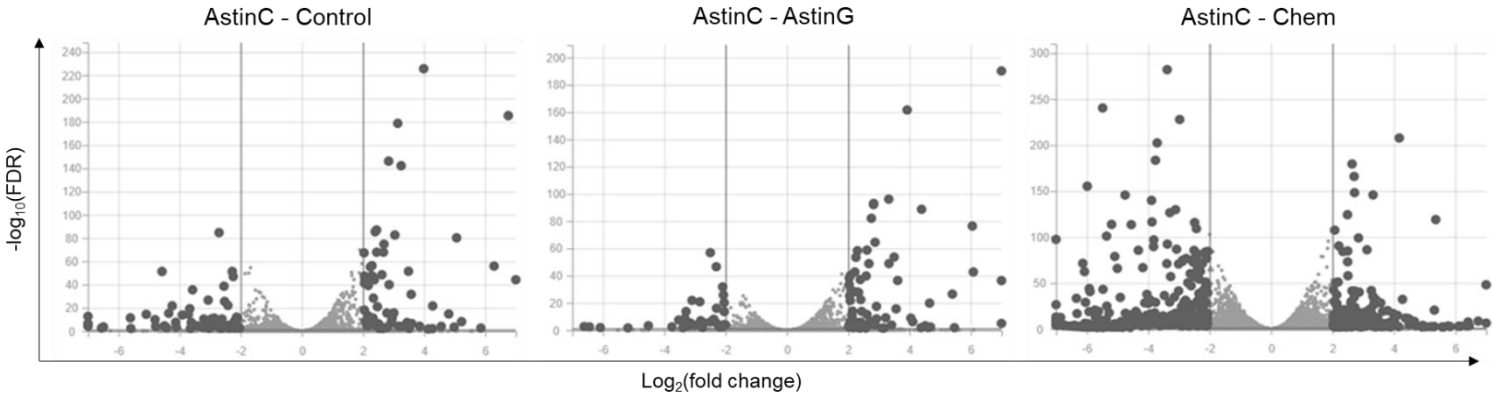

B

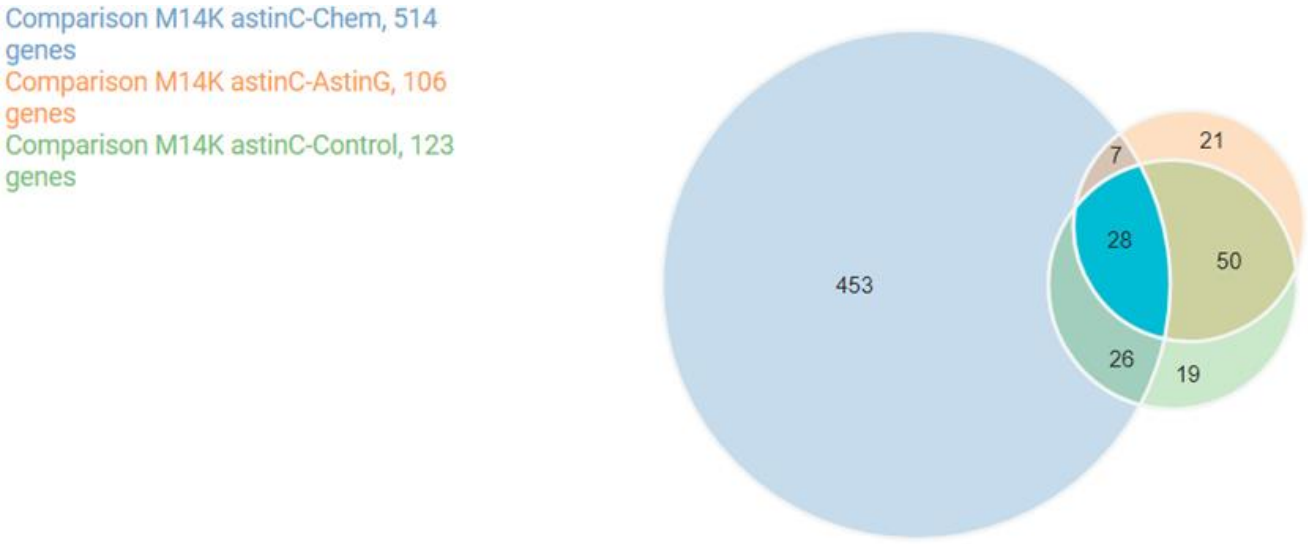

C

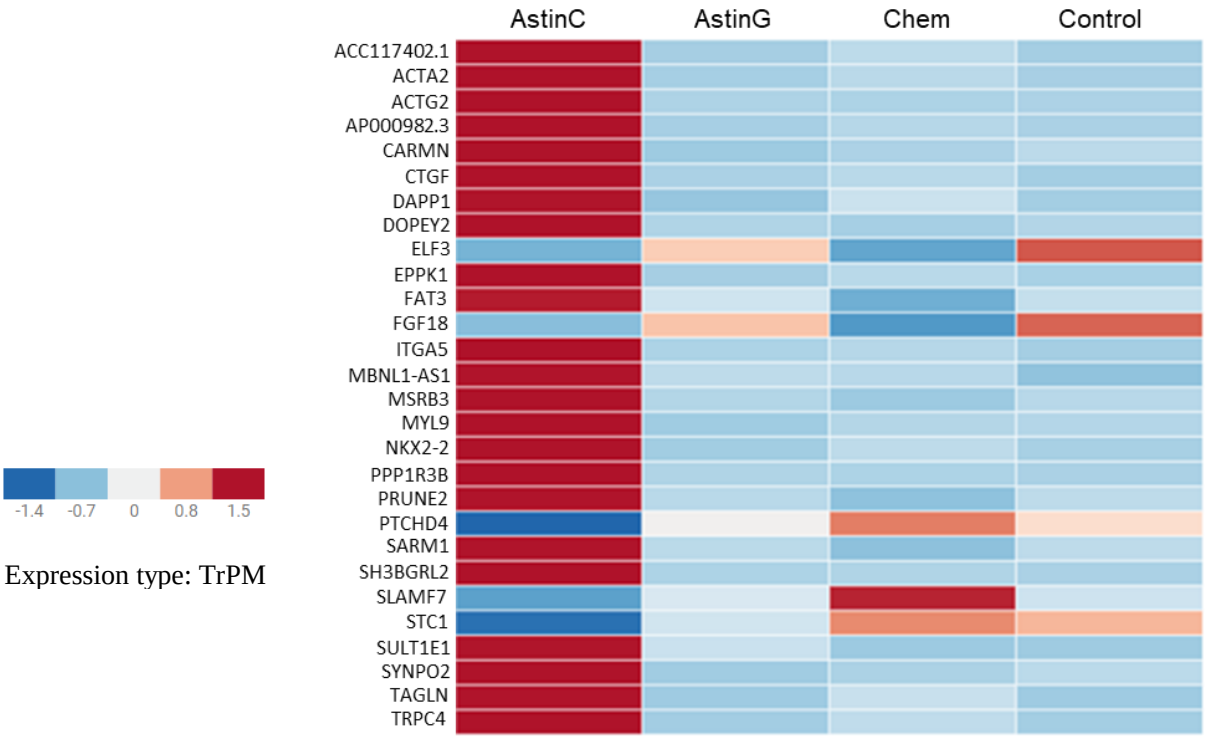

Figure 16. Genes differentially expressed in M14K cells treated with astin C
(A) Volcano plots of differentially expressed genes of cells treated with astin C compared to untreated cells, cells treated with astin G and with chemotherapeutic agents. The volcano plot shows the genes that are differentially expressed between two treatments (astin C vs Control, astin C vs astin G and astin C vs Chem). The x axis represents the $\log_2$(fold change) and the y axis represents the negative $\log_{10}$ of the FDR. Each point on the plot corresponds to a gene with a particular log2(fold change) and -$\log_{10}$(FDR). The genes with high difference in expression level and high statistical confidence were selected and regrouped in a gene set (points indicated in bold) by setting up a $\log_2$(fold change) and a FDR threshold (vertical and horizontal lines) of ±2 and 0.05 respectively for each volcano plot. **(B) Venn diagram of gene sets selected from the volcano plots.** The Venn diagram shows the overlap between different gene sets and therefore the genes that are shared among those. In this case, the three gene sets provided by the volcano plots (astin C vs control, astin C vs astin G and astin C vs Chem) were used in the Venn diagram to highlight the genes that are commonly differentially expressed in M14K cells treated with astin C. **(C) Heat map of the genes commonly differentially expressed in M14K cells treated with astin C.** This graph shows the expression level of the genes selected from the Venn diagram in each individual sample. The rows represent the gene symbols and the columns represent the different samples. A color chart is used to facilitate comparison of gene expression level between the different samples**.**

D

Symbols	Process*	AstinC - Control	AstinC - AstinG	AstinC - Chem
ACC117402.1	/	5.23	6.08	3.36
ACTA2	Mesenchyme migration and regulation of gene expression	6.75	7.45	4.17
ACTG2	Mesenchyme migration and regulation of gene expression	9.56	7.14	9.07
AP000982.3	/	4.28	5.40	3.63
CARMN	Regulation of gene expression at the posttranscriptional level**	4.98	8.00	5.76
CTGF	Cell adhesion, cell death and signal transduction	3.14	2.76	2.64
DAPP1	Signal transduction	2.92	2.41	2.19
DOPEY2	Protein transport	2.78	2.92	2.83
ELF3	Regulation of transcription and cell differentiation	-3.58	-3.10	2.25
EPPK1	Organization of the cytoskeleton and negative regulation of cell migration	3.49	3.50	2.87
FAT3	Cell-cell adhesion	2.33	2.09	5.36
FGF18	MAPK cascade, cell-cell signaling and signal transduction	-2.53	-2.29	2.52
ITGA5	Cell surface adhesion and signal transduction	2.29	2.28	2.16
MBNL1-AS1	/	2.55	2.08	2.36
MSRB3	Oxidation-reduction process and response to oxidative stress	2.05	2.03	2.49
MYL9	Regulation of muscle contraction and platelet aggregation	2.40	2.83	2.49
NKX2-2	Regulation of transcription and development of diverse organs	2.65	2.18	2.83
PPP1R3B	Glycogen metabolic process	3.04	2.88	3.12
PRUNE2	Apoptotic process and polyphosphate catabolic process	3.44	2.72	8.22
PTCHD4	Cell surface signaling pathway	-2.62	-2.38	-2.88
SARM1	Regulation of apoptotic process and innate immune response	2.34	2.34	3.26
SH3BGRL2	/	2.33	2.44	2.45
SLAMF7	Immune system process, cellular defense and cell-cell adhesion	-3.65	-3.75	-5.55
STC1	Negative regulation of cell migration and cellular calcium ion homeostasis	-4.13	-3.22	-4.06
SULT1E1	Sulfation and estrogen catabolic and metabolic processes	4.27	2.38	5.04
SYNPO2	Positive regulation of actin filament bundle assembly	2.80	2.39	2.86
TAGLN	Epithelial cell differentiation and muscle organ development	3.99	3.92	2.72
TRPC4	Cellular calcium ion homeostasis	3.58	3.61	2.73

*Data provided by the National Center for Biotechnology Information (NCBI) and PANTHER.

** Spizzo and al, 2010

Table 1. Comparison table of the genes commonly differentially expressed in M14K cells treated with astin C

This table contains the $\log_2$(fold change) values of the genes that are differentially expressed in the three gene sets and the biological processes in which they are involved (NCBI Gene. Accessed 11 Jun. 2018; GENEONTOLOGY PANTHER Classification System. Accessed 11 Jun. 2018). A color chart is attributed to the $\log_2$(fold change) to facilitate comparison.

2.2. EXPRESSION OF KEY GENES INVOLVED IN CELL CYCLE REGULATION

Based on the observation that the different treatments affect the cell cycle, a targeted analysis was performed. For this purpose, the genes that regulate the cell cycle were selected on the Geneious platform and the expression of the latter was examined in M14K cells treated with astin C, astin G, chemotherapeutic agents and in untreated M14K cells. The results appear in a heat map, the rows representing the gene symbols and the columns representing the different samples.

In M14K cells treated with astin C, cyclin D1 and 2 (CCND1 and CCND2), CDK4, CDK6 and E2F2 are downregulated and Rb1 is upregulated regarding the genes involved in G0-G1 phase. Concerning the genes implied in G1-S phase, S-G2 phase and G2-M phase, only the cyclin A1 is slightly underexpressed, other genes are overexpressed or remain fairly unchanged. Finally, all the genes that inhibit different phases of the cell cycle are downregulated or are not differently expressed (Figure17).

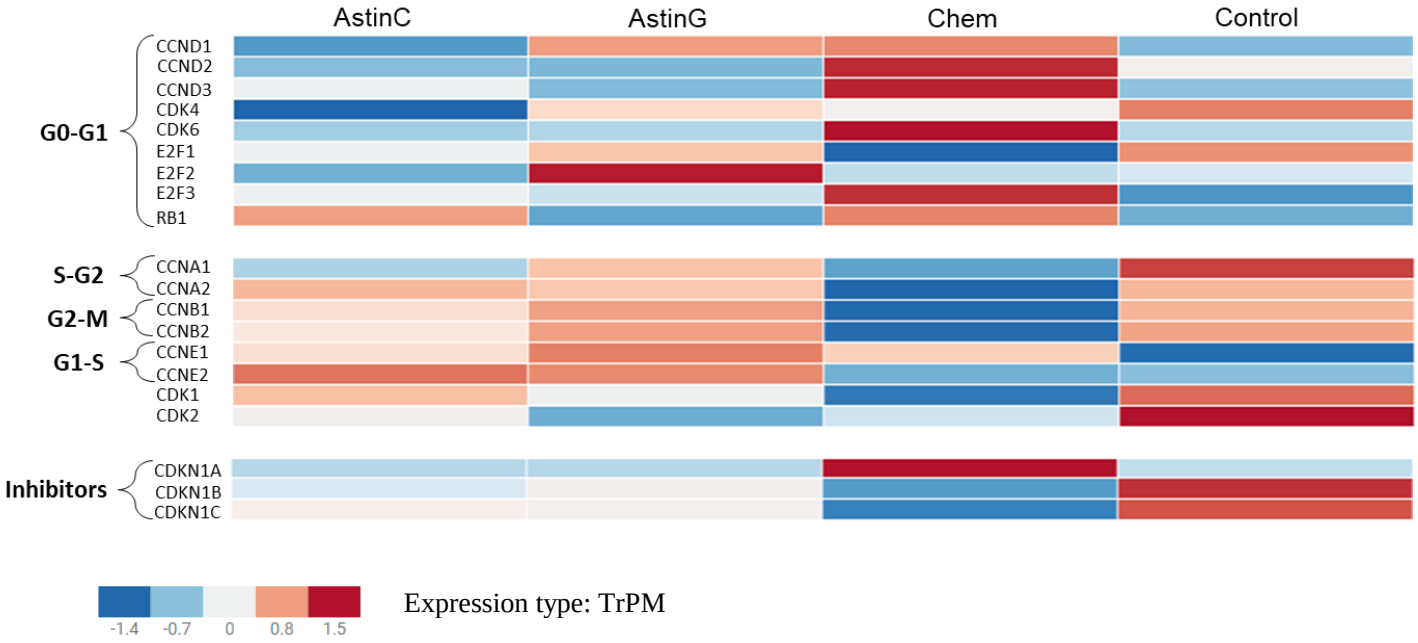

Figure 17. Heat map of the expression of the main genes controlling the cell cycle in M14K cells untreated and treated with astin C, astin G and chemotherapeutic agents
This graph shows the expression level of the genes implicated in cell cycle in each individual sample. The rows represent the gene symbols and the columns represent the different samples. A color chart is used to facilitate comparison of gene expression level between the different samples.

2.3. CELL DEATH AND MAJOR BIOLOGICAL PATHWAYS IMPLICATED IN ASTIN C CYTOTOXIC EFFECT

The determination of the cell death and biological pathways involved in the cytotoxic effect of astin C against M14K cells was performed through the use of the GSEA platform. This platform contains a collection of gene sets corresponding to different biological pathways, each gene set being composed of genes annotated by the same gene ontology terms. The GO terms describe the gene function along three aspects: the molecular function, the cellular component and the biological process.

All genes differentially expressed (with a log2(fold change) different from 0 and a FDR higher than 0.05) in M14K cells treated with astin C by comparison to untreated cells and cells treated with astin G and chemotherapeutic agents were selected. Then, a list of the genes selected with their log_2(fold change) was established and loaded on the GSEA platform. Once loaded, the GSEA software computed the overlaps between the genes of the list and the gene sets annotated to determine which biological pathways are differently regulated in the presence of astin C. In addition to this, the ES, NES, FDR and p-value were calculated and are required to interpret the GSEA results. The ES value determines the degree to which the genes present in the list are overrepresented in an annotated gene set. Then, if a gene is present in the gene set, the ES value increases, otherwise it decreases and the magnitude of this increase or decrease depends on the log_2(fold change) associated to the gene. The NES value corresponds to the normalization of the ES value by considering the number of genes expressed in the gene set in correlation with the size of the gene set to obtain comparable values between the different deregulated pathways. Finally, the FDR and the p-value represent the statistical significance of the NES and the ES values respectively. As a comparison between the different biological pathways is performed, the NES and the FDR values are used because they consider the normalization.

Once the GSEA analysis was performed, the presence of cell death pathways (including apoptosis, necroptosis, necrosis, autophagy and senescence) was examined in the list of the differently regulated biological pathways. Only the cell death pathways found in the list with a FDR < 0,3 and a NES > 1,65 were considered. As shown in table 2A, extrinsic apoptotic pathways are upregulated in M14K cells treated with astin C by comparison to untreated cells and cells treated with astin G. Concerning the comparison of astin C treatment to the chemotherapy treatment, no cell death pathways differently regulated were highlighted.

In addition to the determination of cell death pathways involved in the astin C activity, the first five biological pathways present in the list obtained from the GSEA platform were selected and analyzed. In fact, those pathways appear in descending order of NES, meaning that the first ones are the most differently regulated as they have the highest NES values. As shown in the table 2B, the mesenchyme morphogenesis and platelet aggregation are two pathways upregulated in M14K cells treated with astin C by comparison to untreated cells and cells treated with astin G. In the same way, the myofibril assembly pathway is upregulated when M14K cells are in the presence of astin C compared to untreated cells and cells treated with chemotherapeutic agents. Also, the pathway involving filopodium is upregulated in M14K cells treated with astin C by comparison to cells treated with astin G and chemotherapeutic agents. Finally, it appears that a few genes belonging to the list established in the previous section are involved in some biological pathways differentially regulated, namely “Go mesenchyme morphogenesis” (ACTA2, ACTG2), “Go platelet aggregation” (MYL9), “Go myosin complex” (ACTG2), “Go filopodium” (ACTA2, ACTG2) and “Go cell substrate junction” (SYNPO2, ITGA5).

A

Cell death pathways	ES	NES	P-value	FDR
AstinC - Control				
Go positive regulation of extrinsic apoptotic signaling pathway -INHBA;TGFB2;TIMP3;THBS1;BMPR1B;TNFRSF12A;SKIL;ATF3;PMAIP1	0.56	1.71	0.000	0.281
AstinC - AstinG				
Go regulation of extrinsic apoptotic pathway signaling pathway in absence of ligand -CSF2;INHBA;TGFB2;IL1A;UNC5B;FYN;DAPK3;BCL2;FAS;FGFR1;MAPK7;HSPA1A	0.67	1.89	0.002	0.043
Go regulation of extrinsic apoptotic signaling pathway -CSF2;INHBA;TGFB2;TRAF1;TIMP3;G0S2;TNFAIP3;SERPINE1;ITGAV;TNFRSF12A;IL1A;THBS1; UNC5B;ATF3;ICAM1	0.49	1.73	0.002	0.134
Go positive regulation of extrinsic apoptotic signaling pathway -INHBA;TGFB2;TIMP3;G0S2;TNFRSF12A;THBS1;ATF3;DAPK3;PMAIP1;FAS;BMPR1B;SKIL;BCL10	0.57	1.65	0.010	0.164
AstinC - Chem				
/	/	/	/	/

B

Differentially regulated biological pathways	ES	NES	P-value	FDR
AstinC - Control				
Go mesenchyme morphogenesis -ACTG2;ACTA2;FOXC2;TGFB2;FOXC1;TBX20;SOX9;ACTA1	0,76	2,13	0,000	0,003
Go platelet aggregation -CSRP1;MYL9;ACTN1;ACTB;FERMT3;ACTG1;MYH9;VCL;ILK;FLNA;TLN1;MYL12A	0,77	2,12	0,000	0,004
Go actin filament -LCP1;TPM1;ACTN1;FERMT2;AIF1L;DPYSL3;ACTG1;TPM4;FLNA;APC2;TEK;PALLD;FYN;ACTA1; MYO5A	0,64	2,07	0,000	0,022
Go myosin complex -ACTG2;MYL7;MYL9;MYH11;MYH3;MYO1E;MYH10;MYH9;MYO5C;MYL6;MYL12A;MYO5A;MYO15A ;SHROOM1;MYO3A	0,70	2,07	0,000	0,009
Go myofibril assembly -LMOD1;LDB3;MYH11;TPM1;ANKRD1;MYH3;FHOD3;MYH10;ACTG1;SRF;ACTA1;CFLAR;ACTN2; WDR1	0,71	2,03	0,000	0,023
AstinC - AstinG				
Go mesenchyme morphogenesis -ACTA2;ACTG2;FOXC2;TGFB2;ACTA1;FOXC1;SOX9	0,79	2,12	0,000	0,010
Go filopodium -ACTA2;ACTG2;LCP1;ACTA1;SRCIN1;ITGAV;VASP;AKAP5;NLGN1;ENAH;FSCN1;ITGA3;MSN;TWF2 ;MYO10	0,65	2,07	0,000	0,017
Go cell substrate junction -LCP1;CSPG4;CNN1;CSRP1;NEXN;SYNPO2;ITGA5;LIMS2;PHLDB2;SPRY4;CIB2;ACTN1; ARHGAP22;FBLN7;SRCIN1	0,53	2,06	0,000	0,011
Go negative regulation of coagulation -EDN1;THBD;VTN;SERPINE1;UBASH3B;PTGER3;PDGFB;PRKG1;SERPINB2;PLAT;F12;PLAU; PRKCD	0,79	2,04	0,000	0,014
Go platelet aggregation -MYL9;CSRP1;ACTN1;FERMT3;ACTB;ACTG1;MYH9;VCL;FLNA;ILK;GAS6;MYL12A;HSPB1;TLN1	0,78	2,04	0,000	0,012
AstinC - Chem				
Go actomyosin structure organisation -LMOD1;LDB3;FHOD3;NEBL;CNN1;MYH10;MYLK3;ACTG1;MYH3;ACTA1;PDGFRB;MYH9;TPM1; SRF;KIF23	0,62	2,08	0,000	0,033
Go myofibril assembly -LMOD1;LDB3;FHOD3;NEBL;MYH10;MYLK3;ACTG1;MYH3; ACTA1;PDGFRB;TPM1;SRF	0,69	2,03	0,000	0,037
Go condensed nuclear chromosome -HSPA2;HUS1B;SUN2;KIFAP3;RAD9B;TEX12;PLK1;CENPA;BUB1;CCNB1;ADD3;CHEK1;BUB1B; RAD51	0,59	2,02	0,000	0,031
Go positive regulation of filopodium assembly -NLGN1;BCAS3;GPM6A;DPYSL3	0,76	2,00	0,000	0,030
Go regulation of filopodium assembly -NLGN1;BCAS3;GPM6A;PPP1R9A;DPYSL3	0,69	1,97	0,000	0,047

Table 2. Analyses of the biological pathways involved in astin C cytotoxic effect against M14K cells through the GSEA platform

The genes differentially expressed in cells treated with astin C by comparison to untreated cells and cells treated with astin G and chemotherapeutic agents were loaded on the GSEA platform. To this end, all the genes with a log2(fold change) different from 0 and a FDR higher than 0.05 were selected from the previously established volcano plots. Then, the list of the genes obtained for each volcano plot with their log2(fold change) values were loaded on the GSEA platform. From this list of genes, the GSEA software determines which gene sets are involved in specific biological pathways. In addition to this, it calculates four key statistics, namely the ES, NES, FDR and p-value. The results of the GSEA analyses appear as a table containing the differentially regulated pathways and the four statistical parameters. **(A) Cell death pathways differentially regulated in M14K cells treated with astin C.** This table shows the pathways involved in cell death that are significantly deregulated when the astin C treatment is compared to the control and cells treated with astin G and chemotherapeutic agents. **(B) Major biological pathways differentially regulated in M14K cells treated with astin C.** This table illustrates the five biological pathways that are the most deregulated when the astin C treatment is compared to the control and cells treated with astin G and chemotherapeutic agents.

DISCUSSION AND PERSPECTIVES

Astins are natural compounds that are produced by an endophyte fungus named *Cyanodermella asteris* living inside the plant tissues (Jahn and al, 2017; Jahn and al, 2017). In total, fifteen different forms of astin were discovered, ranging from A-I and K-P, and differ from a structural point a view (Morita and al, 1996; Xu and al, 2013). The anticancer activity of these cyclopeptides has been reported, but the mechanisms involved are unknown. Notwithstanding, it was demonstrated that only astins with a cyclic backbone and a cis-dichlorinated proline residue, namely astin A, B and C have the potential to generate an antineoplastic activity (Morita and al, 1996; Morita and al, 1995; Itokawa and al, 2000; Rossi and al, 2004; Saviano and al, 2004).

The interest devoted to astins relies on their future contribution to the development of more efficacious therapeutic treatments. In fact, the standard chemotherapy treatment currently used against mesothelioma is subjected to the development of resistances, considerably decreasing its efficiency (Behnam-Motlagh and al, 2012). Therefore, the objectives of this work consisted in studying the cytotoxic effect of astin C and astin C combined with the standard chemotherapeutic agents directed against mesothelioma cells, demonstrating the importance of the two chlorides in astin structure and determining the potential genes and mechanisms of action involved in the cytotoxic effect.

1. Astin C exhibits a cytotoxic effect

The analysis of the cell cycle demonstrated that astin C has a cytotoxic effect against M14K mesothelioma cells. The apoptotic death of M14K cells triggered by astin C was also confirmed by the observation of fragmented nuclei by fluorescent microscopy. In addition, the astin C treatment was found to be more effective than the chemotherapy treatment (Figures 12, 13 and 14). Those results are in line with the scientific literature regarding the cytotoxic effect of astin C on different malignant human cell lines (Rossi and al, 2004; Saviano and al, 2004; Cozzolino and al, 2005). However, no studies that relate to the comparison between astin C and chemotherapy treatment were reported.

2. Astin C improves the chemotherapy treatment

Currently, the standard chemotherapy treatment, consisting in the administration of cisplatin plus pemetrexed, is one of the most commonly applied medical protocol for patients suffering from MPM. However, the emergence of resistances considerably reduces the efficiency of this treatment (Cortes-Dericks and al, 2014; Pistolesi and Rusthoven, 2004). Therefore, the effect of the co-administration of astin C plus chemotherapeutic agents on the cytotoxic activity was examined (Figure 12 and 13). The results showed that this association provides additional efficacy compared to the standard chemotherapy treatment. Although the combination of cisplatin plus pemetrexed exhibits a weak cytotoxic activity,

supplementation with astin C significantly increases this activity. This result can be explained by the fact that astin C induces a differential gene expression compared to chemotherapy treatment in M14K cells, leading to alternative mechanisms of action (Figure 16C, 17, Table 1 and 2). Thence, the combination of drugs with different mechanisms of action can strengthen the cytotoxic effect (Vandermeers and al, 2009; Takimoto and Awada, 2008).

3. Chlorides are implicated in the cytotoxic effect of astin C

In order to determine the importance of the two chlorides in the astin C structure, the effect of astin C and astin G on M14K mesothelioma cells was compared. Indeed, astin C is a structural analog of astin G that differs only by the presence of two adjacent chlorides on the proline residue, which are replaced by two hydroxyls in astin G structure (Morita and al, 1995). Following the analysis of the cell cycle and the images obtained from fluorescent microscopy, it was demonstrated that astin G does not have a cytotoxic effect (Figure 12, 13 and 14). Then, the fact that astin C exhibits a cytotoxic activity and not astin G is attributed to the presence of cis-dichloroproline residue in its structure (Morita and al, 1996).

The specific structure of astin C could be involved in its cytotoxic activity through the formation of crosslinks with DNA molecules, as it is the case for several anticancer drugs containing chlorides in their structure. In fact, once astin C enters into the cell, the low concentration in chloride ions could trigger the hydrolysis of astin C. This results in the creation of a very reactive species that could form bonds with DNA bases (Siddik, 2002; Schärer, 2005; Goodsell, 2006). The detection of crosslinks could be verified by hydrolysis (thermal or mild acid) or enzymatic digestion (nuclease P1, DNase I, phosphodiesterase, and alkaline phosphatase) of DNA, followed by an enrichment of the DNA adducts by separating them from unmodified DNA bases using HPLC (to prevent suppression of ionization resulting from high level of unmodified bases and contaminants) and lastly detected by electrospray ionization-mass spectrometry (Singh and Farmer, 2006; Gavina and al, 2014; Zhang and al, 2016; Gaskell and al, 2007).

The identification of stalled replication forks induced by DNA adducts could also be highlighted by performing a comet assay. This test consists in several steps including: labeling of cell DNA with a thymidine analog, the bromodeoxyuridine (BrdU), which is incorporated during replication; embedding of cells in agarose gel; cell lysis; alkaline treatment to denature DNA; alkaline electrophoresis and labeling with monoclonal anti-BrdU. During the electrophoresis, DNAs with high molecular weight cannot move through the gel. However, damaged DNAs resulting from stalled replication forks or strand breaks display an increased migration (Dekant and al, 2009; Mórocz and al, 2013).

The two chlorides could also be involved in the interaction of astin C with other macromolecules (see section 7) by forming covalent links with nucleophilic centers (Siddik, 2002). In fact, loss of the chloride

ions leads to the formation of strong electrophiles that can bind nucleophilic groups (sulfhydryl and carboxyl) as it is the case for various alkylating agents containing chlorides in their structure (Scholar, 2008).

4. Astin C does not block M14K cells in S and G2-M phases

Several antineoplastic agents are responsible for the arrest of the cell cycle in a particular phase. For example, the antimetabolites act mainly on S phase cells, while vinca alkaloids are more specific to G2-M phase cells (Shapiro and Harper, 1999; Waldman and al, 1996; Payne and Miles, 2008). Then, following the general overview of the effect of astin C on the cell cycle, it was decided to determine whether this compound could block cells in S and G2-M phases. The results showed that astin C does not induce a blockage of M14K cells in S phase, in contrast to chemotherapy treatment (Figure 12 and 13). Moreover, bioinformatics analyses confirmed that astin C does not imply cell cycle arrest in S phase. In fact, the complexes cyclin A/Cdk1 and cyclin A/Cdk2 which regulate the transition of cells from S phase through G2 phase are not underexpressed except cyclin A1 (CCNA1) that is slightly downregulated. However, M14K cells treated with chemotherapeutic agents show a strong underexpression of cyclin A1 (CCNA1), cyclin A2 (CCNA2), Cdk1 and Cdk2, supporting the cell cycle arrest in S phase (Figure 17) (Chiu and Dawes, 2012; Aleem and Arceci, 2015; Zafonte and al, 2000; Castanedo and al, 2006). Concerning the G2-M phase, the same results have been obtained. The astin C treatment does not block M14K cells in G2-M phase (Figure 12 and 13). This is supported by bioinformatics analyses indicating that the complex cyclin B/Cdk1 which controls the progression of cells from G2 phase through M phase is not downregulated (Figure 17) (Lim and Kaldis, 2013; Vermeulen and al, 2003).

Cell cycle checkpoints control is regulated by the tumor suppressor protein p53 (Pietenpol and Stewart, 2002; Harris, 1996). In response to DNA damages, genotoxic stress and abnormal oncogenic events, acetylation of p53 at different sites (DNA binding domain and C-terminal domain) occurs, leading to its stabilization and activation (Brooks and Gu, 2011; Tang and al, 2008). Once activated, p53 can block cells in a particular phase through its transcriptional activity on genes involved in cell cycle arrest (p21, Cdc25C, and GADD45) (Giono and Manfredi, 2006). Following the cell cycle analysis of M14K cells treated with astin C, it can be assumed that p53 was inactivated as no cell cycle arrest in S or G2/M phase was observed (Figure 12 and 13).

The loss of p53 function could be due to genetic alteration. Indeed, a mutation in its exon 5 in M14K cells was highlighted by Urso and al, leading to a premature codon stop causing the formation of a truncated protein (Urso and al, 2017). To reveal a potential mutation, the DNA of M14K cells could be extracted and the exons could be amplified by PCR using specific primer pairs. Then, a sequencing would be performed and the sequences obtained would be compared to reference sequences (Urso and al, 2017). Another possibility concerns the overexpression of p53 inhibitors, MDM2 and MDM4, that

bind the p53 protein through their RING finger domain and inactivate it by different mechanisms (Brooks and Gu, 2011; Tang and al, 2008). The MDM2 and MDM4 proteins can be detected in astin C treated cells by performing a Western Blot analysis with antibodies directed against those compounds. Thereafter, the involvement of those inhibitors in p53 inactivation could be determined by transfecting cells with siRNAs specific for MDM2 or MDM4 and analyzing the impacts on the cell cycle (Tang and al, 2008). Finally, as the acetylation of p53 is required for its activation and blocks the interaction between p53 and the inhibitors, deacetylation could also be at the origin of the loss of p53 function. The immunoprecipitation of p53 protein by anti-p53 antibody followed by a Western Blot using site specific antibodies to detect acetylation on lysines 164, 120 and on lysines of the C-terminal domain (lack of acetylation at all those sites suppresses p53 activity) could be conducted to confirm this hypothesis (Brooks and Gu, 2011; Tang and al, 2008).

5. Astin C induces polyploidy

Regarding the results obtained from the analysis of the cell cycle and more precisely of polyploid cells, the figure 12 and 13 demonstrated that astin C induces M14K cell polyploidization. Polyploidy corresponds to the state in which a cell possesses a DNA content that is multiple of the original DNA content. Besides polyploidy, cells with abnormal number of chromosomes (aneuploid cells) were also observed (Pfau and Amon, 2012; Shu and al, 2018; Davoli and Lange, 2011; Salmela and al, 2012). Three main mechanisms are involved in polyploidization: (i) cell-cell fusion (ii) endoreplication that consists in DNA replication without undergoing cell division (cycle without mitosis) and, (iii) deficiencies in progression through cell cycle (cytokinesis failure and exit from anaphase or metaphase) (Bastida-Ruiz; 2016; Davoli and Lange, 2011). The hypothesis of cell-cell fusion, endoreplication and deficiencies in progression through the cell cycle could be approached by microscopy. Indeed, the analysis of mitotic stages and interactions between cells treated with astin C could be revealed through the labeling of the DNA and the microtubule network and the use of a time-lapse confocal microscope (Cselenyák and al, 2010; Chen and al, 2016).

The involvement of astin C in cell membrane fusion could be confirmed in vitro through the use of liposomes and fluorescent probes. The liposomes are vesicles surrounded by one or more lipid bilayers and the lipidic composition of the bilayer can be adapted to mimic cell membranes as closely as possible. The principle consists in the incorporation of fluorophores in high concentration into some of the liposomes, leading to self-quenching. Then, fluorescently labeled and unlabeled liposomes are inserted in the same through under controlled conditions and the astin C is added. In case of liposomes fusion, fluorophores diffuse into a higher content resulting in an increase in fluorescence that is detected by a spectrofluorometer (Blumenthal and al, 2002; Mingeot-Leclercq and al, 2002; Lorin and al, 2004).

In some cases, polyploid cells can re-initiate mitosis leading to the formation of aneuploid cells following multipolar divisions, chromosome missegregation, and cytokinesis failure. This process could also be highlighted by immunofluorescence (Chen and al, 2016; Mason and al, 2017; Shu and al, 2018).

Currently, a new strategy in cancer therapy consists in generating genomic imbalance that overcome the adaptation capacity of cancer cells. In fact, some drugs are able to induce aberrant mitosis leading to aneuploid and/or polyploid cancer cells that subsequently underwent apoptosis. (Mason and al, 2017; Salmela and al, 2012; Sehdev and al, 2012). To highlight a potential correlation between polyploid M14K cells and apoptosis, analyses of the cell cycle after 24H and 48H of astin C treatment could be conducted. Indeed, the decrease in polyploid and aneuploid cells combined with an increased in apoptotic cells over time could reveal a plausible link (Sehdev and al, 2012).

6. Astin C induces apoptosis

The analysis of the cell cycle of M14K cells treated with astin C revealed a high percentage of apoptosis. Similarly, the images obtained via fluorescent microscopy showed fragmented nuclei which is a feature of cell death by apoptosis. Therefore, those experiments conducted in vitro lead to state that astin C kills M14K mesothelioma cells through apoptosis (Figure 12, 13 and 14).

Concerning bioinformatics analyses, the study of cell death pathways induced by astin C indicated that the extrinsic apoptotic pathway is upregulated compared to untreated cells and cells treated with astin G (Table 2A).

The extrinsic apoptosis consists in a programmed cell death mediated by death receptors, belonging to the tumor necrosis factor receptor family (TNFR), through the formation of death-inducing-signaling-complex (DISC). Once formed, DISC activates a cascade of caspases leading to cell apoptosis (Matsuura and al, 2016; Su and al, 2015).

The results obtained could be supported by measuring the activity of the different caspases involved in extrinsic apoptotic pathway via the use of fluorogenic peptide substrates. Another possibility would consist in determining the percentage of apoptotic cells after their treatment with caspase inhibitors (i.e. against caspase 8 for extrinsic apoptosis). However, the intrinsic apoptotic pathway is also characterized by the activation of caspases. Then, the expression level of death receptor molecules could be assessed by conducting Western Blot analysis (Yang and al, 2011; Lee and al, 2016; Cozzolino and al, 2005). In complement to those in vitro experiments, bioinformatics analyses could be performed to compare expression level of molecules involved in extrinsic apoptotic pathway between M14K cells treated with astin C and untreated cells.

7. Astin C disrupts actin cytoskeleton

The main mechanism of action that could be involved in astin C cytotoxicity concerns the disruption of the actin cytoskeleton. In fact, the analysis of the biological pathways and the genes deregulated in the presence of astin C revealed that actin proteins (ACTG, ACTA) and actin binding proteins (FLNA, TPM) are upregulated and involved in most biological pathways (Figure 16C, Table 1 and 2). Besides, the morphological changes observed in M14K cells treated with astin C support the actin cytoskeletal derangement (Figure 14).

Actin is a protein involved in cell mobility, contraction, endocytosis or cytokinesis, composed of regular arrays of filaments (Behrmann and al, 2012; Pollard and Cooper, 2009). Actin can be found in monomeric form (G-actin) but under physiological conditions, actin monomers polymerize into a helical polymer forming stable filaments (F-actin) (Pollard and Cooper, 2009; Reisler and Egelman, 2007). The interaction between actin and myosin filaments results in actomyosin complex formation leading to cell contraction (Behrmann and al, 2012; Zaidel-Bar and al, 2015).

Knowing that (i) the actin binding proteins (ABP) upregulated, filamin (FLN) and tropomyosin (TPM), are involved in the orthogonal actin branching and the stabilization of actin fibers respectively (Desouza and al, 2012) and, (ii) that the pathways differentially expressed “Go actin filament”, “Go platelet aggregation”, “Go filopodium” and “Go mesenchyme morphogenesis” are involved in actin remodeling (Bonello and al, 2009; Shankar and Nabi, 2015; Haynes and al, 2011; Rumbaut and Thiagarajan, 2010), our data show that astin C induces actin polymerization and reorganization. Therefore, the effect of astin C on actin cytoskeleton could be triggered by its binding to actin subunits or actin regulatory proteins, as it is the case for actin-targeting compounds (Bonello and al, 2009). The increase in F actin content could be analyzed by labeling with rhodamine-phalloidin the M14K cells treated with astin C, subsequently analyzed by flow cytometry (Moulding and al, 2007).

The polymerization and stabilization of actin by astin C could be at the origin of the polyploidy and aneuploidy observed in M14K cells (Figure 12 and 13). In fact, actin filaments aggregation and delocalization could be responsible for cytokinesis failure and mitosis disturbance. The aggregation of F actin close to the mitotic chromosomes, around the mitotic spindle and between spindle poles can prevent the attachment and segregation of chromosomes by microtubules. In addition, the distribution of F actin aggregates through the cytoplasm can compromise the furrow cleavage formation or can directly impede the actomyosin contractile ring formation inhibiting the last step of cell division (Moulding and al, 2007).

The perturbation of actin cytoskeleton could initiate cell death through different mechanisms (Desouza and al, 2012). Firstly, the signaling intermediates and regulators that are localized throughout the F-actin

aggregates can be disrupted. For example, actin fibers can bring members of DISC together leading to its activation or it can delocalize anti-apoptotic regulators leading to their inactivation (White and al, 2001). Secondly, the aneuploid and polyploid cells generated by actin cytoskeleton disruption can subsequently undergo mitotic catastrophe. The mitotic catastrophe is a type of cell death caused by an impairment of mitotic checkpoints leading to inappropriate mitosis. Those defects in mitotic checkpoints can lead to accelerated mitosis producing lethal genomic instability (Mason and al, 2017; Colombo and al, 2010; Tardif and al, 2011; Vakifahmetoglu and al, 2008; Castedo and al, 2004). Lastly, the loss of adhesion between the cells and the extracellular matrix (ECM), phenomenon known as anoikis, can lead to apoptosis (Paoli and al, 2013; Bonello and al, 2012). The attachment of the cells to ECM is conducted by focal adhesions (FAs) which are composed of transmembrane proteins (integrins), structural proteins (actinin, taline, vinculin) and signaling proteins (focal adhesion kinase) (Gilmore and Burridge, 1996; Vicente-Manzanares and al, 2009; Delon and Brown, 2007). The outer domain of integrins binds the ECM that activates intracellular signaling preventing apoptosis and the cytoplasmic domain is linked to the actin cytoskeleton through structural proteins. Therefore, actin cytoskeleton disruption induced by astin C can affect the protein complex that connects actin to integrins which can result in a destabilization of adhesions leading ultimately to their disassembly (Vicente-Manzanares and al, 2009). The inhibition of anoikis process followed by the measurement of apoptotic M14K cells could highlight the involvement of this mechanism in the cytotoxic activity of astin C. Recent studies have demonstrated that the disruption of integrins-matrix interactions activates the Hippo pathway kinase LATS1/2 resulting in YAP inactivation, thereby inducing anoikis. In fact, increased levels of YAP prevent anoikis through the downregulation of Bcl2-L11 and also by overcoming the signaling pathway initiated by tumor necrosis factor alpha and Fas ligand. Then, the inhibition of LATS1/2 leading to the activation of YAP could be used to establish a potential correlation between anoikis and cytotoxic activity of astin C (Frisch and al, 2013; Zhao and al, 2012; Overholtzer and al, 2006; Zanconato and al, 2016).

Finally, it is important to underline that the disruption of actin cytoskeleton, responsible for cell morphological changes, can be both a target and an inducer of apoptosis (White and al, 2001).

8. Astin C upregulates a microRNA

CARMN, also identified by MIR143HG (MIR 143 host gene) is a long non-coding RNA from which the miR-143 and the miR-145 derive (Figure 16C and Table 1). The miRNAs consist in 18 to 24 nucleotides of noncoding RNAs that are involved in the regulation of genes at a posttranscriptional level by interfering with the stability and translation of mRNAs. The expression of miR-143/145 and their host gene is most commonly decreased is several human cancers (lung, breast, colon, prostate) and their overexpression is associated with antitumorigenic activity as well as an increased sensitivity of tumor cells to chemotherapy (Wang and al, 2017; Gomes and al, 2018; Zhao and al, 2018; Spizzo and al, 2010; Zhou and al, 2017).

One important target of the miR-143 is the cyclin D1 (CCND1) whose expression is significantly decreased when miR-143 is upregulated in breast cancer (Zhou and al, 2017). The cyclin D1 which interacts with CDK4/CDK6 is involved in the transition of cells from G0 to G1 phase and is a well-defined human oncogene as it enables the proliferation of tumoral cells. In addition to miR-143, other molecules such as p21, p27 and p57 can induce the inhibition of the cyclin D1 (Schwaederlé and al, 2014; Musgrove and al, 2011; Chiu and Dawes, 2012).

According to the bioinformatics analyses, the expression level of cyclin D1 (CCND1), CDK4, CDK6, E2F2, p21 (CDKN1A), p27 (CDKN1B) and p57(CDKN1C) was decreased or remained fairly unchanged whereas CARMN and RB1 were upregulated (Figure 16C, 17 and Table 1). If so, the expression of the cyclin D1 could be downregulated by miR-143 as the other main inhibitors are underexpressed.

Indeed, considering that MIR143HG is overexpressed in M14K cells treated with astin C, it can be assumed that the biogenesis of miR-143 is therefore increased. Following the synthesis of miR-143, the expression level of cyclin D1 should be decreased. Due to the downregulation of cyclin D1, the tumor suppressor protein RB (RB1) is not phosphorylated. Hence, the unphosphorylated RB protein can bind the transcription factor E2F resulting in the inhibition of the expression of E2F-regulated genes involved in cell cycle progression (Figure 18) (Musgrove and al, 2011; Chiu and Dawes, 2012; Zafonte and al, 2000).

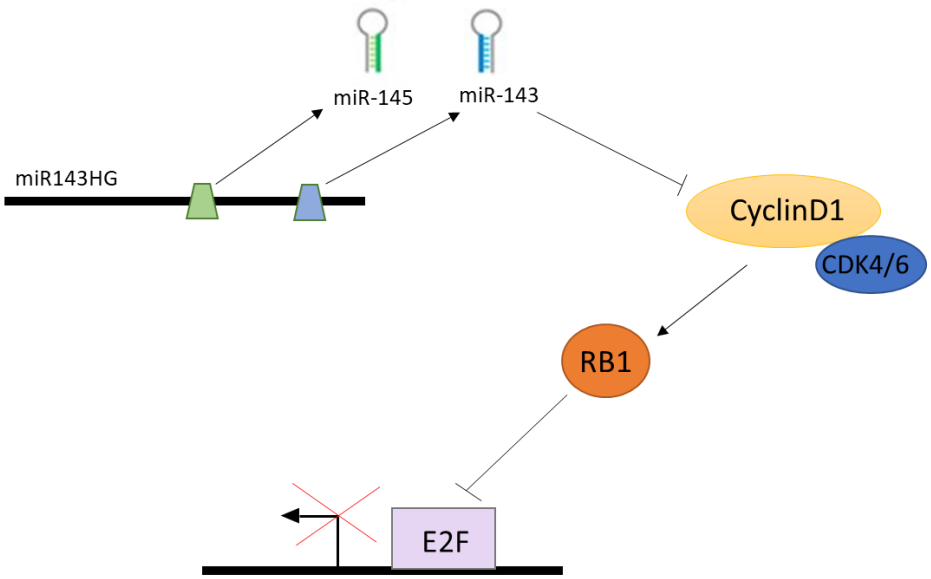

Figure 18. Model of hypothetic inhibition of cyclin D1 by miR-143 in M14K cells treated with astin C

Astin C induces the upregulation of miR143HG resulting in the biogenesis of miR-143. Once synthetized, the miR-143 decreases the expression level of cyclin D1/CDK4/6 that, therefore, cannot phosphorylate the RB protein. In its unphosphorylated form, the RB protein can interact with the transcription factor E2F leading to the inhibition of downstream genes involved in cell cycle progression.

The downregulation of cyclin D1 by miR-143 could be confirmed by transfecting M14K cells treated with astin C with miR-143 inhibitor (Tang and al, 2017; Zhou and al, 2017). After the cell transfection, the expression level of cyclin D1 could be assessed by Western Blot and the impact on the G0-G1 phase could be determined through the analysis of the cell cycle (Zhou and al, 2017).

CONCLUSION

In conclusion, this work demonstrated the cytotoxic activity of astin C against mesothelioma cells and the additional effect conferred by this compound to the standard chemotherapy treatment. Bioinformatics analyses further provided information about the mechanisms involved. These data may be instrumental for the development of improved therapies against mesothelioma.

BIBLIOGRAPHY

Aleem, E., & Arceci, R. J. (2015). Targeting cell cycle regulators in hematologic malignancies. *Frontiers in Cell and Developmental Biology*, **3**(16).

Alley, E. W., Katz, S. I., Cengel, K. A., & Simone II, C. B. (2017). Immunotherapy and radiation therapy for malignant pleural mesothelioma. *Translational Lung Cancer Research*, **6**(2), 212–219.

Alsaab, H. O., Sau, S., Alzhrani, R., Tatiparti, K., Bhise, K., Kashaw, S. K., & Iyer, A. K. (2017). PD-1 and PD-L1 checkpoint signaling inhibition for cancer immunotherapy: mechanism, combinations, and clinical outcome. *Frontiers in Pharmacology*, **8**(561).

Bastida-Ruiz, D., Van Hoesen, K., & Cohen, M. (2016). The dark side of cell fusion. *International Journal of Molecular Sciences*, **17**(5), 638.

Behnam-Motlagh, P., Andreas, T., Johansson, A., Tyler, A., Brännström, T., Karlsson, T., & Grankvist, K. (2012). 'Cisplatin Resistance in Malignant Pleural Mesothelioma' in Zubritsky, A. (ed.) *Synonyms and Definition, Epidemiology, Etiology, Pathogenesis, Cyto-Histopathological Features, Clinic, Diagnosis, Treatment, Prognosis*. 3 edn. INTECH Open Access Publisher, 1353–1416.

Behrmann, E., Müller, M., Penczek, P. A., Mannherz, H. G., Manstein, D. J., & Raunser, S. (2012). Structure of the rigor actin-tropomyosin-myosin complex. *Cell*, **150**(2), 327–338.

Bianchi, C., & Bianchi, T. (2014). Global mesothelioma epidemic: Trend and features. *Indian Journal of Occupational and Environmental Medicine*, **18**(2), 82.

Bianchi, C., & Bianchi, T. (2007). Malignant mesothelioma: global incidence and relationship with asbestos. *Industrial Health*, **45**(3), 379–387.

Blanáthoma, O. V., Jelínková, I., Szöor, Á., Skender, B., Souček, K., Horváth, V., … Kozubík, A. (2011). Cisplatin and a potent platinum (IV) complex-mediated enhancement of TRAIL-induced cancer cells killing is associated with modulation of upstream events in the extrinsic apoptotic pathway. *Carcinogenesis*, **32**(1), 42–51.

Blumenthal, R., Gallo, S. A., Viard, M., Raviv, Y., & Puri, A. (2002). Fluorescent lipid probes in the study of viral membrane fusion. *Chemistry and Physics of Lipids*, **116**(1–2), 39–55.

Bonello, T. T., Stehn, J. R., & Gunning, P. W. (2009). New approaches to targeting the actin cytoskeleton for chemotherapy. *Future Medicinal Chemistry*, **1**(7), 1311–1331.

Bonello, T., Coombes, J., Schevzov, G., Gunning, P., & Stehn, J. (2012). 'Therapeutic Targeting of the Actin Cytoskeleton in Cancer' in Kavallaris M. (eds) *Cytoskeleton and Human Disease*. NewYork: Humana Press, 181–200.

Boutin, C., Schlesser, M., Frenay, C., & Astoul, P. (1998). Malignant pleural mesothelioma. *European Respiratory Journal*, **12**(4), 972–981.

Boyles, M., Stoehr, L., Schlinkert, P., Himly, M., & Duschl, A. (2014). The Significance and Insignificance of Carbon Nanotube-Induced Inflammation. *Fibers*, **2**(1), 45–74.

Brooks, C. L., & Gu, W. (2011). The impact of acetylation and deacetylation on the p53 pathway. *Protein and Cell*, **2**(6), 456–462.

Browning, R. J., Reardon, P. J. T., Parhizkar, M., Pedley, R. B., Edirisinghe, M., Knowles, J. C., & Stride, E. (2017). Drug Delivery Strategies for Platinum-Based Chemotherapy. *ACS Nano*, **11**(9), 8560–8578.

CAROL, ONCOBOURGOGNE, ONCOCHA, ONCOLIE & ONCOLOR. (2017). Mésothéliome Pleural. [online] OncoLogiK. Available at: http://oncologik.fr/referentiels/interregion/mesotheliome-pleural [Accessed 27 Feb. 2018].

Castanedo, G., Clark, K., Wang, S., Tsui, V., Wong, M., Nicholas, J., … Sutherlin, D. (2006). CDK2/cyclinA inhibitors: Targeting the cyclinA recruitment site with small molecules derived from peptide leads. *Bioorganic and Medicinal Chemistry Letters*, **16**(6), 1716–1720.

Castedo, M., Perfettini, J. L., Roumier, T., Andreau, K., Medema, R., & Kroemer, G. (2004). Cell death by mitotic catastrophe: A molecular definition. *Oncogene*, ***23***(2), 2825–2837.

Ceresoli, G. L., Gridelli, C., & Santoro, A. (2007). Multidisciplinary Treatment of Malignant Pleural Mesothelioma. *The Oncologist*, **12**(7), 850–863.

Chen, S., Stout, J. R., Dharmaiah, S., Yde, S., Calvi, B. R., & Walczak, C. E. (2016). Transient endoreplication down-regulates the kinesin-14 HSET and contributes to genomic instability. *Molecular Biology of the Cell*, **27**(19), 2911–2923.

Chiu, J., & Dawes, I. W. (2012). Redox control of cell proliferation. *Trends in Cell Biology*, **22**(11), 592–601.

Cinausero, M., Rihawi, K., Sperandi, F., Melotti, B., & Ardizzoni, A. (2018). Chemotherapy treatment in malignant pleural mesothelioma: a difficult history. *Journal of Thoracic Disease*, **10**(Suppl 2), S304–S310.

Colombo, R., Caldarelli, M., Mennecozzi, M., Giorgini, M. L., Sola, F., Cappella, P., … Moll, J. (2010). Targeting the mitotic checkpoint for cancer therapy with NMS-P715, an inhibitor of MPS1 kinase. *Cancer Research*, **70**(24), 10255–10264.

Cortes-Dericks, L., Froment, L., Boesch, R., Schmid, R. A., & Karoubi, G. (2014). Cisplatin-resistant cells in malignant pleural mesothelioma cell lines show ALDHhighCD44+ phenotype and sphere-forming capacity. *BMC Cancer*, **14**(304), 1471–2407.

Cozzolino, R., Palladino, P., Rossi, F., Calì, G., Benedetti, E., & Laccetti, P. (2005). Antineoplastic cyclic astin analogues kill tumour cells via caspase-mediated induction of apoptosis. *Carcinogenesis*, **26**(4), 733–739.

Cselenyak, A., Pankotai, E., Horvath, E. M., Kiss, L., Zsombor, L. (2010). Mesenchymal stem cells rescue cardiomyoblasts from cell death in an in vitro ischemia model via direct cell-to-cell connections. *BMC Cell Biology*, **11**(29), 1471–2121.

Dasari, S., & Tchounwou, P. B. (2015). Cisplatin in cancer therapy: molecular mechanisms of action. *Eur J Pharmacol*, **5**(0), 364–378.

Davoli, T., & de Lange, T. (2011). The Causes and Consequences of Polyploidy in Normal Development and Cancer. *Annual Review of Cell and Developmental Biology*, **27**(1), 585–610.

Dekant, W. (2009). 'The role of biotransformation and bioactivation in toxicity' in Luch, A (ed.) *Molecular, Clinical and Environmental Toxicology*. 1edn. Birkhäuser Basel, 57–86.

Delgermaa, V., Takahashi, K., Park, E.-K., Le, G. V., Hara, T., & Sorahan, T. (2011). Global mesothelioma deaths reported to the World Health Organization between 1994 and 2008. *Bulletin of the World Health Organization*, **89**(10), 716–724.

Delon, I., & Brown, N. H. (2007). Integrins and the actin cytoskeleton. *Current Opinion in Cell Biology*, **19**(1), 43–50.

Desouza, M., Gunning, P. W., & Stehn, J. R. (2012). The actin cytoskeleton as a sensor and mediator of apoptosis. *BioArchitecture*, **2**(3), 75–87.

DeVita, V. T., & Chu, E. (2008). A history of cancer chemotherapy. *Cancer Research*, **68**(21), 8643–8653.

Dogan, A. U., Baris, Y. I., Dogan, M., Emri, S., Steele, I., Elmishad, A. G., & Carbone, M. (2006). Genetic predisposition to fiber carcinogenesis causes a mesothelioma epidemic in Turkey. *Cancer Research*, **66**(10), 5063–5068.

Dozier, J., Zheng, H., & Adusumilli, P. S. (2017). Immunotherapy for malignant pleural mesothelioma: current status and future directions. *Translational Lung Cancer Research*, **6**(3), 315–324.

Ellis, P., Davies, A. M., Evans, W. K., Haynes, A. E., & Lloyd, N. S. (2006). The use of chemotherapy in patients with advanced malignant pleural mesothelioma: A systematic review and practice guideline. *Journal of Thoracic Oncology*, **1**(6), 591–601.

Espinosa, E., Zamora, P., Feliu, J., & González Barón, M. (2003). Classification of anticancer drugs - A new system based on therapeutic targets. *Cancer Treatment Reviews*, **29**(6), 515–523.

Florea, A.-M., & Büsselberg, D. (2011). Cisplatin as an Anti-Tumor Drug: Cellular Mechanisms of Activity, Drug Resistance and Induced Side Effects. *Cancers*, **3**(4), 1351–1371.

Frisch, S. M., Schaller, M., & Cieply, B. (2013). Mechanisms that link the oncogenic epithelial–mesenchymal transition to suppression of anoikis. *Journal of Cell Science*, **126**(1), 21–29.

Galmarini, D., Galmarini, C. M., & Galmarini, F. C. (2012). Cancer chemotherapy: A critical analysis of its 60 years of history. *Critical Reviews in Oncology/Hematology*, **84**(2), 181–199.

Gaskell, M., Kaur, B., Farmer, P. B., & Singh, R. (2007). Detection of phosphodiester adducts formed by the reaction of benzo[a]pyrene diol epoxide with 2′-deoxynucleotides using collision-induced dissociation electrospray ionization tandem mass spectrometry. *Nucleic Acids Research*, **35**(15), 5014–5027.

Gavina, J. M. A., Yao, C., & Feng, Y. L. (2014). Recent developments in DNA adduct analysis by mass spectrometry: A tool for exposure biomonitoring and identification of hazard for environmental pollutants. *Talanta*, **130**, 475–494.

GENEONTOLOGY. PANTHER Classification System Home. [online] Available at: http://pantherdb.org/ [Accessed 11 Jun. 2018].

Gilmore, A. P., & Burridge, K. (1996). Molecular mechanisms for focal adhesion assembly through regulation of protein – protein interactions. *Cell*, **4**(6), 647–651.

Giono, L. E., & Manfredi, J. J. (2006). The p53 tumor suppressor participates in multiple cell cycle checkpoints. *Journal of Cellular Physiology*, **209**(1), 13–20.

Gomes, S. E., Pereira, D. M., Roma-Rodrigues, C., Fernandes, A. R., Borralho, P. M., & Rodrigues, C. M. P. (2018). Convergence of miR-143 overexpression, oxidative stress and cell death in HCT116 human colon cancer cells. *PLOSONE*, **13**(1), e0191607.

Goodsell, D. S. (2006). The Molecular Perspective: Cisplatin. *Stem Cells*, **24**(3), 514–515.

Grégoire, M. (2010). What's the place of immunotherapy in malignant mesothelioma treatments? *Cell Adhesion and Migration*, **4**(1), 153–161.

Hanauske, a R., Chen, V., Paoletti, P., & Niyikiza, C. (2001). Pemetrexed disodium: a novel antifolate clinically active against multiple solid tumors. *The Oncologist*, **6**(4), 363–373.

Hannun, Y. (1997). Apoptosis and the Dilemma of Cancer Chemotherapy. *The Journal of The American Society of Hematology*, **89**(6), 1845–1853.

Harris, C. C. (1996). Structure and function of the p53 tumor suppressor gene: clues for rational cancer therapeutic strategies. *Journal of the National Cancer Institute*, **88**(20), 1442–1455.

Haynes, J., Srivastava, J., Madson, N., Wittmann, T., & Barber, D. L. (2011). Dynamic actin remodeling during epithelial-mesenchymal transition depends on increased moesin expression. *Molecular Biology of the Cell*, **22**(24), 4750–4764.

Hazarika, M., White, R. M., Booth, B. P., Wang, Y.-C., Ham, D. Y. L., Liang, C. Y., … Pazdur, R. (2005). Pemetrexed in malignant pleural mesothelioma. *Clinical Cancer Research: An Official Journal of the American Association for Cancer Research*, **11**(3), 982–92.

Ho, L., Sugarbaker, D., & Skarin, A. T. (2001). 'Malignant Pleural Mesothelioma' in Ettinger D.S. (eds). *Thoracic Oncology*. Boston: Springer US, 327–373.

Housman, G., Byler, S., Heerboth, S., Lapinska, K., Longacre, M., Snyder, N., & Sarkar, S. (2014). Drug Resistance in Cancer: An Overview. *Cancers*, **6**(3), 1769–1792.

Hrycay, E.G., & Bandiera S. (2015). 'Monooxygenase, Peroxidase and Peroxygenase Properties and Mechanisms of Cytochrome P450' in Hrycay E., Bandiera S. (eds) *Monooxygenase, Peroxidase and Peroxygenase Properties and Mechanisms of Cytochrome P450*. Springer, 1–61.

Huijbers, M. M. E., Montersino, S., Westphal, A. H., Tischler, D., & Van Berkel, W. J. H. (2013). Flavin dependent monooxygenases. *Archives of Biochemistry and Biophysics*, **544**, 2–17.

Husain, A. N., Colby, T., Ordonez, N., Krausz, T., Attanoos, R., Beasley, M. B., … Wick, M. (2013). Guidelines for pathologic diagnosis of malignant mesothelioma: 2012 update of the consensus statement from the International Mesothelioma Interest Group. *Archives of Pathology and Laboratory Medicine*, **137**(5), 647–667.

Institut national de la santé et de la recherche medicale (2008). 'Classification histologique et pathologie moléculaire' in Inserm, DL (ed.). *Cancer et Environnement*. Paris : Les Éditions Inserm, 175–186.

Iqbal, M. S. (2017). Pleural Mesothelioma. Symptoms, Causes, Treatment Options. [online] CENTRAMIC. Available at : https://centramic.com/pleural-mesothelioma-symptoms-causes/ [Accessed 30 Jun. 2018].

Ismail-Khan, R., Robinson, L. A., Williams, C. C., Garrett, C. R., Bepler, G., & Simon, G. R. (2006). Malignant pleural mesothelioma: A comprehensive review. *Cancer Control*, **13**(4), 255–263.

Itokawa H., Takeya K., Hitotsuyanagi Y. & Morita H., (2000). Antitumor compounds isolated from higher plants. *Stud. Nat. Prod. Chem.* **24**, 269–350.

Jahn, L. (2015). Characterization of a new endophytic astin producer Pelliciarosea asterica, from Aster tataricus, 1–154.

Jahn, L., Schafhauser, T., Pan, S., Weber, T., Wohlleben, W., Fewer, D., … Ludwig-Müller, J. (2017). Cyanodermella asteris sp. nov. (Ostropales) from the inflorescence axis of Aster tataricus. *Mycotaxon Issn*, **132**(1), 107–123.

Jahn, L., Schafhauser, T., Wibberg, D., Rückert, C., Winkler, A., Kulik, A., … Wohlleben, W. (2017). Linking secondary metabolites to biosynthesis genes in the fungal endophyte Cyanodermella asteris: The anti-cancer bisanthraquinone skyrin. *Journal of Biotechnology*, **257**(June), 233–239.

Jänne, P. A., Wozniak, A. J., Belani, C. P., Keohan, M.-L., Ross, H. J., Polikoff, J. A., … Obasaju, C. K. (2006). Pemetrexed Alone or in Combination with Cisplatin in Previously Treated Malignant Pleural Mesothelioma: Outcomes from a Phase IIIB Expanded Access Program. *Journal of Thoracic Oncology*, **1**(6), 506–512.

Jasani, B., & Gibbs, A. (2012). Mesothelioma not associated with asbestos exposure. *Archives of Pathology and Laboratory Medicine*, **136**(3), 262–267.

Johnstone, R. W., Ruefli, A. A., & Lowe, S. W. (2002). Apoptosis: A link between cancer genetics and chemotherapy. *Cell*, **108**(2), 153–164.

Kanbay, A., Ozer Simsek, Z., Tutar, N., Yilmaz, I., Buyukoglan, H., Canoz, O., & Demir, R. (2014). Non-Asbestos-related Malignant Pleural Mesothelioma. *Internal Medicine*, **53**(17), 1977–1979.

Kapuscinski, J. (1995). DAPI: a DNA-Specific Fluorescent Probe. *Biotechnic & Histochemistry*, **70**(5), 220–233.

Kartalou, M., & Essigmann, J. M. (2001). Mechanisms of resistance to cisplatin. *Mutation Research/Fundamental and Molecular Mechanisms of Mutagenesis*, **478** (1–2), 23–43.

Kaufman, A. J., & Flores, R. M. (2011). Surgical treatment of malignant pleural mesothelioma. *Current Treatment Options in Oncology*, **12**(2), 201–216.

Kazan-Allen, L. (2015). The global mesothelioma landscape. *National center for asbestos related diseases*, (April), 1–25.

Kim, Y. K., Kim, J. S., Lee, K. W., Yi, C. A., Koo, J. M., & Jung, S. H. (2016). Multidetector CT findings and differential diagnoses of malignant pleural mesothelioma and metastatic pleural diseases in Korea. *Korean Journal of Radiology*, **17**(4), 545–553.

Kindler, H. L. (2000). Malignant Pleural Mesothelioma. *Current Treatment Options in Oncology*, **1**, 313–326.

Lee, C.-F., Yang, J.-S., Tsai, F.-J., Chiang, N.-N., Lu, C.-C., Huang, Y.-S., … Chen, F.-A. (2016). Kaempferol induces ATM/p53-mediated death receptor and mitochondrial apoptosis in human umbilical vein endothelial cells. *International Journal of Oncology*, **48**(5), 2007–2014

Lim, S., & Kaldis, P. (2013). Cdks, cyclins and CKIs: roles beyond cell cycle regulation. *Development*, **140**(15), 3079–3093.

Lorin, A., Flore, C., Thomas, A., & Brasseur, R. (2004). Les liposomes: Description, fabrication et applications. *Biotechnology, Agronomy and Society and Environment*, **8**(3), 163–176.

Luqmani, Y. A. (2005). Mechanisms of Drug Resistance in Cancer Chemotherapy. *Medical Principles and Practice*, **14**(1), 35–48.

Magnani, C., Agudo, A., González, C. A., Andrion, A., Calleja, A., Chellini, E., … Terracini, B. (2000). Multicentric study on malignant pleural mesothelioma and non-occupational exposure to asbestos. *British Journal of Cancer*, **83**(1), 104–11.

Manning, C. B., Vallyathan, V., & Mossman, B. T. (2002). Diseases caused by asbestos: Mechanisms of injury and disease development. *International Immunopharmacology*, **2**(2–3), 191–200.

Marieb, E., & Hoehn, K. (2007). Human anatomy & physiology. 7 edn. San Francisco: Pearson Benjamin Cummings Publications.

Martin, R. M., Leonhardt, H., & Cardoso, M. C. (2005). DNA labeling in living cells. *Cytometry Part A*, **67**(1), 45–52.

Mason, J. M., Wei, X., Fletcher, G. C., Kiarash, R., Brokx, R., Hodgson, R., … Mak, T. W. (2017). Functional characterization of CFI-402257, a potent and selective Mps1/TTK kinase inhibitor, for the treatment of cancer. *Proceedings of the National Academy of Sciences*, **114**(12), 3127–3132.

Matsuura, K., Canfield, K., Feng, W., & Kurokawa, M. (2016). Metabolic Regulation of Apoptosis in Cancer. *International Review of Cell and Molecular BiologyInternational Review of Cell and Molecular Biology*, **327**, 43–87.

Mendus, D. (2010). Cisplatin-induced DNA damage in normal and malignant cells: Mechanisms of drug resistance and side effects and strategies for their prevention, 1–116.

Miller, B. R., & Gulick, A. M. (2016). Nonribosomal Peptide and Polyketide Biosynthesis. *Methods Mol Biol***, 1401**(716), 3–29.

Mingeot-Leclercq, M. P., Lins, L., Bensliman, M., Van Bambeke, F., Van Der Smissen, P., Peuvot, J., … Brasseur, R. (2002). Membrane destabilization induced by β-amyloid peptide 29-42: Importance of the amino-terminus. *Chemistry and Physics of Lipids*, **120**(1–2), 57–74.

Mitchell, C. A., Shi, C., Aldrich, C. C., & Gulick, A. M. (2012). Structure of PA1221, a nonribosomal peptide synthetase containing adenylation and peptidyl carrier protein domains. *Biochemistry*, **51**(15), 3252–3263.

Morita, H., Nagashima, S., Uchiumi, Y., Kuroki, O., Takeya, K., & Itokawa, H. (1996). Cyclic peptides from higher plants. XXVIII. Antitumor activity and hepatic microsomal biotransformation of cyclic pentapeptides, astins, from Aster tataricus. *Chemical & Pharmaceutical Bulletin*, **44**(5), 1026–1032.

Morita, H., Nagashima, S., Takeya, K., Itokawa, H., & Iitaka, Y. (1995). Structures and conformation of antitumour cyclic pentapeptides, astins A, B and C, from Aster tataricus. *Tetrahedron*, **51**(4), 1121–1132.

Morita, H., Nagashima, S., Shirota, O., Takeya, K., and Itokawa, H. (1993a). Two novel monochlorinated cyclic pentapeptides, astins D and E from Aster tataricus. *Chemistry Letters*, **22**(11), 1877–1880.

Morita, H., Nagashima, S., Takeya, K., and Itokawa, H. (1993b). Astins A and B, antitu- mor cyclic pentapeptides from Aster tataricus. *Chemical & Pharmaceutical Bulletin*, **41**(5), 992–993.

Mórocz, M., Gali, H., Raskó, I., Downes, C. S., & Haracska, L. (2013). Single Cell Analysis of Human RAD18-Dependent DNA Post-Replication Repair by Alkaline Bromodeoxyuridine Comet Assay. *PLoS ONE*, **8**(8), e70391.

Mossman, B. T., & Marsh, J. P. (1989). Evidence supporting a role for active oxygen species in asbestos-induced toxicity and lung disease. *Environmental Health Perspectives*, **81**, 91–94.

Moulding, D. A., Blundell, M. P., Spiller, D. G., White, M. R. H., Cory, G. O., Calle, Y., … Thrasher, A. J. (2007). Unregulated actin polymerization by WASp causes defects of mitosis and cytokinesis in X-linked neutropenia. *The Journal of Experimental Medicine*, **204**(9), 2213–2224.

Mujoomdar, A. A., Tilleman, T. R., Richards, W. G., Bueno, R., & Sugarbaker, D. J. (2010). Prevalence of in vitro chemotherapeutic drug resistance in primary malignant pleural mesothelioma: Result in a cohort of 203 resection specimens. *Journal of Thoracic and Cardiovascular Surgery*, **140**(2), 352–355.

Musgrove, E. A., Caldon, C. E., Barraclough, J., Stone, A., & Sutherland, R. L. (2011). INK4 family Cyclin D as a therapeutic target in cancer. *Nature*, **11**, 558–572.

NCBI. Gene. [online] Available at : https://www.ncbi.nlm.nih.gov/gene/ [Accessed 11 Jun. 2018].

Nowak, A. K. (2012). Chemotherapy for malignant pleural mesothelioma: a review of current management and a look to the future. *Annals of Cardiothoracic Surgery*, **1**(4), 508–15.

O'Reilly, K. M. A., Mclaughlin, A. M., Beckett, W. S., & Sime, P. J. (2007). Asbestos-related lung disease. *American Family Physician*, **75**(5), 683–8.

Overholtzer, M., Zhang, J., Smolen, G. A., Muir, B., Li, W., Sgroi, D. C., … Haber, D. A. (2006). Transforming properties of YAP, a candidate oncogene on the chromosome 11q22 amplicon. *Proceedings of the National Academy of Sciences*, **103**(33), 12405–12410.

Pabla, N., & Dong, Z. (2008). Cisplatin nephrotoxicity: Mechanisms and renoprotective strategies. *Kidney International*, **73**(9), 994–1007.

Paoli, P., Giannoni, E., & Chiarugi, P. (2013). Anoikis molecular pathways and its role in cancer progression. *Biochimica et Biophysica Acta - Molecular Cell Research*, **1833**(12), 3481–3498.

Payne, S., & Miles, D. (2008). 'Mechanisms of Anticancer Drugs' in Gleeson M.(ed.) *Scott-Brown's Otorhinolaryngology: head and neck surgery*. 7 edn. Boca Raton: CRC Press, 34–46.

Peake, M. D. (2009). Pemetrexed in the treatment of malignant pleural mesothelioma. *Therapy*, **6**(4), 569–575.

Perrot, M. de, Wu, L., Wu, M., & Cho, B. C. J. (2017). Radiotherapy for the treatment of malignant pleural mesothelioma. *The Lancet Oncology*, **18**(9), e532–e542.

Pfau, S. J., & Amon, A. (2012). Chromosomal instability and aneuploidy in cancer: From yeast to man. *EMBO Reports*, **13**(6), 515–527.

Philippeaux, M. M., Pache, J. C., Dahoun, S., Barnet, M., Robert, J. H., Mauël, J., & Spiliopoulos, A. (2004). Establishment of permanent cell lines purified from human mesothelioma: Morphological aspects, new marker expression and karyotypic analysis. *Histochemistry and Cell Biology*, **122**(3), 249–260.

Pietenpol, J., & Stewart, Z. (2002). Cell cycle checkpoint signaling: Cell cycle arrest versus apoptosis. *Toxicology*, **181–182**, 475–481.

Pistolesi, M., & Rusthoven, J. (2004). Malignant pleural mesothelioma: Update, current management, and newer therapeutic strategies. *Chest*, **126**, 1318–1329.

Pollard, T. D., & Cooper, J. A. (2009). Actin, a Central Player in Cell Shape and Movement. *Spatial Cell Biology*, **326**, 2008-2011.

Powell, S.F., & Dudek. (2009). Tailoring treatment of nonsmall cell lung cancer by tissue type: Role of pemetrexed. *Pharmacogenomics and Personalized Medicine*, **2**(1), 21–37.

Rabik, C. A., & Dolan, M. E. (2007). Molecular mechanisms of resistance and toxicity associated with platinating agents. *Cancer Treatment Reviews*, **33**(1), 9–23.

Raja, S., Murthy, S. C., & Mason, D. P. (2011). Malignant pleural mesothelioma. *Current Oncology Reports*, **13**(4), 259–264.

Ramalingam, S. S., & Belani, C. P. (2008). Recent advances in the treatment of malignant pleural mesothelioma. *Journal of Thoracic Oncology*, **3**(9), 1056–1064.

Reisler, E., & Egelman, E. H. (2007). Actin structure and function: What we still do not understand. *Journal of Biological Chemistry*, **282**(50), 36133–36137.

Robinson, B. M. (2012). Malignant pleural mesothelioma: an epidemiological perspective. *Annals of Cardiothoracic Surgery*, **1**(4), 491–6.

Røe, O. D., & Stella, G. M. (2015). Malignant pleural mesothelioma: History, controversy and future of a manmade epidemic. *European Respiratory Review*, **24**(135), 115–131.

Rosenzweig, K. E., & Giraud, P. (2017). Radiothérapie des mésothéliomes malins pleuraux. *Cancer/Radiotherapie*, **21**(1), 73–76.

Rossi, F., Zanotti, G., Saviano, M., Iacovino, R., Palladino, P., Saviano, G., … Benedetti, E. (2004). New antitumour cyclic astin analogues: Synthesis, conformation and bioactivity. *Journal of Peptide Science*, **10**(2), 92–102.

Rumbaut, RE., Thiagarajan, P. (2010). 'Platelet Aggregation' in Granger D.N., Granger J. (eds) *Platelet-Vessel Wall Interactions in Hemostasis and Thrombosis.* San Rafael (CA): Morgan & Claypool Life Sciences.

Ruth, S. Van, Baas, P., & Zoetmulder, F.A.N. (2003). Surgical Treatment of Malignant Pleural. *Chest*, **123**, 551–561.

Salmela, A. L., Pouwels, J., Kukkonen-Macchi, A., Waris, S., Toivonen, P., Jaakkola, K., … Kallio, M. J. (2012). The flavonoid eupatorin inactivates the mitotic checkpoint leading to polyploidy and apoptosis. *Experimental Cell Research*, **318**(5), 578–592.

Sanchez, V. C., Pietruska, J. R., Miselis, N. R., Hurt, R. H., & Agnes, B. (2010). Biopersistence and potential adverse health impacts of fibrous nanomaterials: what have we learned from asbestos? *Wiley Interdiscip Rev Nanomed Nanobiotechnol*, **1**(5), 511–529.

Sartorius, U. A., & Krammer, P. H. (2002). Upregulation of Bcl-2 is involved in the mediation of chemotherapy resistance in human small cell lung cancer cell lines. *International Journal of Cancer*, **97**(5), 584–592.

Saviano, G., Benedetti, E., Cozzolino, R., De Capua, A., Laccetti, P., Palladino, P., … Rossi, F. (2004). Influence of conformational flexibility on biological activity in cyclic astin analogues. *Biopolymers - Peptide Science Section*, **76**(6), 477–484.

Schafhauser, T., Kirchner, N., Kulik, A., Huijbers, M. M. E., Flor, L., Caradec, T., … Van Pée, K. H. (2016). The cyclochlorotine mycotoxin is produced by the nonribosomal peptide synthetase CctN in Talaromyces islandicus ('Penicillium islandicum'). *Environmental Microbiology*, **18**(11), 3728–3741.

Schärer, O. D. (2005). DNA interstrand crosslinks: Natural and drug-induced DNA adducts that induce unique cellular responses. *ChemBioChem*, **6**, 27– 32.

Schärer, O. D. (2013). Nucleotide Excision Repair in Eukaryotes. *Cold Spring Harb Perspect Biol*, **5**, a012609

Scholar, E. (2008). 'Chemotherapeutic agents: Alkylating Agents' in Enna S.J., Bylund D.B. (eds) *xPharm: The Comprehensive Pharmacology Reference*. Amsterdam: Elsevier.

Schumacherr, K. K., Jiang, J., & Joullié, M. M. (1998). Synthetic studies toward astins A, B and C. Efficient syntheses of cis-3,4-dihydroxyprolines and (−)-(3S,4R)-dichloroproline esters. *Tetrahedron*, **9**, 47–53.

Schwaederlé, M., Daniels, G. A., Piccioni, D. E., Fanta, P. T., Schwab, R. B., Shimabukuro, K. A., … Kurzrock, R. (2014). Cyclin alterations in diverse cancers: Outcome and co-amplification network. *Oncotarget*, **6**(5), 3033–3042.

Sehdev, V., Katsha, A., Ecsedy, J., Zaika, A., Belkhiri, A., & El-Rifai, W. (2012). The combination of alisertib, an investigational Aurora kinase A inhibitor, and docetaxel promotes cell death and reduces tumor growth in preclinical cell models of upper gastrointestinal adenocarcinomas. *Cancer*, **119**(4), 904–914.

Selcuk, Z. T., Coplu, L., Emri, S., Kalyoncu, A. F., Sahin, A. A., & Baris, Y. I. (1992). Malignant pleural mesothelioma due to environmental mineral fiber exposure in Turkey; Analysis of 135 cases. *Chest*, **102**(3), 790–796.

Shankar, J., & Nabi, I. R. (2015). Actin cytoskeleton regulation of epithelial mesenchymal transition in metastatic cancer cells. *PLoS ONE*, **10**(3), 1–12.

Shapiro, G. I., & Harper, J. W. (1999). Anticancer drug targets: Cell cycle and checkpoint control. *Journal of Clinical Investigation*, **104**(12), 1645–1653.

Shen, D.-W., Pouliot, L. M., Hall, M. D., & Gottesman, M. M. (2012). Cisplatin Resistance: A Cellular Self-Defense Mechanism Resulting from Multiple Epigenetic and Genetic Changes. *Pharmacological Reviews*, **64**(3), 706–721.

Shu, Z., Row, S., & Deng, W. M. (2018). Endoreplication: The Good, the Bad, and the Ugly. *Trends in Cell Biology*, **28**(6), 465–474.

Siddik, Z. H. (2002). 'Mechanisms of Action of Cancer Chemotherapeutic Agents: DNA-Interactive Alkylating Agents and Antitumour Platinum-Based Drugs' in Alison M.R. (ed.) *The cancer handbook*. 1 edn. London: Nature Pub. Group, 1295–1313.

Singh, R., & Farmer, P. B. (2006). Liquid chromatography-electrospray ionization-mass spectrometry: The future of DNA adduct detection. *Carcinogenesis*, **27**(2), 178–196.

Spizzo, R., Nicoloso, M. S., Lupini, L., Lu, Y., Fogarty, J., Rossi, S., … Calin, G. A. (2010). MiR-145 participates with TP53 in a death-promoting regulatory loop and targets estrogen receptor-α in human breast cancer cells. *Cell Death and Differentiation*, **17**(2), 246–254.

Stayner, L., Welch, L. S., & Lemen, R. (2013). The Worldwide Pandemic of Asbestos-Related Diseases. *Annual Review of Public Health*, **34**(1), 205–216.

Sterman, D., & Albelda, S. (2005). Advances in the diagnosis, evaluation, and management of malignant pleural mesothelioma. *Respirology*, **10**(3), 266–283.

Strieker, M., Tanović, A., & Marahiel, M. A. (2010). Nonribosomal peptide synthetases: Structures and dynamics. *Current Opinion in Structural Biology*, **20**(2), 234–240.

Su, S. (2009). Mesothelioma: Path to Multimodality Treatment. *Seminars in Thoracic and Cardiovascular Surgery*, **21**(2), 125–131.

Su, Z., Yang, Z., Xu, Y., Chen, Y., & Yu, Q. (2015). Apoptosis, autophagy, necroptosis, and cancer metastasis. *Molecular Cancer*, **48**(14).

Sugarbaker, D. J., & Wolf, A. S. (2010). Surgery for malignant pleural mesothelioma. *Expert Review of Respiratory Medicine*, **4**(3), 363–372.

Takimoto, C. H., & Awada, A. (2008). Safety and anti-tumor activity of sorafenib (Nexavar®) in combination with other anti-cancer agents: A review of clinical trials. *Cancer Chemotherapy and Pharmacology*, **61**(4), 535–548

Tang, Y.-Y., Zhao, P., Zou, T.-N., Duan, J.-J., Zhi, R., Yang, S.-Y., … Wang, X.-L. (2017). Circular RNA hsa_circ_0001982 Promotes Breast Cancer Cell Carcinogenesis Through Decreasing miR-143. *DNA and Cell Biology*, **36**(11), 901–908.

Tang, Y., Wenhui, Z., Chen, Y., Zhao, Y., & Gu, W. (2008). Acetylation Is Indispensable for p53 Activation. *Cell*, **133**(4), 612–626.

Tano, Z. E., Chintala, N. K., Li, X., & Adusumilli, P. S. (2017). Novel immunotherapy clinical trials in malignant pleural mesothelioma. *Annals of Translational Medicine*, *5*(11), 245–245.

Tardif, K. D., Rogers, A., Cassiano, J., Roth, B. L., Cimbora, D. M., McKinnon, R., … Williams, B. L. (2011). Characterization of the Cellular and Antitumor Effects of MPI-0479605, a Small-Molecule Inhibitor of the Mitotic Kinase Mps1. *Molecular Cancer Therapeutics*, **10**(12), 2267–2275.

Théatre, A., & Jacques, P. (2017). Design of a fungal biofilm reactor for the production of astin, an anticancerous secondary metabolite.

Tomek, S., Emri, S., Krejcy, K., & Manegold, C. (2003). Chemotherapy for malignant pleural mesothelioma: Past results and recent developments. *British Journal of Cancer*, **88**(2), 167–174.

Tsao, A. S., Wistuba, I., Roth, J. A., & Kindler, H. L. (2009). Malignant pleural mesothelioma. *Journal of Clinical Oncology*, **27**(12), 2081–2090.

Uraguchi, K., Saito, M., Noguchi, Y., Takahashi, K., Enomoto, M., & Tatsuno, T. (1972). Chronic toxicity and carcinogenicity in mice of the purified mycotoxins, luteoskyrin and cyclochlorotine. *Food and Cosmetics Toxicology*, **10**(2), 193–207.

Urso, L., Cavallari, I., Silic-Benussi, M., Biasini, L., Zago, G., Calabrese, F., … Pasello, G. (2017). Synergistic targeting of malignant pleural mesothelioma cells by MDM2 inhibitors and TRAIL agonists. *Oncotarget*, **8**(27), 44232–44241.

Vakifahmetoglu, H., Olsson, M., & Zhivotovsky, B. (2008). Death through a tragedy: Mitotic catastrophe. *Cell Death and Differentiation*, **15**(7), 1153–1162.

Van Pée, K. H., & Patallo, E. P. (2006). Flavin-dependent halogenases involved in secondary metabolism in bacteria. *Applied Microbiology and Biotechnology*, **70**(6), 631–641.

Vandermeers, F., Hubert, P., Delvenne, P., Mascaux, C., Grigoriu, B., Burny, A., … Willems, L. (2009). Valproate, in combination with pemetrexed and cisplatin, provides additional efficacy to the treatment of malignant mesothelioma. *Clinical Cancer Research*, **15**(8), 2818–2828.

Vermeulen,K.,Van Bockstaele,D.R.,Berneman, Z. N., Vermeulen, K., Van Bockstaele, D. R., & Berneman, Z. N. (2003). The cell cycle:a review of regulation,deregulation and therapeutic targets in cancer. *Cell Proliferation*, **36**(3), 131–149.

Vicente-Manzanares, M., Choi, C. K., & Horwitz, A. R. (2009). Integrins in cell migration - the actin connection. *Journal of Cell Science*, **122**(9), 1473–1473.

Waite, K., & Gilligan, D. (2007). The Role of Radiotherapy in the Treatment of Malignant Pleural Mesothelioma. *Clinical Oncology*, **19**(3), 182–187.

Waldman, T., Lengauer, C., Kinzler, K. W., & Vogelstein, B. (1996). Uncoupling of S phase and mitosis induced by anticancer agents in cells lacking p21. *Nature*, **381**(JUNE), 713–716.

Wang, J., Seebacher, N., Shi, H., Kan, Q., & Duan, Z. (2017). Novel strategies to prevent the development of multidrug resistance (MDR) in cancer. *Oncotarget*, **8**(48), 84559–84571.

Wang, S., Liu, J. C., Ju, Y., Pellecchia, G., Voisin, V., Wang, D.-Y., … Zacksenhaus, E. (2017). microRNA-143/145 loss induces Ras signaling to promote aggressive Pten-deficient basal-like breast cancer. *JCI Insight*, **2**(15), e93313.

White, S. R., Williams, P., Wojcik, K. R., Sun, S., Hiemstra, P. S., Rabe, K. F., & Dorscheid, D. R. (2001). Initiation of apoptosis by actin cytoskeletal derangement in human airway epithelial cells. *American Journal of Respiratory Cell and Molecular Biology*, **24**(3), 282–294.

WHO. (2007). Cancer Control: Knowledge Into Action: WHO Guide for Effective Programmes-WHO prevention module 2. [online] Geneva: World Health Organization. Available at: http://www.who.int/cancer/modules/Prevention%20Module.pdf [Accessed 22 Feb. 2018].

Wylie, A. G. (2017). 'Asbestos and Fibrous Erionite' in Testa J. (eds.) *Asbestos and Mesothelioma, Current Cancer Research*. 8 edn. Cham: Springer International Publishing, 11–41.

Xu, H. M., Zeng, G. Z., Zhou, W. B., He, W. J., & Tan, N. H. (2013). Astins Kvol-P, six new chlorinated cyclopentapeptides from Aster tataricus. *Tetrahedron*, **69**(37), 7964–7969.

Xu, J., & Mao, W. (2016). Overview of Research and Development for Anticancer Drugs. *Journal of Cancer Therapy*, **7**(10), 762–772.

Yang, H., Testa, J.R., & Carbone, M. (2009). Mesothelioma Epidemiology, Carcinogenesis and Pathogenesis. *Current Treatment Options in Oncology*, **9**(2-3), 147–157.

Yang, T. Y., Chang, G. C., Chen, K. C., Hung, H. W., Hsu, K. H., Wu, C. H., … Hsu, S. L. (2011). Pemetrexed induces both intrinsic and extrinsic apoptosis through ataxia telangiectasia mutated/p53-dependent and -independent signaling pathways. *Molecular Carcinogenesis*, **52**(3), 183–194.

Yardley, D. A. (2013). Drug Resistance and the Role of Combination Chemotherapy in Improving Patient Outcomes. *International Journal of Breast Cancer*, **2013**(137414), 1–15.

Yu, P., Cheng, S., Xiang, J., Yu, B., Zhang, M., Zhang, C., & Xu, X. (2015). Expectorant, antitussive, anti-inflammatory activities and compositional analysis of Aster tataricus. *Journal of Ethnopharmacology*, **164**, 328–333.

Zafonte, B. T., Hulit, J., Amanatullah, D. F., Albanese, C., Wang, C., Rosen, E., … Pestell, R. G. (2000). 938 2. Introduction 2.1. Inherited Breast Cancer Susceptibility Genes 2.2. Breast Adenocarcinoma Pathology 3. The Cell Cycle and Pathogenesis of Breast Cancer 3.1. The p27 Kip1 Tumor. *Frontiers in Bioscience*, **5**, 938–961.

Zaidel-Bar, R., Zhenhuan, G., & Luxenburg, C. (2015). The contractome - a systems view of actomyosin contractility in non-muscle cells. *Journal of Cell Science*, **128**(12), 2209–2221.

Zanconato, F., Cordenonsi, M., & Piccolo, S. (2016). YAP/TAZ at the Roots of Cancer. *Cancer Cell*, **29**(6), 783–803.

Zandwijk, N. Van, Clarke, C., Henderson, D., Musk, A. W., Fong, K., Nowak, A., … Penman, A. (2013). Guidelines for the diagnosis and treatment of malignant pleural mesothelioma. *Journal of Thorac Disease*, **5**(6), E254–E307.

Zhang, N., Song, Y., Wu, D., Xu, T., Lu, M., Zhang, W., & Wang, H. (2016). Detection of 1,N2-propano-2'-deoxyguanosine adducts in genomic DNA by ultrahigh performance liquid chromatography-electrospray ionization-tandem mass spectrometry in combination with stable isotope dilution. *Journal of Chromatography A*, **1450**, 38–44.

Zhang, H. tao, Tian, M., He, Q. wei, Chi, N., Xiu, C. ming, & Wang, Y. bo. (2017). Effect of Aster tataricus on production of inflammatory mediators in LPS stimulated rat astrocytoma cell line (C6) and THP-1 cells. *Saudi Pharmaceutical Journal*, **25**(3), 370–375.

Zhao, B., Li, L., Wang, L., Wang, C. Y., Yu, J., & Guan, K. L. (2012). Cell detachment activates the Hippo pathway via cytoskeleton reorganization to induce anoikis. *Genes and Development*, **26**(1), 54–68.

Zhao, L., Pan, Y., Gang, Y., Wang, H., Jin, H., Tie, J., … Fan, D. (2009). Identification of GAS1 as an epirubicin resistance-related gene in human gastric cancer cells with a partially randomized small interfering RNA library. *Journal of Biological Chemistry*, **284**(39), 26273–26285.

Zhao, Q., Sun, X., Liu, C., Li, T., Cui, J., & Qin, C. (2018). Expression of the microRNA-143/145 cluster is decreased in hepatitis B virus-associated hepatocellular carcinoma and may serve as a biomarker for tumorigenesis in patients with chronic hepatitis B. *Oncology Letters*, **15**(5), 6115–6122.

Zhou, L. L., Dong, J. L., Huang, G., Sun, Z. L., & Wu, J. (2017). MicroRNA-143 inhibits cell growth by targeting ERK5 and MAP3K7 in breast cancer. *Brazilian Journal of Medical and Biological Research*, **50**(8), e5891.

Zhu, X., De Laurentis, W., Leang, K., Herrmann, J., Ihlefeld, J., Pée, K-H & Naismith, J-H. (2009). Structural Insights into Regioselectivity in the Enzymatic Chlorination of Tryptophan. *J Mol Bio*, **391**(1), 74–85.